

CORRECTIONS FOR BEAM PATTERN RESIDUALS IN  
BACKSCATTER IMAGERY FROM THE KONGSBERG-  
SIMRAD EM300 MULTIBEAM ECHOSOUNDER

by

Kristian Charles Llewellyn

B.Sc.Eng, Mechanical, University of New Brunswick, 2002

A Report Submitted in Partial Fulfillment of  
the Requirements for the Degree of

Masters of Engineering

in the UNB Ocean Mapping Group,  
Department of Geodesy & Geomatics Engineering

Supervisor: Dr. John E. Hughes Clarke, PhD  
Associate Professor, Department of Geodesy &  
Geomatics Engineering  
Chair, UNB Ocean Mapping Group

Examining Board: Dr. David Wells, PhD  
Professor Emeritus, Department of Geodesy &  
Geomatics Engineering

Dr. Karl Butler, PhD  
Associate Professor, Department of Geology  
Director, Geological Engineering

THE UNIVERSITY OF NEW BRUNSWICK

January, 2006

© Kristian Llewellyn, 2006

## **ABSTRACT**

This report outlines the research and subsequent software development to correct for beam pattern residuals in backscatter mosaics derived from the Kongsberg-Simrad EM300 multibeam system installed on the Canadian Coast Guard Ship Amundsen. Since 2003, the UNB Ocean Mapping Group (OMG) has been tasked with the acquisition, processing, management, and distribution of all hydrographic data from the ship as part of the Canadian Arctic Shelf Exchange Study and ArticNet projects organized and financed through the Natural Sciences and Engineering Research Council of Canada and the Canadian Foundation for Innovation.

In addition to the typical bathymetric products available from multibeam sonar systems, backscatter mosaics are also needed to support other scientific objectives on board the vessel, particularly ongoing paleo-oceanographic research. This involves boxcore and piston-core samples taken from the surface and sub-surface of the seabed in the high Canadian arctic. Having accurate seafloor backscatter information is vital to choosing appropriate locations for these activities. It is therefore crucial to provide such backscatter products with all apparent changes in such products due to actual changes in seafloor geology and not due to beam pattern fluctuations from the sonar system.

There is a great deal of calibration performed automatically by the Simrad system on raw backscatter data, and OMG beam correction software exists to further calibrate backscatter in several different ways. Even so, residual beam pattern effects still exist in the resulting mosaics from the Amundsen due to additional complications with the EM300. This report describes the ship and the ArcticNet program in general, discusses the technical details of the EM300 sonar system, and reviews some general and Simrad-specific backscatter theory as well as current OMG beam pattern correction practices. Finally, it describes further research and software development created for this project to correct for residual beam pattern effects in the Amundsen EM300 data.

## **DEDICATION**

*For my parents, Gary and Carol Llewellyn,  
for their never-ending support.*

## **ACKNOWLEDGEMENTS**

I would like to thank the officers, crew, and scientists aboard the Canadian Coast Guard Ship Amundsen and CSIRO Research Vessel Southern Surveyor, as well as Howard Ingals and James Leslie, skippers for the CHS/OMG Canadian Survey Launch Heron with whom I worked. Aboard these three vessels I was able to obtain a large amount of hydrographic field experience during the course of this degree, as well as much experience using Kongsberg-Simrad multibeam sonar systems and related oceanographic and hydrographic equipment.

Thanks go to the University of Washington in the United States and the University of Newcastle in Australia for the use of multibeam sonar data from the RV Thomas Thompson and CSIRO Southern Surveyor for this research.

Thanks go to The Natural Sciences and Engineering Research Council of Canada and the Canadian Foundation for Innovation for their financial and logistical support of the Canadian CASES and ArticNet projects, through which this research was undertaken.

I would also like to thank Jonathon Beaudoin, research assistant and PhD candidate in the UNB Ocean Mapping Group, for continued support and assistance using and developing OMG software tools.

Lastly I thank my supervisor, Dr. John E. Hughes Clarke, for all his guidance and support over the last two years, and for making the research and worldwide ocean surveying opportunities I have experienced possible.

# TABLE OF CONTENTS

ABSTRACT.....	ii
DEDICATION.....	iii
ACKNOWLEDGEMENTS.....	iv
TABLE OF CONTENTS.....	v
LIST OF FIGURES .....	vi
LIST OF TABLES.....	vii
1. INTRODUCTION .....	1
2. THE CANADIAN COAST GUARD SHIP AMUNDSEN.....	4
3. THE KONGSBERG-SIMRAD EM300 MULTIBEAM ECHOSOUNDER .....	7
3.1 System Parameters.....	7
3.2 EM300 Ice Window Installation.....	7
3.3 Principles of Multi-Sector Yaw Stabilization and Multi-Mode Multibeam Sonar Systems.....	10
3.4 Transmit Beam Pattern Ice Window Adjustments.....	17
4. MULTIBEAM BACKSCATTER OVERVIEW .....	20
5. CORRECTION SOFTWARE FOR BACKSCATTER BEAM PATTERN RESIDUALS.....	27
6. BACKSCATTER BEAM PATTERN ISSUES AND NEW SOFTWARE DEVELOPMENT SOLUTIONS.....	32
6.1 Determination of Angular Sector Boundaries.....	35
6.2 Redefinition of Launch Angles Using Raw Angle Determination .....	43
6.3 Automatic Mode-Intelligent Beam Pattern Correction Software for Multi-Mode, Multi-Sector Multibeam Systems.....	47
6.4 Inter-Beam Interpolation Within Beam Pattern Models.....	55
7. CONCLUSION.....	61
REFERENCES.....	64
APPENDIX A: Comparisons of Default EM300 Transmit Beam Pattern Adjustments with those Modified to Account for the Ice Window Installation aboard the CCGS Amundsen.....	65
APPENDIX B: Quantitative Comparisons of Beam Pattern Modeling .....	70
APPENDIX C: Overview of Angular Definitions.....	86
CURRICULUM VITAE	

## LIST OF FIGURES

Figure 1. The CCGS Amundsen .....	4
Figure 2. The Canadian survey area .....	6
Figure 3. Typical arctic survey conditions encountered by the Amundsen .....	8
Figure 4. EM300 protective polymer-titanium ice window.....	9
Figure 5. EM300 transmit array.....	9
Figure 6. EM300 receive array .....	9
Figure 7. Multibeam beam vector shown as a product of transmit and receive beams ...	11
Figure 8. Principle of multibeam yaw stabilization.....	13
Figure 9. Illustration of sounding geometry with and without yaw stabilization .....	14
Figure 10. Multiple transmit sectors used by the EM300.....	15
Figure 11. EM300 performance envelope as installed on the CCGS Amundsen showing the range performance of each mode of the EM300 system .....	17
Figure 12. Backscatter mosaics illustrating differing transmit sector strength offsets ....	18
Figure 13. Spherical spreading of an acoustic wave.....	22
Figure 14. Temperature dependence for oceanic waters .....	22
Figure 15. Ensonified area of the seabed .....	23
Figure 16. Seabed angular response curve.....	25
Figure 17. Simrad backscatter corrections for seafloor angular response .....	26
Figure 18. Illustration of multiple backscatter values recorded within the footprint of one beam of a Simrad multibeam system .....	29
Figure 19. Beam pattern from the EM300 as installed on the Amundsen, showing variations in beam pattern intensities as well as imperfect angular response modeling .....	31
Figure 20. Differences of output from the OMG backscatter production software showing the importance of beam pattern corrections .....	32
Figure 21. Sector boundary beam pattern residuals in Amundsen EM300 data.....	34
Figure 22. Sequential firing sequence of the EM300 multiple transmit sectors.....	36
Figure 23. Angular conventions for the depression and sector angles .....	36
Figure 24. Angular conventions for the depression and sector angles .....	38
Figure 25. Individual angular components used to calculate the sector angle.....	41
Figure 26. Differing methods of launch angle determination.....	45
Figure 27. EM300 backscatter mosaiced using raw angle determination .....	46
Figure 28. EM300 beam patterns showing the effects of changing pulse length and the number of transmit sectors fired .....	49
Figure 29. EM300 backscatter mosaiced with differing beam pattern corrections applied.....	51
Figure 30. EM300 beam patterns with differing angular swaths.....	53
Figure 31. Automatic beam pattern corrections for the EM300 Extra Deep mode .....	54
Figure 32. EM300 beam pattern with missing and artificial beam pattern data .....	56
Figure 33. EM300 beam pattern with inter-beam interpolation .....	59
Figure 34. EM300 backscatter mosaiced using interpolated beam pattern model corrections.....	60
Figure 35. Backscatter mosaics showing the results of using the improved beam pattern correction software tools.....	63

Figure C-1. Individual angular components used to calculate the sector angle.....	88
Figure C-2. Convention used for sector and launch angles .....	89
Figure C-3. Azimuth and depression angles .....	90
Figure C-4. Seabed incidence angle.....	91

## LIST OF TABLES

Table 1. Ping Modes of the EM300 .....	16
Table 2. Sample Data from a Typical Beam Pattern Structure.....	30
Table 3. EM300 Sector Boundaries Provided to OMG by Kongsberg-Simrad.....	37
Table 4. EM300 Sector Boundaries in use on CCGS Amundsen as Calculated Using Sector Angle = $90^{\circ}$ – Depression Angle .....	40
Table 5. EM300 Sector Boundaries in Use by the System on CCGS as Calculated Using Raw Angular Measurements .....	42
Table 6. Sample Data from a Beam Pattern Structure Resulting from Using Conventional OMG Beam Pattern Correction Software .....	56
Table 7. Sample Data from a Beam Pattern Structure Resulting from Using Inter-Beam Interpolated Beam Pattern Correction Software.....	58
Table A-1. EM300 Relative Sector Transmit Strengths. ....	66
Table A-2. EM300 Transmit Sector Crossover Angles .....	67
Table A-3. EM300 Transmit Sector Beam Boresite Pointing Angles.....	68
Table A-4. EM300 Across-Track Transmit Sector Beamwidths.....	69
Table B-1. Numerical Beam Pattern Structure as Shown Graphically in Figure 25 Comparing Launch Angle Calculation of Sounding Depth and Across-Track Distance Transformation versus Raw Angle Determination ....	71
Table B-2. Numerical Beam Pattern Structure as Shown Graphically in Figure 26 Comparing Beam Pattern Statistics Calculated for Each Used Mode in a Survey Line versus an Average of the Entire Line .....	76
Table B-3. Numerical Beam Pattern Structure as Shown Graphically in Figures 30 and 31 Comparing Original Beam Pattern Modeling versus Inter-Beam Interpolation Modeling .....	81



## 1. INTRODUCTION

This report is a summary of the research and subsequent software developments undertaken to improve products derived from the Kongsberg-Simrad EM300 multibeam swath sonar system installed on the Canadian Coast Guard Ship (CCGS) Amundsen. The ship operates as the primary platform for the Canadian ArcticNet project, a major marine research project funded through The Natural Sciences and Engineering Research Council of Canada and the Canadian Foundation for Innovation. Installed on board the ship are several marine echosounders used to map the surface and sub-surface of the seabed, the primary one being the EM300 multibeam system.

The two major products derived from this system are the maps of bathymetry and backscatter strength. The backscatter products have proven to be an important part of the geology and paleo-oceanography science programs on board, which use these products as a guide in choosing locations for taking boxcore or piston core samples on and beneath the seabed. It is therefore crucial for the backscatter mosaics used by this team of people to represent true geological features, and not to contain sonar beam pattern residuals often present in the backscatter mosaics produced by commercial multibeam processing software suites. Software exists within the Ocean Mapping Group which will correct for most beam pattern effects in these types of mosaics, however there are a few complications with the EM300 system as installed on the Amundsen which results in several acoustic artifacts remaining in the backscatter products after processing.

The first issue is the advanced motion compensation capabilities of the system. This includes the ability to compensate for sudden changes in heading, or yawing, of the vessel, a feature which has a major impact on its overall operation. It requires that the transmit fan be split into 3 or 9 frequency-coded transmit sectors. These are fired within

a few milliseconds of each other with independent active steering according to vessel roll, pitch and yaw to ensure that the resulting swath remains close to perpendicular to the survey line. This multi-sector type of system will often operate with slightly different returned acoustic strength results for each separate transmit sector, leaving beam pattern residuals along its sector boundaries in the resulting backscatter mosaics.

The second issue is the type of installation the transducer required in order to be outfitted aboard the Amundsen. The ship is a class 1200 icebreaker and routinely works in and around ice fields as its primary field area is above the Arctic Circle. The major issue upon installing the system was the question of survivability. In order to withstand the bombardment of ice flow underneath the vessel, the transmit and receive transducers were installed inside an acoustic well built within the keel, and protected by titanium bars encased in a polymer shell. This type of multibeam installation has been found to cause increased beam pattern effects along the boundaries of the transmit sectors as they propagate through the protective ice window. As such, the calibration performed automatically by the Simrad system on raw backscatter data, as well as the standard suite of OMG beam pattern correction tools, are not always sufficient to remove all beam pattern effects from the data.

The motive for this work was to discover a way to remove these sector boundary residuals from the Amundsen data, and ensure that all backscatter products in the future are free from all residual sonar effects. The course of the project work became one primarily of computer programming, requiring both the modification of current OMG software, as well as the development of new software. This report will discuss the technical details of each of these issues, as well as outline the ongoing software

development solutions created to remove these unwanted sector boundary residuals in the Amundsen EM300 backscatter data.

## 2. THE CANADIAN COAST GUARD SHIP AMUNDSEN

The Canadian Coast Guard Ship (CCGS) Amundsen is a Class 1200 state of the art refurbished icebreaker, one of 3 sister icebreakers operated by the Canadian Coast Guard. Formerly the Sir John Franklin, she was recommissioned as the Amundsen in 2003. She is shown in Figure 1.



Figure 1. The CCGS Amundsen steaming through the Canadian Arctic. Photo courtesy of M. Fortier.

Since her refit, the Amundsen has been the primary science platform for the Canadian Arctic Shelf Exchange Study (CASES). This was a program dedicated to scientific research to better understand the ecosystem in the western arctic, particularly along the Mackenzie Shelf. As of the fall of 2004, the CASES project was completed and the Amundsen is scheduled to work for up to the next 14 years as part of ArcticNet, a major federal initiative funded by The Natural Sciences and Engineering Research

Council of Canada and the Canadian Foundation for Innovation to conduct multi-disciplinary scientific arctic research, as well as to increase the government's presence in the Canadian north and improve health services for Canada's northern communities. The Ocean Mapping Group at UNB has been tasked with operating all seabed mapping equipment aboard the ship, as well as handling the processing, management, and distribution of all related data.

The ship is a double-propeller vessel, 98 meters in length, with an endurance of 44 days (or 5,000 nautical miles) at 14 knots. The vessel offers accommodation for 46 scientists, 9 officers, and 22 crew, and is capable of twenty-four hour operation. For science operations she has 4 deck cranes, 2 10-ton A-frames, 5 scientific winches, an internal moonpool, 3 launches/barges, a BO 125 helicopter with helideck, and 400 m<sup>2</sup> of wet and dry laboratory working space [CCGS Amundsen 2004].

Its sonar and related equipment include the Simrad EM300 multibeam swath mapping system, a Knudsen 320R 3.5 kHz sub-bottom profiler, inboard ADCPs for current measurements, and a Simrad EK50 echosounder at 38, 120, and 200 kHz. GPS and orientation data is obtained from an Applanix POS/MV 320 system, with differential corrections from the C&C Technologies C-Nav global GPS corrections service. The manufacturer's stated accuracies are in the order of 0.02° for roll and pitch, 0.05° for heading, and < 1m positioning with the DGPS signal at the 95% confidence level. Water column control is obtained with 2 carousel rosette systems and a Brooke Ocean MVP300 moving vessel profiler with towfish. Both are outfitted with Seabird 911 + conductivity, temperature, and depth (CTD) sensors. The MVP is capable of being towed behind the

vessel in ice-free waters down to 300m at 12 knots, with a dipping motion constantly collecting water column information along the travel path of the vessel.

As shown in Figure 2, the science and survey area comprises all northern Canadian waters, with the priority thus far in the Northwest Passage and western Arctic area. Each field season takes place during the summer and fall seasons, while her winter is spent out of her home port of Quebec City undergoing standard Coast Guard ice-breaking activities in the St. Lawrence river.

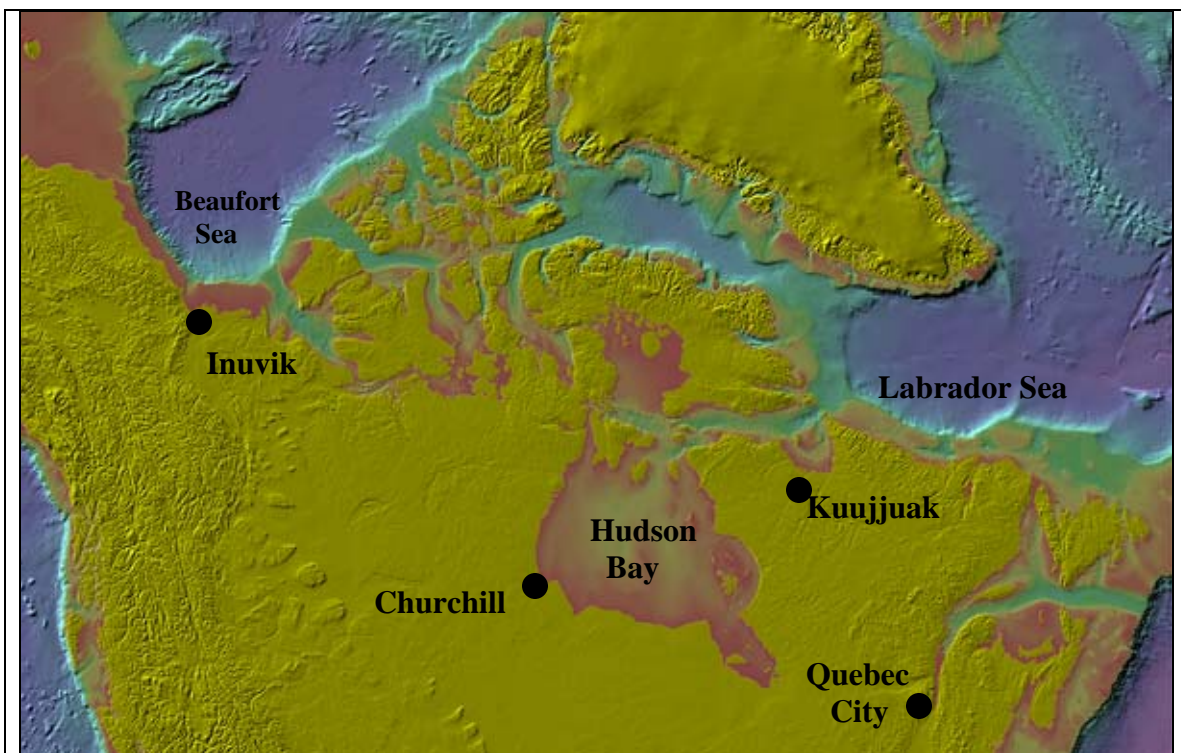


Figure 2. The Canadian survey area showing the locations of the Amundsen's home port of Quebec City, and the towns of Inuvik, Churchill, and Kuujjuak where 2004 crew changes took place. Image derived from topographic and bathymetric Canadian map created by Jonathan Beaudoin.

### **3. THE KONGSBERG-SIMRAD EM300 MULTIBEAM ECHOSOUNDER**

#### **3.1 System Parameters**

One of the primary geophysical tools aboard the CCGS Amundsen is the Kongsberg-Simrad EM300 multibeam swath sonar mapping system. This system uses a single 30 kHz Mills Cross array and is capable of swath mapping with depth ranges between 10 m and 5000m. It runs with up to  $\pm 75^\circ$  angular swath with 135 beams per ping, and features dynamically variable beamwidth configurations in the range of  $1^\circ$  to  $4^\circ$  to achieve both high spatial resolution in deep water and avoidance of nearfield effects in shallow water. It is fully stabilized for ship motion through 3 or 9 frequency-coded transmit sectors fired within a few milliseconds of each other with independent active steering according to vessel roll, pitch and yaw to ensure a swath close to perpendicular to the survey line. For all sectors, a choice of equiangular, equidistant, or in-between beam spacing is available. The swath width may be set to either a fixed angular sector, or a fixed maximum swath width. The ping rate is dependant on the round trip travel time in the water up to a maximum of 10 Hz, and the manufacturer's stated system vertical accuracy is 0.2% of water depth at nadir, and 0.5% of water depth between  $60^\circ$  and  $70^\circ$  off-nadir at the 95% confidence level [Kongsberg-Simrad, 2002].

#### **3.2 EM300 Ice Window Installation**

The major concern for installing a multibeam system on an icebreaker is its ability to survive while the ship is traveling through ice. Very often ice is pushed under the ship which would shear any protruding parts of the transducer off the ship's keel if installed in



the standard fashion. A typical ocean scene within the Amundsen's science and survey area is shown in Figure 3.



Figure 3. Typical arctic survey conditions encountered by the Amundsen. Photo courtesy of M. Fortier.

When the EM300 was chosen to be the multibeam system on the vessel, the first issue was one of survivability. For its protection, Simrad included an ice window with the transducer installation. This is comprised of titanium rods encased in a polymer shell which sits underneath the transducer. The transducer itself sits in an acoustic well which was cut out of the bottom of the ship while the system was being installed, as shown in Figure 4. As expected, this ice window compromises the performance of the system in open ocean conditions. Both the transmit and receive arrays were required to be installed inside the hull surface which reduces the achievable angular sector by 10 degrees per side. In addition to this, the receive array was tilted 6 degrees due to a lack of available flat level surfaces on the lower hull which further limits the available angular sector. It



has been found that  $65^\circ$  to port and  $60^\circ$  to starboard are the practical operational limits.

Illustrations of both the transmit and receive arrays are shown in Figures 5 and 6.

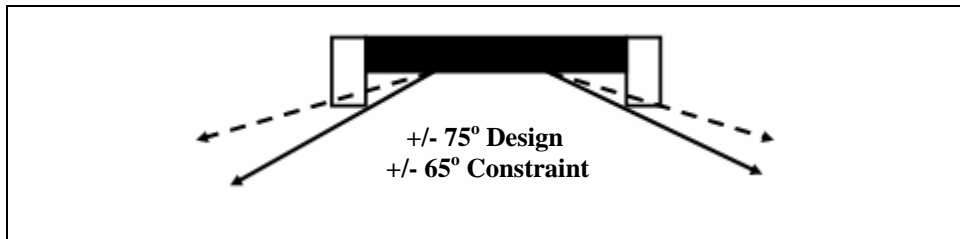


Figure 5. EM300 transmit array.

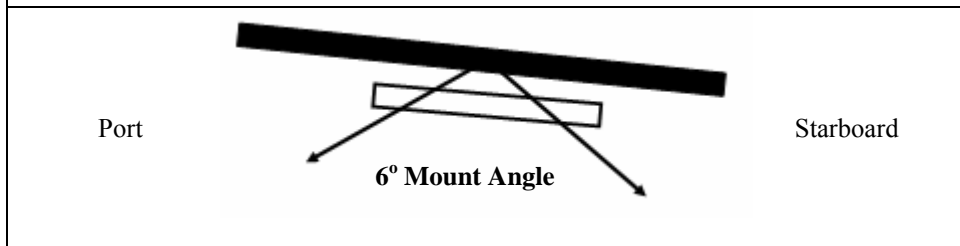
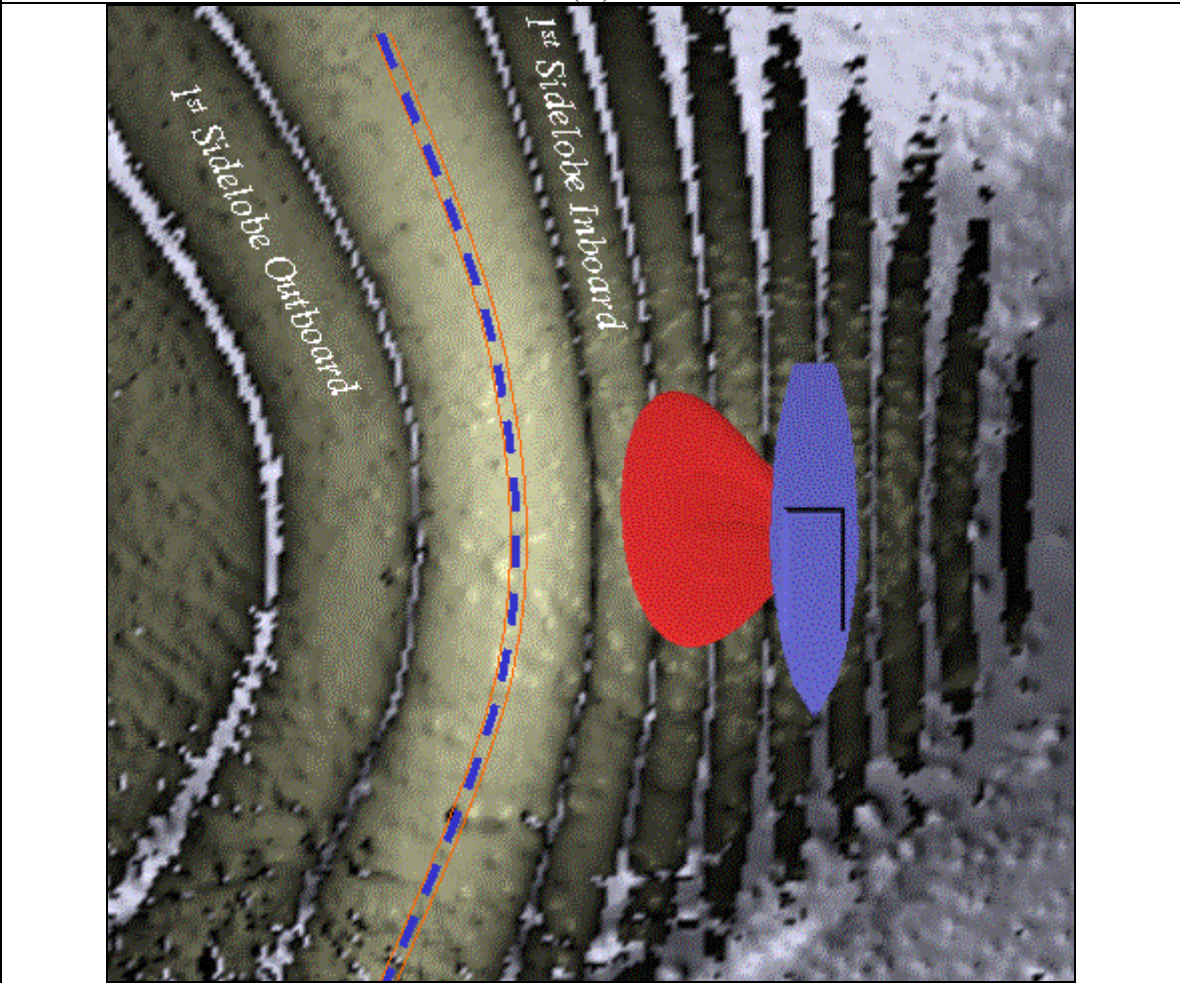
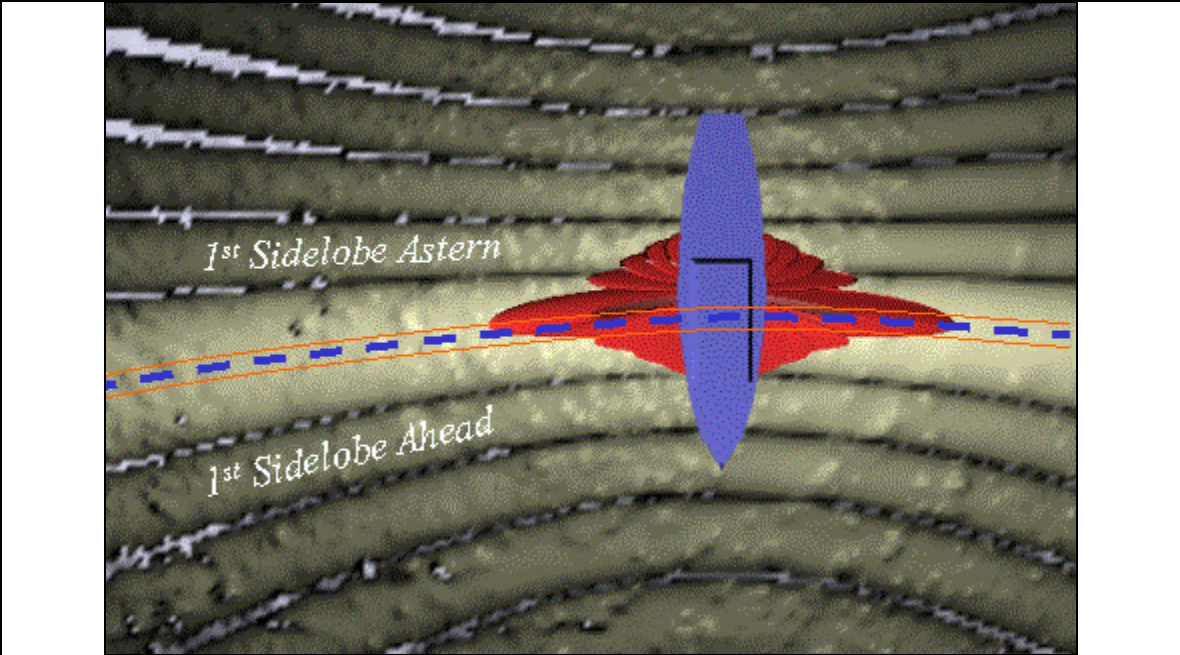


Figure 6. EM300 receive array.

Another complication is the propagation of the sound through the ice window, which causes a reduction in range performance and a lower signal-to-noise ratio. A ~10 decibel (dB) net loss occurs as a combination of propagation through the window for each product of the transmit and receive beams [Bartlett, 2004]. Lastly, bubble-washdown occurs quite frequently as the transducer is mounted flush with the bottom of the hull. An EM300 transducer is typically mounted in a gondola unit installed below the survey vessel. This keeps the transmit and receive arrays at a distance from the keel of the ship, allowing the majority of all air bubbles to pass above and around the gondola rather than along the transducer face. A system installed in this fashion is therefore much less sensitive to ship motion on the sea surface, and has been seen to be capable of full coverage mapping in seastate 7. In contrast, the combination of issues arising from the ice window installation on board the Amundsen renders the system vulnerable to bubbles in seastates above 3.

### **3.3 Principles of Multi-Sector Yaw Stabilization and Multi-Mode Multibeam Sonar Systems**

Modern multibeam systems will typically execute electronic beam steering to compensate for the dynamic motion of the survey vessel on the ocean surface and maintain a constant geometry of soundings on the seabed. This is quite common in the along and across-track directions to compensate for the pitch and the roll of the vessel as the swath can be electronically steered in either of these directions. The final beam vector is a product of both the transmit and receive beams, as shown in Figure 7.





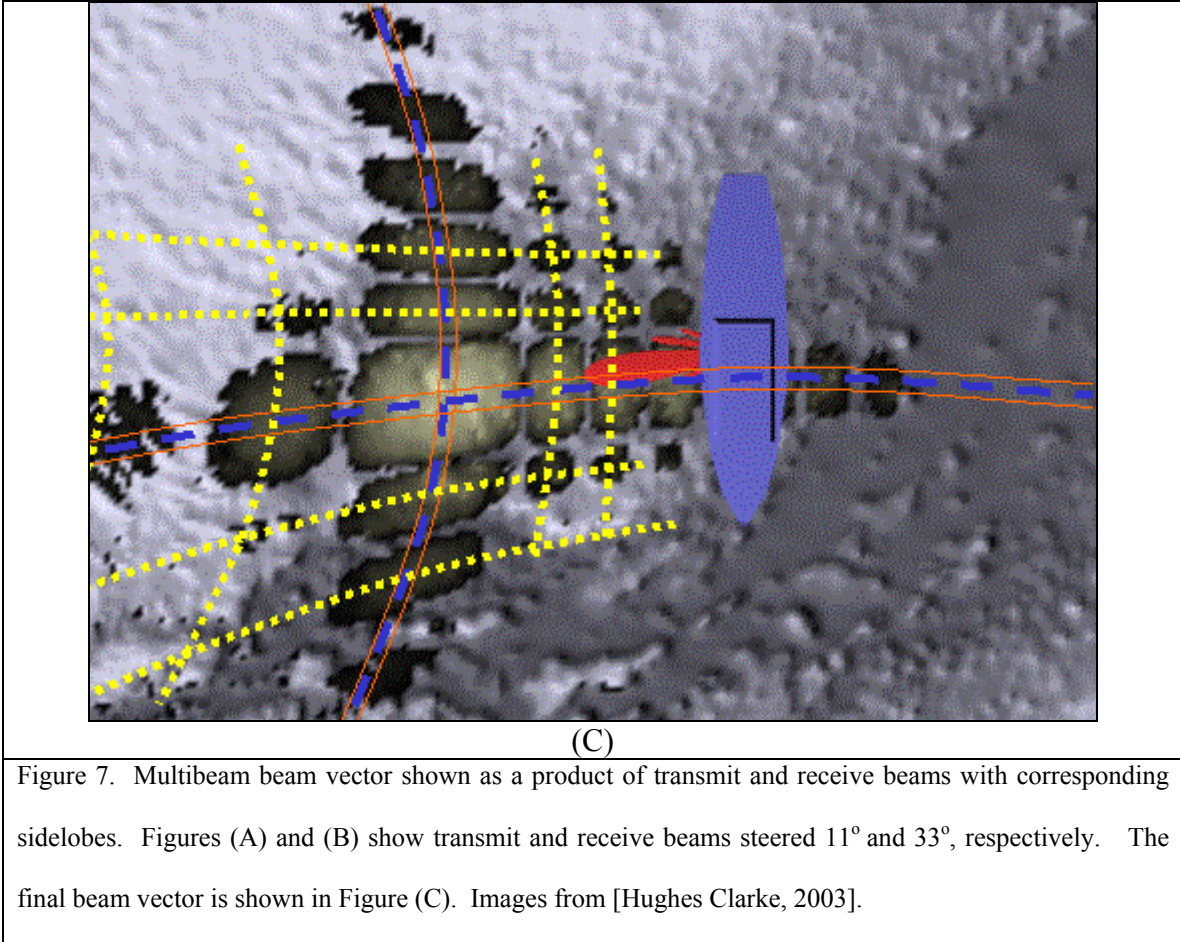
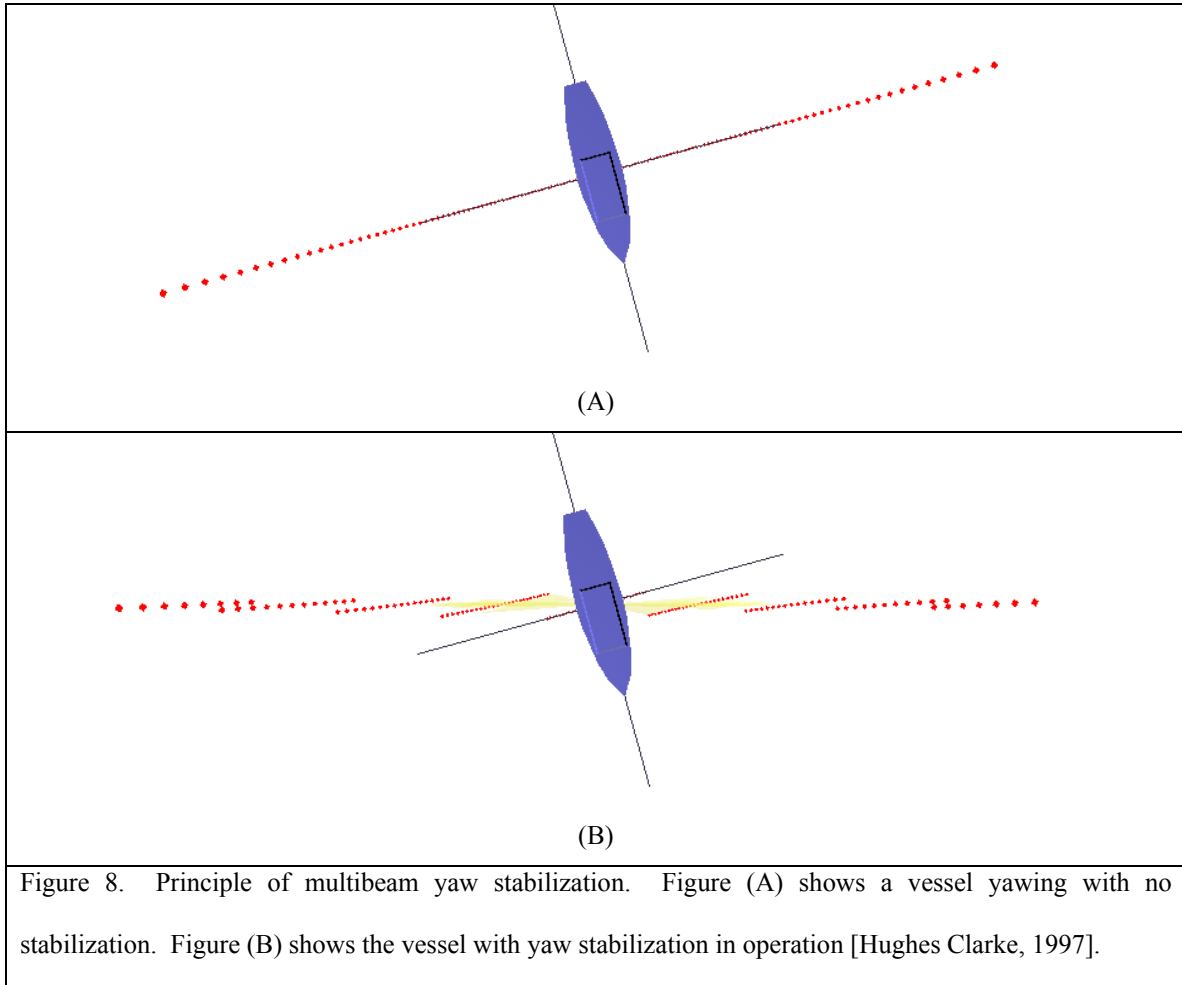


Figure 7. Multibeam beam vector shown as a product of transmit and receive beams with corresponding sidelobes. Figures (A) and (B) show transmit and receive beams steered  $11^\circ$  and  $33^\circ$ , respectively. The final beam vector is shown in Figure (C). Images from [Hughes Clarke, 2003].

Motion compensation is accomplished by beam steering in the along-track direction on transmit to compensate for pitch, and steering each receive channel in the across-track direction to compensate for roll.

Compensating for yawing of a vessel must be accomplished by some other method since it is not possible to twist or manipulate a swath in some way to account for changes of heading. In the case of the EM300, the swath instead is transmitted as multiple frequency-coded transmit sectors. Instead of firing one wave of acoustic energy across the entire desired angular swath as shown in Figure 7a, the system will fire 3 or 9 of them. The receive channels can differentiate the multiple sectors due to each sector's unique frequency, while the yawing motion of the boat is compensated for by pitch

steering each sector independently depending on the heading of the ship at the instant of transmit. In this way the swath can remain close to perpendicular to the course of the vessel, and is shown in Figures 8 and 9 [Hughes Clarke, 1997].



One drawback of using this frequency-coded multiple transmit sector method is that it limits the available bandwidth for each sector. The system has a maximum available bandwidth of 4 kHz which is required to be distributed over each transmit sector if yaw stabilization is used. The maximum available bandwidth for each transmit sector is therefore equal to the total array bandwidth divided by the number of fired sectors.

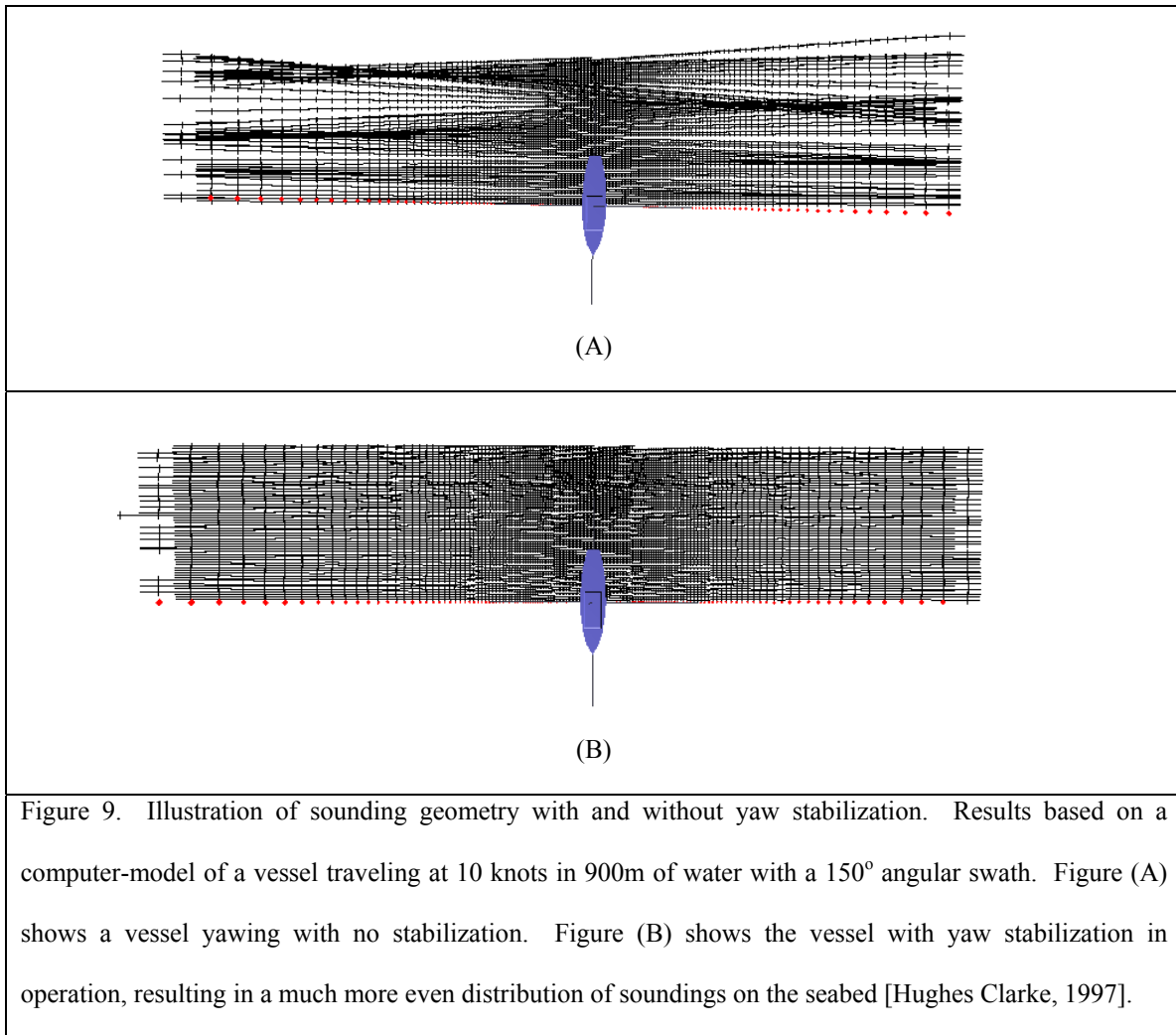
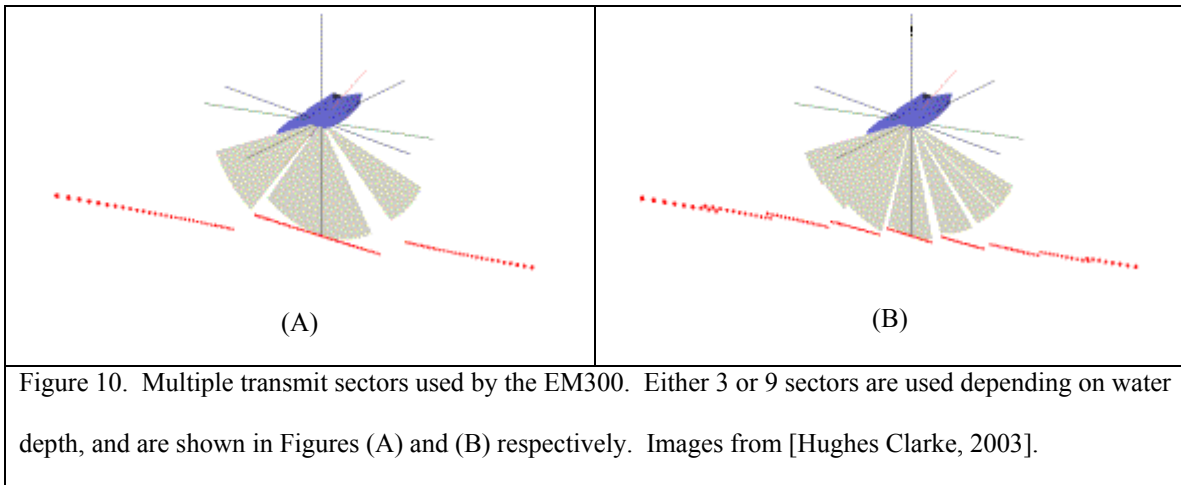


Figure 9. Illustration of sounding geometry with and without yaw stabilization. Results based on a computer-model of a vessel traveling at 10 knots in 900m of water with a 150° angular swath. Figure (A) shows a vessel yawing with no stabilization. Figure (B) shows the vessel with yaw stabilization in operation, resulting in a much more even distribution of soundings on the seabed [Hughes Clarke, 1997].

To accommodate a balance between range resolution and maximum compensation for vessel motion, the system will change the number of sectors it fires depending on the water depth. 3 sectors are used in shallow water (less than 500 meters) which will result in a higher bandwidth for each sector and hence maintain a finer depth resolution, while 9 sectors are fired in deep water (greater than 500 meters) to take advantage of the improved motion compensation. This is important as angular changes in beam steering at the water surface will result in greater differences in the positioning of soundings on the seabed with increasing water depth. In very deep water (below 3000

meters), the system reduces the number of sectors back to 3 as the angular swath is limited to  $\pm 18$  degrees due to attenuation through the water column. In this case the increased range resolution resulting from using fewer sectors once again outweighs the benefits of using 9-sector motion compensation. An illustration of the use of multiple transmit sectors is shown in Figure 10.



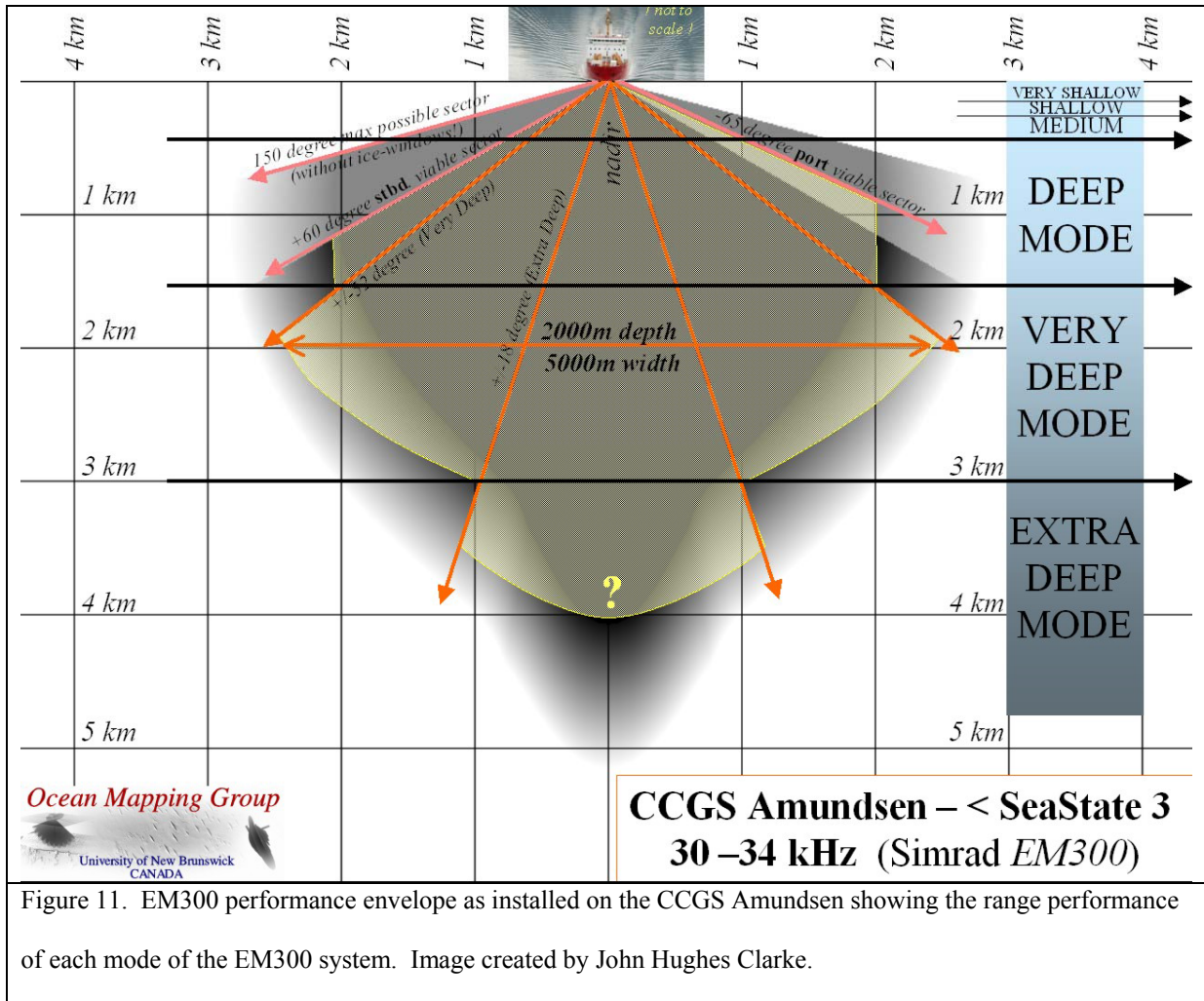
The system performs using 6 operational modes, with each mode controlling the characteristics of the swath depending on the water depth. The number of sectors fired, the acoustic pulse length, and angular sector will change with system mode. These details are shown in Table 1.

Table 1. Ping Modes of the EM300. From [Kongsberg-Simrad, 2002].

	<b>Very Shallow</b>	<b>Shallow</b>	<b>Medium</b>	<b>Deep</b>	<b>Very Deep</b>	<b>Extra Deep</b>
<b>Minimum Depth (m)</b>	5	30	100	500	1000	3000
<b>Maximum Depth (m)</b>	50	300	1000	3000	6000	6000
<b>Number of Sectors Fired</b>	3	3	3	9	9	3
<b>Pulse Length (ms)</b>	0.7	0.7	2	5	5	15
<b>Maximum Angular Sector (deg)</b>	+/- 75	+/- 75	+/- 75	+/- 75	+/- 52	+/- 18
<b>Minimum Beamwidth (deg)</b>	4	2	1	1	1	1

Figure 11 shows the performance envelope for the EM300 multibeam system as installed on the Amundsen. Each mode is shown along with its corresponding depth range and angular swath, as well as the 60°/65° maximum angular limitation due to the ice window installation geometry. At 30 kHz the system will begin to attenuate below 1000m causing a reduction in angular swath, although the declining signal-to-noise at depths greater than this caused by the ice window installation has typically caused operators to manually change modes to reduce the angular swath and increase pulse length to maintain consistent bottom tracking. Thus far the system has been tested in water depths up to 2600m with reasonable mapping capabilities shown in seastates less than 5. Beyond this depth the performance of the system is as yet untested. A full description of the deep water capabilities of the system can be found in Hughes Clarke et al., [2004].





### 3.4 Transmit Beam Pattern Ice Window Adjustments

Due to the presence of the ice window below the transducers, several calibration settings required altering from the default settings typically used for an EM300 system during the system installation. The parameters which required changing include multiple settings for each fired transmit sector. These settings include:

- 1) The acoustic beam strength
- 2) The across-track beam boresite pointing angle
- 3) The across-track beam width defined by its -3dB limits
- 4) The crossover angles indicating the boundaries between each transmit sector

This need for adjustment was predicted by Simrad, and updated calibration files were implemented in the system on board by OMG personnel and a representative of the Kongsberg-Simrad company during the initial shakedown cruise of the system in the fall of 2003. Appendix A documents both the default EM300 and Amundsen EM300 (as predicted by Simrad) calibration values for each transmit sector variable. Figure 12 shows examples of raw backscatter strength values obtained with the system.

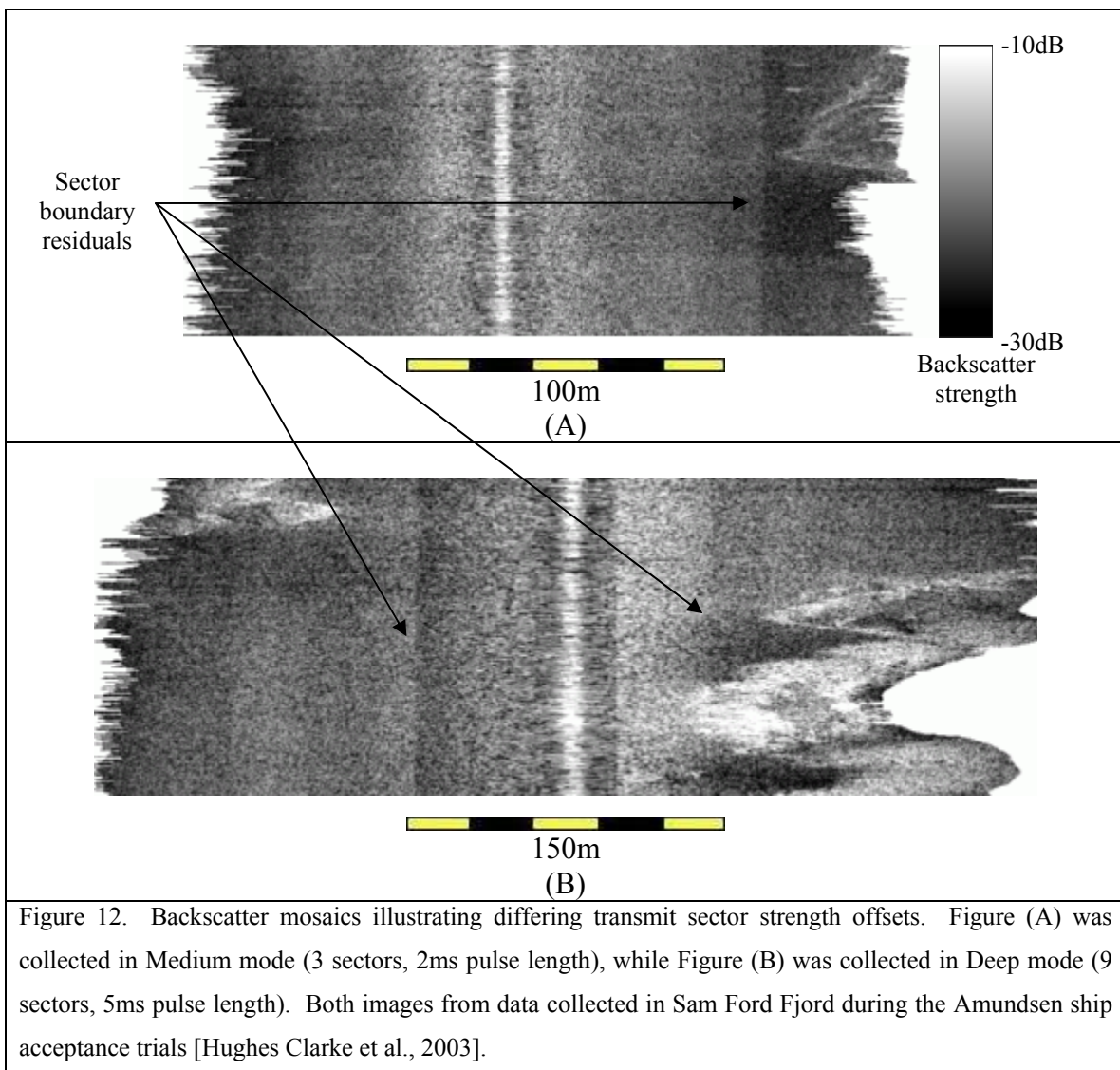


Figure 12. Backscatter mosaics illustrating differing transmit sector strength offsets. Figure (A) was collected in Medium mode (3 sectors, 2ms pulse length), while Figure (B) was collected in Deep mode (9 sectors, 5ms pulse length). Both images from data collected in Sam Ford Fjord during the Amundsen ship acceptance trials [Hughes Clarke et al., 2003].

By examining the images it is clear that each sector would benefit from further adjustment. Calibration trials to accomplish this could be planned, which would involve running repetitive lines over a patch of seafloor with all sector adjustments turned off, thus allowing precise sector intensity values to be determined. However, this would require substantially deep water, a very calm seastate to avoid bubble wash down and retain a high signal-to-noise ratio, and a flat, featureless seafloor. The multi-disciplinary nature of the science activities aboard the Amundsen, along with the typical tight timelines under which these activities are conducted, will most likely negate the possibility of running such trials under these conditions in the near future. As such, changes in sector boundary backscatter strengths are corrected for in post-processing, as will be discussed in detail in section 5 of this report.

## **4. MULTIBEAM BACKSCATTER OVERVIEW**

Two types of information are available from multibeam swath sonar systems. Bathymetry, or water depth, is in common use and is computed from the two-way-travel-time (TTWT), depression angle, and azimuth of each beam of the system through the water column. Of less common use is the backscatter information recorded by each beam. The strength of the return signal, or backscatter strength, is also computed and is used to gather information on the type of seafloor. It is the ratio of the intensity returned by the acoustic wave after traveling to the seafloor and back over the intensity of the wave which was initially transmitted by the transducer. This ratio can give you valuable information about the type of seafloor the vessel is surveying. This information is becoming increasingly important as the inclusion of backscatter products becomes more standard with commercial survey contracts.

The bottom backscatter strength of the seabed has a major impact on the strength of the return signal, however there are many other factors which will affect the strength of the returned signal. Most of these factors are accounted for automatically by Simrad systems and include:

- 1) Absorption coefficient of the water column
- 2) Incidence angle on the seabed
- 3) Acoustic spherical spreading
- 4) Ensonified area of the beam footprint

The use of seabed backscatter strength can be seen in the sonar equation, which represents the total performance of a system [Lurton, 2002]. These variables will affect

both the bottom-detection capability and the backscatter values returned by the sonar system (all measured in dB):

$$SN = SL - 2TL - NL + BTS + DI \quad (1)$$

where:

SN = Signal to noise ratio

SL = Source level (both transmit power and receive gain)

TL = Transmission loss

NL = Noise level

BTS = Bottom target (backscatter) strength

DI = Directivity index

The backscatter strength, or echo level (EL) of the system is the relative amount of energy reflected back by the seabed towards the sonar system. It is computed as the ratio of the return intensity over the transmit intensity of the acoustic wave:

$$EL = 10 \log \left( \frac{I_R}{I_T} \right) \quad (2)$$

The magnitude of the echo level is dependant on three factors: The source level (transmit and receive), transmission losses, and bottom target strength:

$$EL = SL - 2TL + BTS \quad (3)$$

The first variable, source level, is the intensity of the transmit and receive acoustic waves. The transmission loss and bottom target strength are computed by the system. Transmission loss is comprised of two elements: Spherical spreading and the absorption losses in the water column:

$$2TL = 40 \log R + 2\alpha R \quad (4)$$

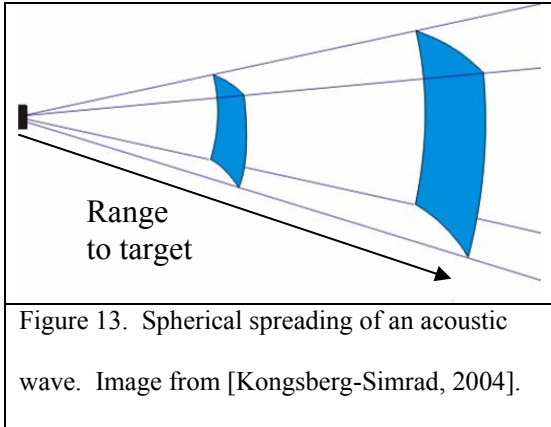


Figure 13. Spherical spreading of an acoustic wave. Image from [Kongsberg-Simrad, 2004].

Here  $R$  is the range to target, and  $\alpha$  is the absorption coefficient of the water column. Since the entire acoustic wave is radiated spherically from the transducer, the energy per unit area of the wave decays with  $1/R^2$  as shown in Figure 13. This is due to the

conservation of acoustic energy which is in effect transmitted onto a larger and larger surface as the wave is projected farther from the source, and is independent of transducer frequency. The energy from the seabed target will also be re-radiated spherically back to the source, therefore the total energy decay is [Hughes Clarke, 2003]:

$$\frac{1}{R^2} \times \frac{1}{R^2} = \frac{1}{R^4} \quad (-40 \log R \text{ expressed logarithmically}) \quad (5)$$

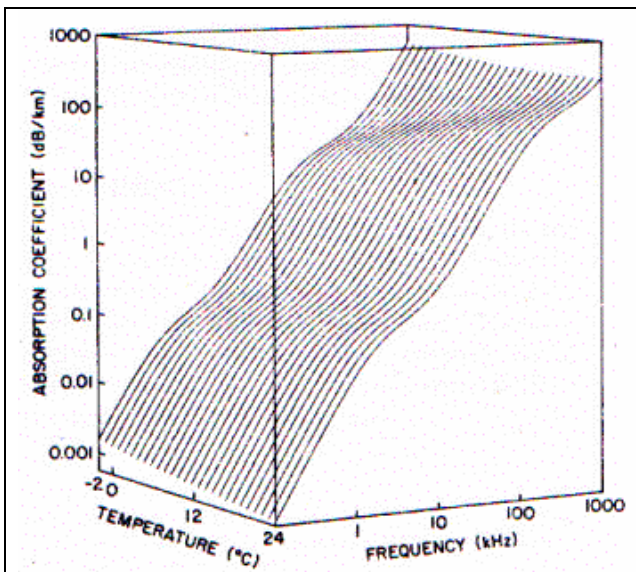


Figure 14. Temperature dependence for oceanic waters (34-36 ppt). Image from [Francois et al., 1982a].

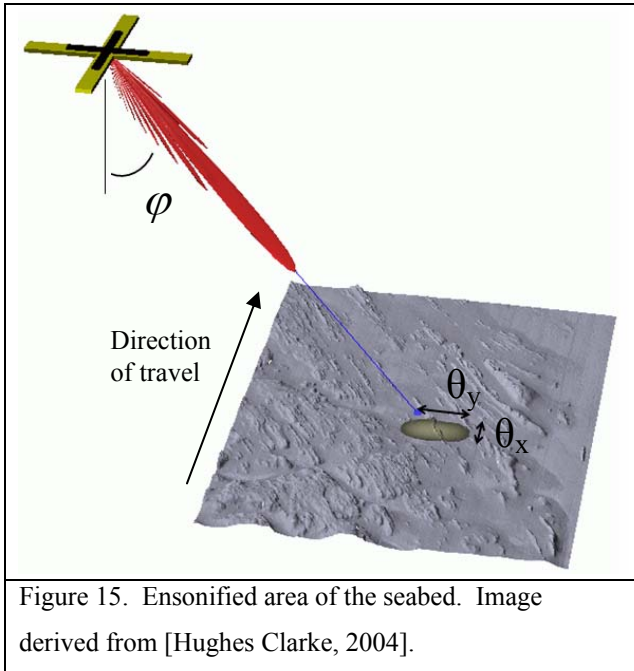
The absorption coefficient,  $\alpha$ , is the extinction rate of the acoustic wave due to absorption and scattering within the water column and is the dominating factor in acoustic propagation. As shown in Figure 14, this is highly dependant on the transducer frequency and water temperature. This acoustic dissipation

is caused by interactions with pure water at all frequencies, magnesium sulfate below 1MHz, as well as boric acid below 10kHz [Francois et al., 1982a,b]. The absorption

coefficient can be calculated if the temperature, salinity, depth, and pH value of the water are known.

The bottom target strength component is comprised of a backscattered area (BA) and a backscatter coefficient (BS):

$$BTS = BA + 10 \log(BS) \quad (6)$$



The backscattered area is the area instantaneously ensonified by the sonar system as shown in Figure 15. At normal incidence (incidence angle  $\phi$ , of 0 degrees) it is a function of the along and across-track beamwidths, while at other incidence angles it is a function of the along-track beamwidth, incidence angle, range to target, and pulse length [Hammerstad, 2000]:

$$BA = 10 \log \theta_x \theta_y R^2 \text{ for } \phi = 0^\circ \text{ (normal incidence)} \quad (7)$$

$$BA = 10 \log \frac{c\tau}{2 \sin \phi} \theta_x R \text{ for } \phi > 0^\circ \text{ (oblique incidence)} \quad (8)$$

where:

$c$  = Speed of sound in water

$\theta_x$  = Along-track beamwidth (measured in radians)

$\theta_y$  = Across-track beamwidth (measured in radians)

$R$  = Range to target

$\phi$  = Incidence Angle

$\tau$  = Pulse Length

Beams are considered to be at normal incidence as long as the receive steering angle is less than the larger of the following limits, where D is water depth:

$$\cos \theta_{L1} = \left(1 + \frac{c\tau}{2D}\right)^{-1} \quad (9)$$

$$\sin \theta_{L2} = -\frac{\theta_y D}{c\tau} + \sqrt{\left(\frac{\theta_y D}{c\tau}\right)^2 + 1} \quad (10)$$

Equation 9 ensures that the depth plus the  $c\tau/2$  term is less than the range to target, while equation 10 ensures that the across-track coverage on the seabed is larger when derived with the beamwidth rather than the pulse length [Hammerstad, 2005]. Note that here the incidence angle is measured as the angle between the beam vector and the vertical in the across-track direction. This is always the case with a Simrad multibeam due to the system's simplifying assumption that the seabed is flat. The true incidence angle on the seabed will depend on the changing orientation of the seabed.

The second component of the bottom target strength is the backscatter coefficient, which is dependant on the incidence angle and properties of the seabed. Simrad multibeam systems record the backscattered intensity time series of the seabed for each receive beam, which is then corrected to remove the effects of changing incidence angles, in addition to the other variables previously discussed. The reflected energy of the receive beams will be higher at low incidence angles, while it will be much less at high incidence angles as more of the acoustic energy will be reflected away from the transducer. Therefore beams with low incidence angles have their gains reduced by the system, while those with high incidence angles have their gain increased, in an effort to reduce the angular response signatures of each receive beam. The system accomplishes this by assuming that the bottom is flat and applying mean backscattering coefficients of



$BS_N$  and  $BS_O$  applied at angles of  $0^\circ$  and a set crossover angle. The backscattering coefficient is assumed to change linearly with angle from  $BS_N$  at  $0^\circ$  to  $BS_O$  at the crossover angle, and change according to Lambert's law at greater angles, as shown graphically in Figure 16:

$$BS = BS_O + 20 \log(\cos \varphi) \quad (11)$$

The crossover angle can be set by the sonar user based on knowledge of the type of seafloor, and has a default value set by Simrad of  $25^\circ$ . With a flat seafloor, an incidence angle of  $25^\circ$  is equivalent to  $R=1.1R_1$ , where  $R$  is the range to target and  $R_1$  is the range to normal incidence. With that in mind, the full model for the estimate of bottom target strength is given in equations 12-14 [Hammerstad, 2000].

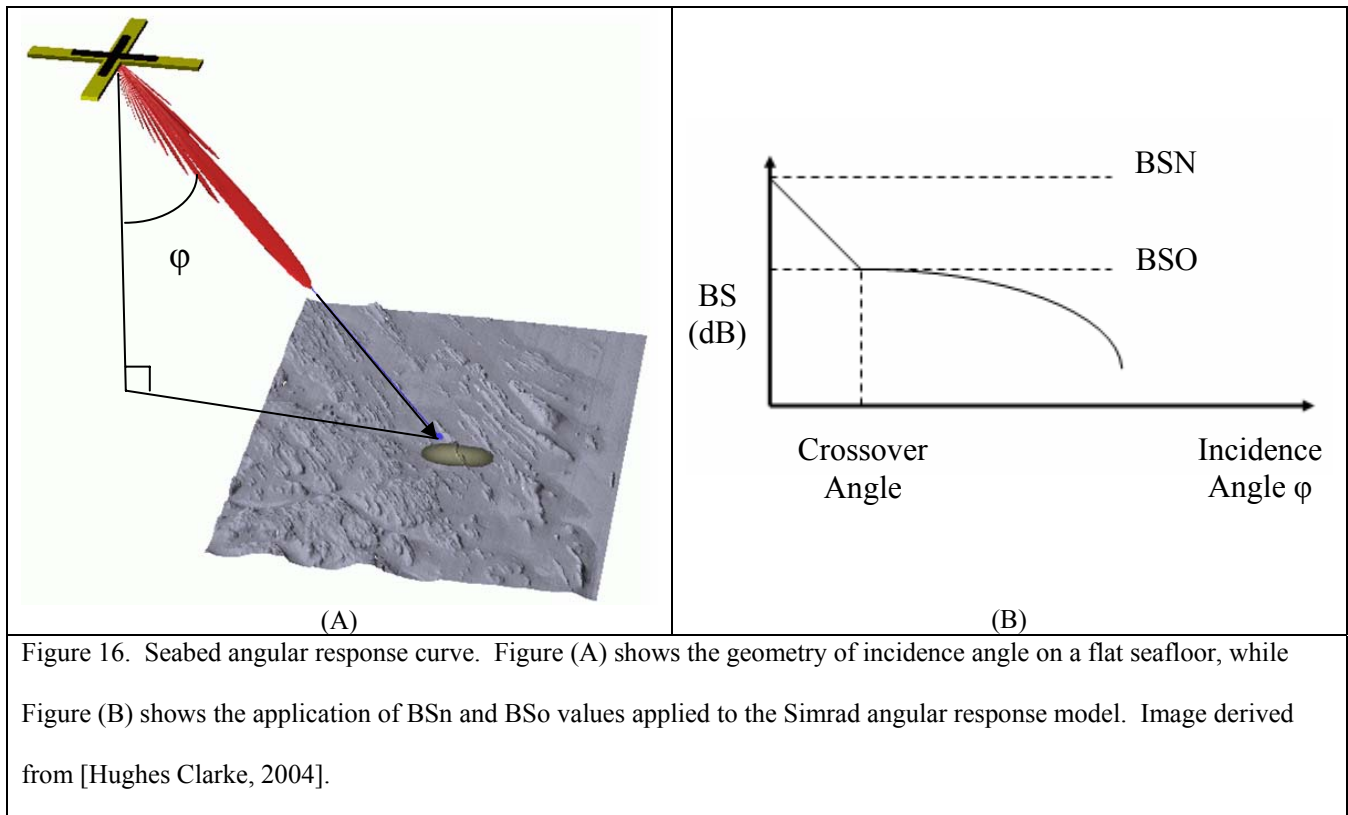


Figure 16. Seabed angular response curve. Figure (A) shows the geometry of incidence angle on a flat seafloor, while Figure (B) shows the application of  $BS_N$  and  $BS_O$  values applied to the Simrad angular response model. Image derived from [Hughes Clarke, 2004].

$$BTS = BS_N + 10 \log \theta_x \theta_y R^2 \text{ for } R \leq R_1 \text{ (before first arrival)} \quad (12)$$

$$BTS = BS_O - 5 \log \left( \frac{R}{R_1} \right)^2 \left[ \left( \frac{R}{R_1} \right)^2 - 1 \right] + 10 \log \frac{c\tau}{2} \theta_x R \text{ for } R \geq 1.1R_1 \text{ (lambert zone)} \quad (13)$$

$$BTS = BS_N + 3.62 \sqrt{R/R_1 - 1} (BS_O - BS_N) - 5 \log \left( \frac{R}{R_1} \right)^2 \left[ \left( \frac{R}{R_1} \right)^2 - 1 \right] + 10 \log \frac{c\tau}{2} \theta_x R \text{ for } R_1 < R \leq 1.1R_1 \text{ (linear near-nadir zone)} \quad (14)$$

This varying model for incidence angle correction is necessary as angular response curves differ for different types of seabeds. Since these curves often change while using the same sonar system, the values of  $BS_O$  and  $BS_N$  are computed by the Simrad system to best approximate the response curve based on the results of preceding pings. An illustration depicting theoretical response curves for different types of seafloor, as well as the end result of the application of the angular response model in equations 12-14 is shown in Figure 17.

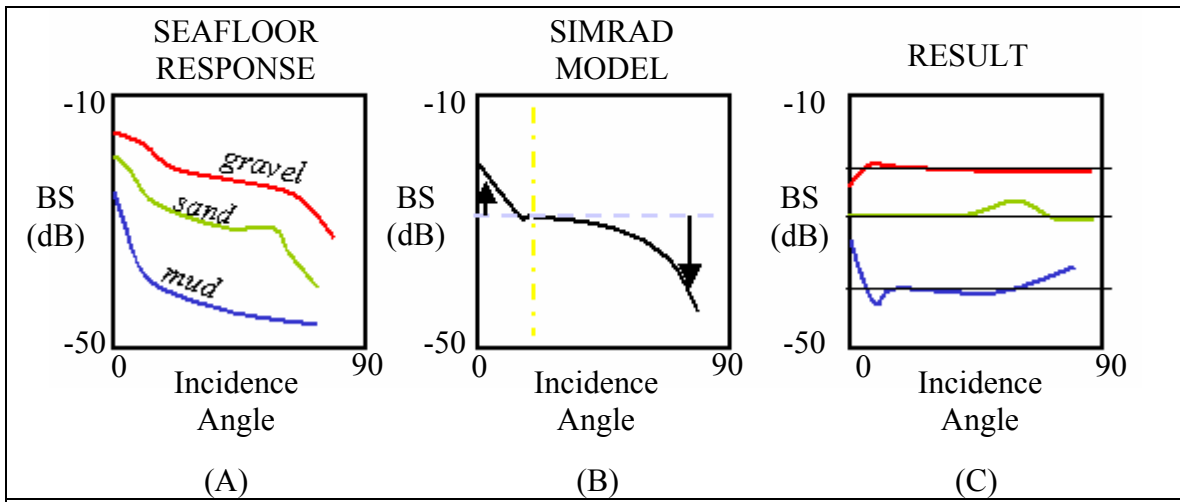


Figure 17. Simrad backscatter corrections for seafloor angular response. Figure (A) depicts the theoretical angular response curves for 3 different types of seafloor. Figure (B) shows the model which Simrad applies to the data. Figure (C) contains the end result of this process. Image derived from [Hughes Clarke, 2004].

## **5. CORRECTION SOFTWARE FOR BACKSCATTER BEAM PATTERN RESIDUALS**

As seen in the preceding section, the multibeam system automatically performs a significant amount of processing to properly reduce the backscatter intensities in the raw logged values. Even so, significant effects remain in the data which must be corrected for in post-processing to avoid having backscatter mosaics which reflect fluctuations in intensities due to sonar geometry rather than true geological changes along the seabed. These effects are generally a result of one or both of two things:

- 1) Angular response of the seabed. Despite the incidence angle normalization algorithm of the Simrad system, imperfect modeling of the seafloor angular response does occur. This algorithm will fail when the seafloor is not flat which the system assumes. As the seabed slope changes across the swath, the beam incidence angles will be changing as well. This will cause changes in the backscatter strengths which will be unaccounted for resulting in increases and decreases in apparent seabed reflectance which could be classified incorrectly as local geological changes. The algorithm will also fail when the theoretical model used by the system to correct for angular response in real-time is unable to account for all types of seabeds (some examples of which were shown in Figure 17a) which can and will change as the vessel steams. This effect is particularly noticed at nadir resulting in strong effects which follow the ship track lines.
- 2) Transducer beam pattern effects. Small yet significant fluctuations in acoustic intensity are generally present among groups of elements of the transducer array. These can be caused by differences in power amplification between each of the roll-stabilized beamforming channels, or by changes in the physical structure of

the transducer elements. The former case will result in vertically-referenced beam pattern effects (as was shown by the sector boundaries in Figure 12), while the latter will cause transducer-relative effects which can be seen to roll with the ship.

Software currently exists within the Ocean Mapping Group to adjust for these beam patterns on a line by line basis. The backscatter mosaicing software package is comprised of 2 separate software programs:

- 1) Beam pattern correction software to determine the required corrections for intensity fluctuations and incorrect angular response modeling.
- 2) Backscatter production software to mosaic the raw data. If the beam pattern correction software has been used then the corrections will be accounted for in this mosaicing process.

The EM300 system records multiple backscatter intensity values for each receive beam as a time series along the beam footprint, as shown in Figure 18. The number of individual values will increase with higher incidence angle as the beam footprints become larger in the across-track direction. At and near nadir it will typically record between one and twenty backscatter values per beam, while upwards to one hundred and above may be collected on the outer edges of the swath where the beam footprints are larger.

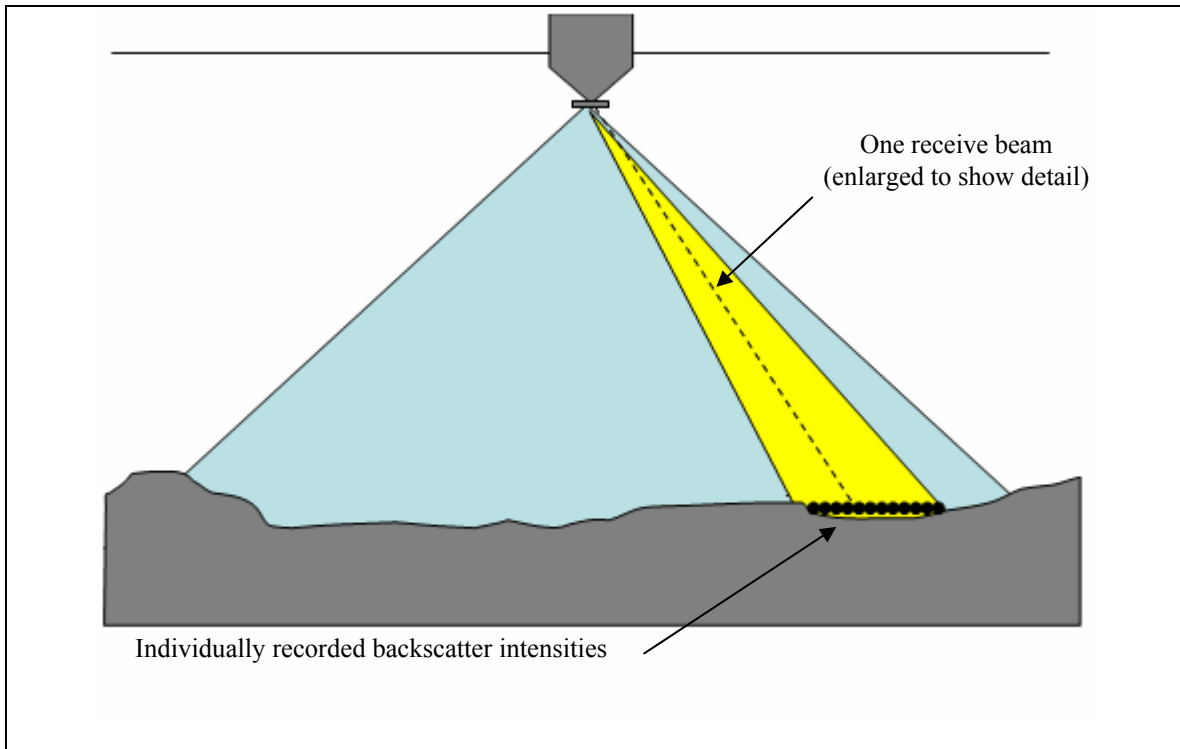


Figure 18. Illustration of multiple backscatter values recorded within the footprint of one beam of a Simrad multibeam system. Image derived from [Kongsberg-Simrad, 2004].

To correct for beam intensity fluctuations, the procedure is as follows:

- 1) Each individual backscatter value is summed for every beam of every ping for an entire logged line, with each beam classified according to its vertically-referenced launch angle below the vessel.
- 2) An average intensity value for each launch angle of the multibeam system is calculated.
- 3) The overall swath intensity is calculated by averaging the average values of each beam, excluding the beams at nadir as they will be most affected by angular response fluctuations.
- 4) The overall average of the swath is then compared to the averages for each launch angle.

The software creates a model of the residual beam pattern of the sonar system in the form of an array of 180 data bins comprised of the results for each launch angle, with one entry for each angle +/- 90° from nadir, rounded to the nearest degree. Each data structure contains the launch angle and its average intensity, the difference between that intensity and the overall averaged intensity for the entire swath, and the number of individual backscatter values used to compute the average value for that launch angle. The difference between the average for that angle and that of the entire swath is the correction factor needed which is passed on to the backscatter production software and included in the mosaicing process to remove the beam pattern effect caused by that deviation in acoustic intensity. A sample of data from a residual beam pattern model is shown in Table 2.

Table 2. Sample Data from a Typical Beam Pattern Structure.

BEAM LAUNCH ANGLE (deg)	AVERAGE BEAM INTENSITY (dB)	DIFFERENCE FROM ARRAY AVERAGE (dB)	NUMBER OF INTENSITY SAMPLES
0.0 .....			
22.0	-27.078682	-6.237802	15264
23.0	-28.196124	-5.120360	31220
24.0	-28.896974	-4.419510	46396
25.0	-29.844290	-3.472194	56602
26.0	-29.775912	-3.540572	57473
..... 180.0			

Shown in Figure 19 is an example of the apparent residual beam pattern from one line of multibeam data produced by the beam pattern correction software for the EM300 system as installed on the CCGS Amundsen. This residual beam pattern produced by the software is a product of the difference between the design and actual beam patterns for each transmit and receive beam, as well as the predicted and actual seabed angular

response curve. This survey line was run in 400m of water over a featureless seafloor on the continental shelf of the Beaufort Sea. It was logged in Medium mode, and was therefore operating with 3 transmit sectors. One can notice the distinct beam intensity fluctuations in the order of 5dB across the swath including the sharp change in response nadir.

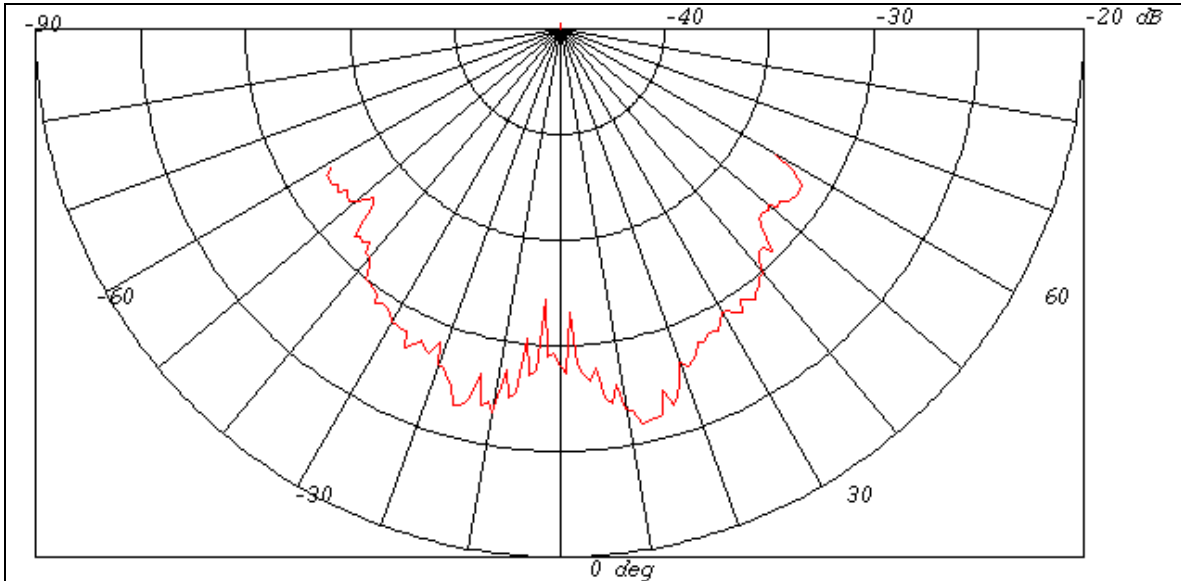


Figure 19. Residual beam pattern from the EM300 on the Amundsen as computed by the beam pattern correction software. Present are variations in beam pattern intensities across the swath, as well as imperfect angular response modeling as can be seen from the change in backscatter strength at nadir.

Figure 20 contains the backscatter information for which the residual beam pattern was shown in Figure 19, indicating the differences between mosaicing the raw backscatter data, the beam corrections which are applied, and mosaicing whilst including the needed intensity correction factors for each launch angle.

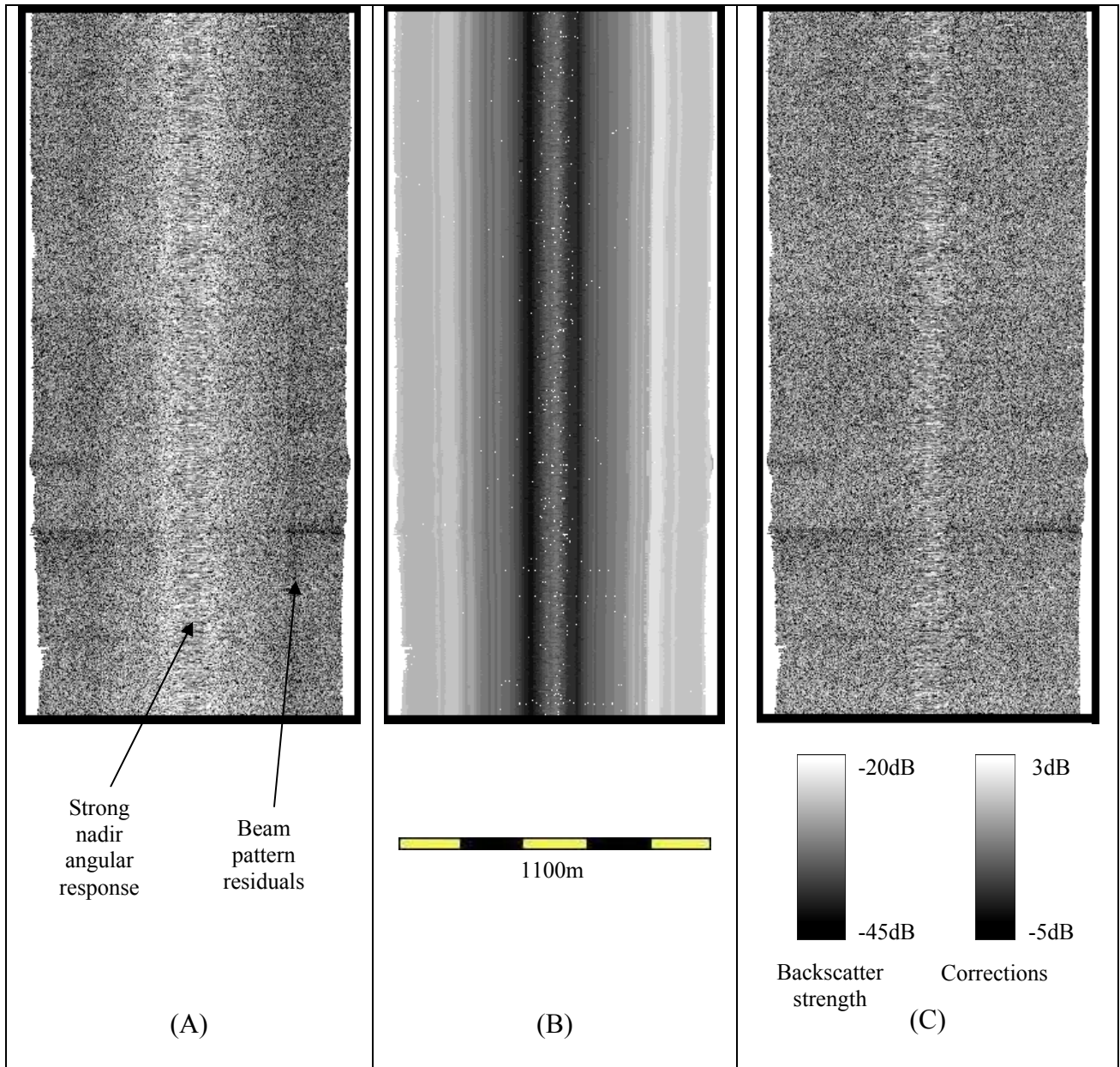


Figure 20. Differences of output from the OMG backscatter production software showing the importance of beam pattern corrections. Figure (A) depicts the raw backscatter from the Simrad system. Figure (B) shows the location and relative magnitude of the corrections applied. Figure (C) depicts the backscatter with corrections applied.

Several assumptions are made in the running of this software. Firstly, it must be understood that both angular response and sonar beam pattern effects are corrected for simultaneously. The program is statistical in nature and therefore does not distinguish between these two occurrences as it calculates the required corrections. It is designed in this way so



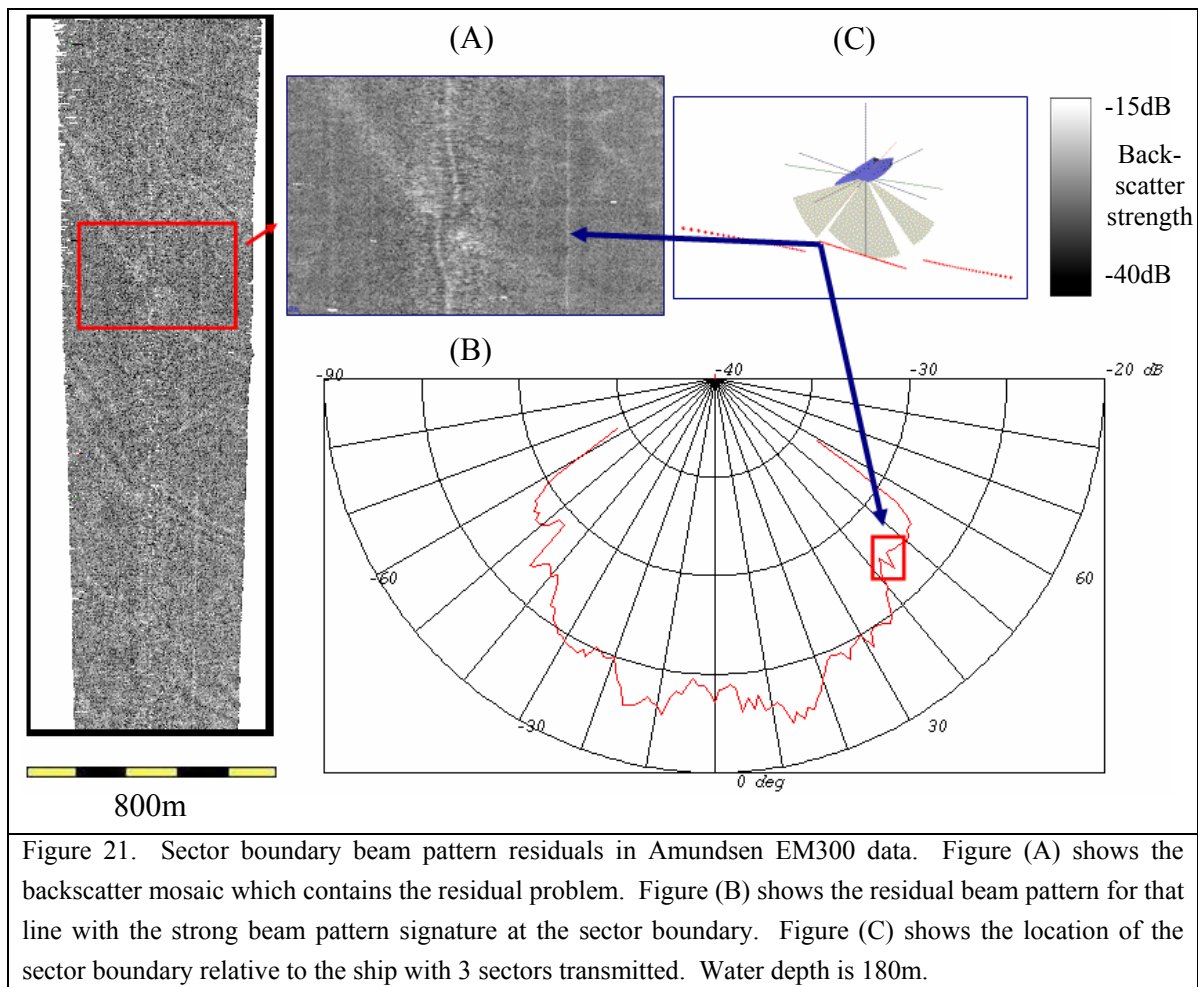
that it can function automatically for all types of sonars and all types of seabeds. The Ocean Mapping Group has undertaken developments for other functionalities of the software, and other types of research into angular response modeling, however they will not be discussed here.

While eliminating changing sonar intensities is almost always desired, visible angular response effects can actually give the user additional geological information regarding the seabed. Seafloor classification may in fact be aided by this type of backscatter data. As well, there is the possibility that the software will eliminate a real feature on the seabed. This would happen in the event of a feature such as rock outcrop which happens to run exactly parallel to the ship track for the entire length of the survey line. In such a case, the software would most likely identify it as a beam pattern anomaly and correct for it, therefore caution should be taken when running very short survey lines. That being said, lines are typically run over considerable distances and comprise thousands of pings, therefore the chances of encountering such a feature is unlikely, and local variations in geology will typically be preserved.

In practice, it has been found that most users prefer studying mosaics with these types of corrections applied. The choice to study either uncorrected or corrected backscatter images, or perhaps both for comparative purposes, is left to the user.

## 6. BACKSCATTER BEAM PATTERN ISSUES AND NEW SOFTWARE DEVELOPMENT SOLUTIONS

Despite the automatic calibration performed by Simrad on raw backscatter values, as well as the existing OMG beam pattern correction software, it was found that some additional beam pattern effects remained in the mosaics from the Amundsen EM300 data. These were in the form of straight lines which ran along the ship track on either side of nadir. They were not affected by any roll of the ship and therefore were an issue of vertically-referenced beam pattern residuals. The positions of these effects were constant relative to nadir and were clearly happening at the boundaries between each transmit sector. Figure 21 shows an image with this effect.



A multi-step solution was implemented to correct for these anomalies. This included:

- 1) Determination of the angular location of each sector boundary
- 2) Redefinition of the angular beam launch vectors computed in both the beam pattern correction and backscatter production software
- 3) Automation of the mode-intelligent features of the beam pattern correction software which produces residual beam pattern models for different pings modes of the system
- 4) Inter-beam interpolation on the produced beam pattern models to account for any beams to which a statistically low amount of data was attributed

Specifics on these steps are discussed in detail in the following sections.

## 6.1 Determination of Angular Sector Boundaries

It was evident that some additional software would be required to remove these visible beam pattern effects in the backscatter data. The first step in this process was to determine exactly where these vertically-referenced sector boundaries lie. In the newer Windows-based SIS Simrad software currently used on board the Amundsen by OMG, the transmit sector to which a beam belongs is logged in the raw data. However up until 2005, the UNIX-based version of the Simrad software was in use which does not record to which sector each beam belongs, therefore it must be calculated using other values which are known. The procedure used by OMG is such:

- 1) Determine the operational mode stored in the Runtime Parameters telegram.
- 2) Determine the sector angle for a given beam of a ping by using the depression angle stored in the depth telegram of the output Simrad file. It is calculated as:

$$\theta_{sector} = 90^{\circ} - \theta_{depression} \quad (15)$$

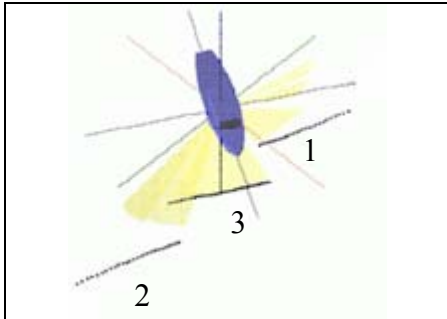


Figure 22. Sequential firing sequence of the EM300 multiple transmit sectors. Image derived from [Hughes Clarke, 2003].

This is performed with the depression angle being measured from the horizontal, and the sector angle being measured from nadir, with the port side being positive. With this information the appropriate sector can then be used for that beam. Each transmit sector is fired sequentially with the outer sectors fired first, as shown in Figure 22. Knowing the sector to

which a beam belongs allows for the proper transmit time to be used in accordance with the changing firing intervals of each sector. The convention used to determine depression and sector angles is shown in Figure 23.

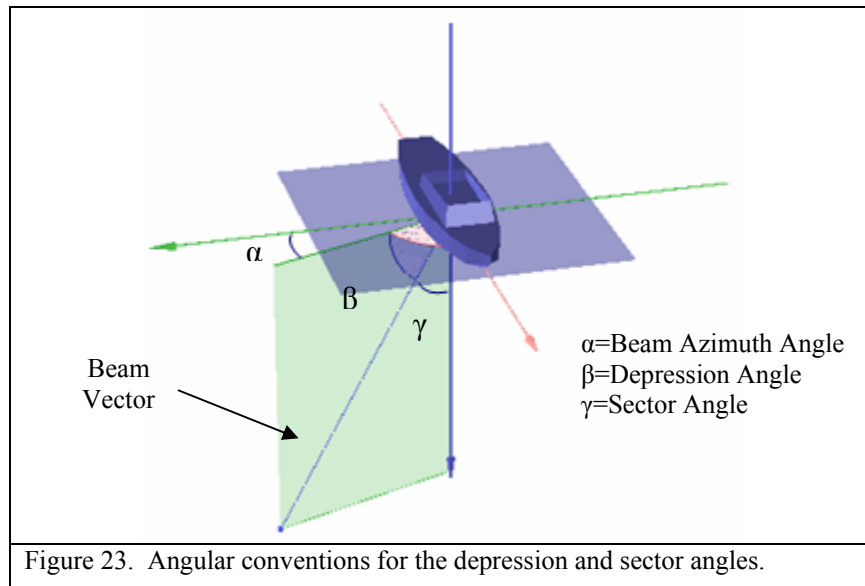


Figure 23. Angular conventions for the depression and sector angles.

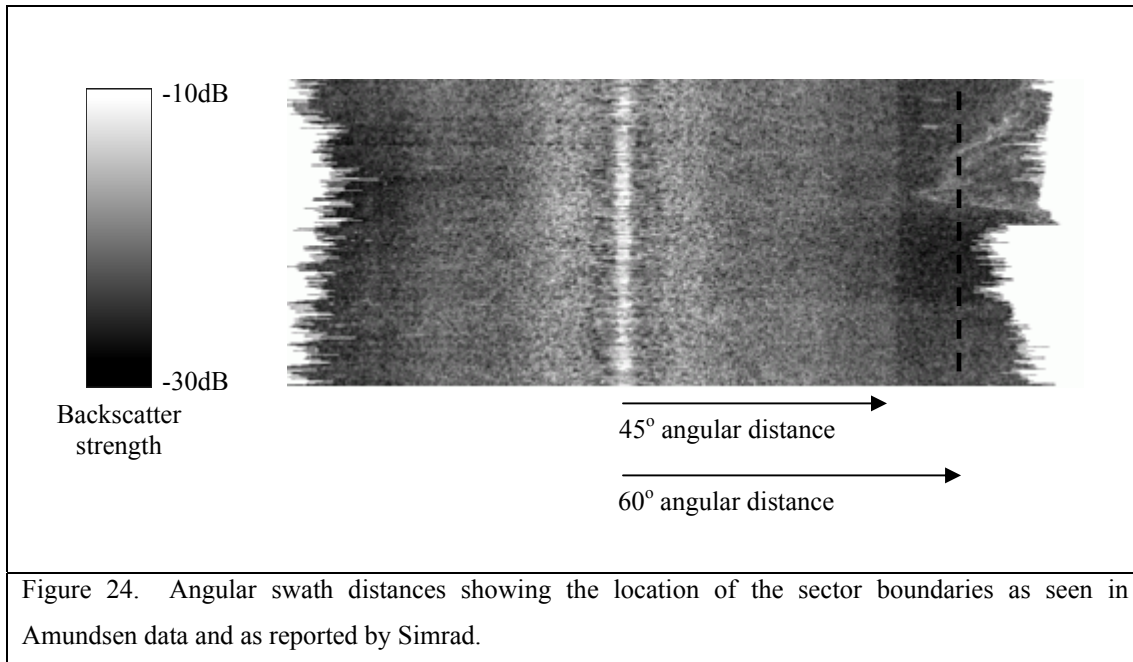
In the fall of 2003 on board the CCGS Amundsen, the Kongsberg Simrad engineer provided some information to OMG personnel describing the angular sector boundaries and firing intervals for the EM300. This is shown in Table 3.

Table 3. EM300 Sector Boundaries Provided to OMG by Kongsberg-Simrad.

Mode	Number of Sectors	Sector Boundaries (degrees) <i>positive=port, negative=starboard</i>	Sector Firing Interval (ms)
Extra-Deep	3	10.5, -10.5	15.51
Very-Deep	9	44,31.5,20.5,10.5 -10.0, -21.0, -31.5, -44.0	5.32
Deep	9	63.4, 44.7, 29.5, 18.4, -17.0, -31.0, -44.7, -63.5	5.32
Medium	3	60.0, -60.0	2.66
Shallow	3	60.0, -60.0	1.11
Very-Shallow	3	60.0, -60.0	1.11

Upon use of the system, it was clear however that these sector boundary angles were not accurate. This was evident in the post-processing stage, and was even noticed on board in the real-time Simrad Merlin display as pitch steering was occurring at angles vastly different from those contained in Table 3. Figure 24 shows a backscatter image in Medium mode of the system (3 sectors) with an obvious sector boundary approximately 45 degrees from nadir. This is shown along with the point which is approximately 60 degrees from nadir, the angular location which Simrad had declared to be where one of the sector boundaries lays for this mode of the system.

Since the operation of the EM300 transmit sectors was significantly different from what the manufacturer claimed it to be, an algorithm was designed to determine where exactly these boundaries lie. This information was paramount to this project, as well as other research happening at the time within OMG with the EM300 used aboard the Amundsen.



Since the sector information is not stored in the raw telegrams, the only way to determine that two adjacent beams belong to different transmit sectors is by examining the pitch steering angles. Since the sectors are independently pitch-steered to compensate for yawing of the survey vessel, any change in this value within the swath must be a change of sector. However, this does not happen for consistent beam numbers, nor do each beam on either side of a sector boundary have consistent sector angles, nor does the system constantly have changing pitch-steering angles within one swath, as it is only needed if there are sudden changes of heading while a survey line is being run.

What this means is that there is no guarantee that the determination of the actual sector boundary locations can be calculated by examining one line of multibeam data. What is known is that the sector boundary beam pattern residuals do occur consistently at a specific angle in the swath (as can be seen in Figure 24), therefore the real sector

boundaries must be a fixed vertically-referenced angular value. The procedure the algorithm uses to devise the true sector boundaries operates as such:

- 1) Determine the beam numbers before and after each pitch steering angle change for one ping from the system, if in fact at least one did occur. This information is taken from the raw range and angle telegram and indicates the presence of a sector boundary between those two beams.
- 2) The sector angles for the corresponding beams are then calculated using the depression angle from the depth telegram, indicating an angular window in which the sector boundary must lie.
- 3) This is then repeated for the next ping in the file. If another sector boundary is found the sector angles on either side of the boundary are calculated in the same way. If either sector angle is within the window determined from the previous ping, the window is then narrowed using the new sector angle as its boundary.
- 4) This process is repeated for all pings in hundreds of Simrad files to converge on all sector boundaries for all six modes of the system.

It was found that the average sector boundaries converged fairly well using this method. The accuracy of measurement for these values is one decimal place, and the process showed a mean standard deviation of 0.14 degrees between boundaries found for each individual line. The results of this are shown in Table 4.

Table 4. EM300 Sector Boundaries in Use on CCGS Amundsen as Calculated Using Sector Angle =  $90^\circ - \text{Depression Angle}$ .

Mode	Number of Sectors	Sector Boundaries (degrees) <i>positive=port, negative=starboard</i>
Extra-Deep	3	5.2, -5.1
Very-Deep	9	36.6, 23.1, 18.1, 5.0 -4.4, -16.2, -24.1, -34.0
Deep	9	53.1, 35.1, 27.1, 9.1 -8.0, -29.0, -36.0, -51.00
Medium	3	47.1, -44.0
Shallow	3	47.3, -43.9
Very Shallow	3	47.6, -43.6

Knowing these values for the angular sector boundaries, the process was then run again computing the sector angles using raw measurements. In lieu of formula (15) to determine the sector angle using the depression angle, it was calculated using measurements of the raw receive beams and transducer installation geometry rather than the final sounding solutions. These include the steering angle of the receive beam, the roll of the ship at the moment of receive, and the roll installation angle of the transducer, as shown in Figure 25 and equation 16:

$$\theta_{sector} = \theta_{steer} + \theta_{roll} + \theta_{installation} \quad (16)$$

where:

$\theta_{steer}$  = Transducer-relative receive steering angle

$\theta_{roll}$  = Horizon-relative vessel roll angle at moment of receive (equal to the angle between the gravity vertical and the transducer boresite)

$\theta_{installation}$  = Vessel-relative transducer installation angle



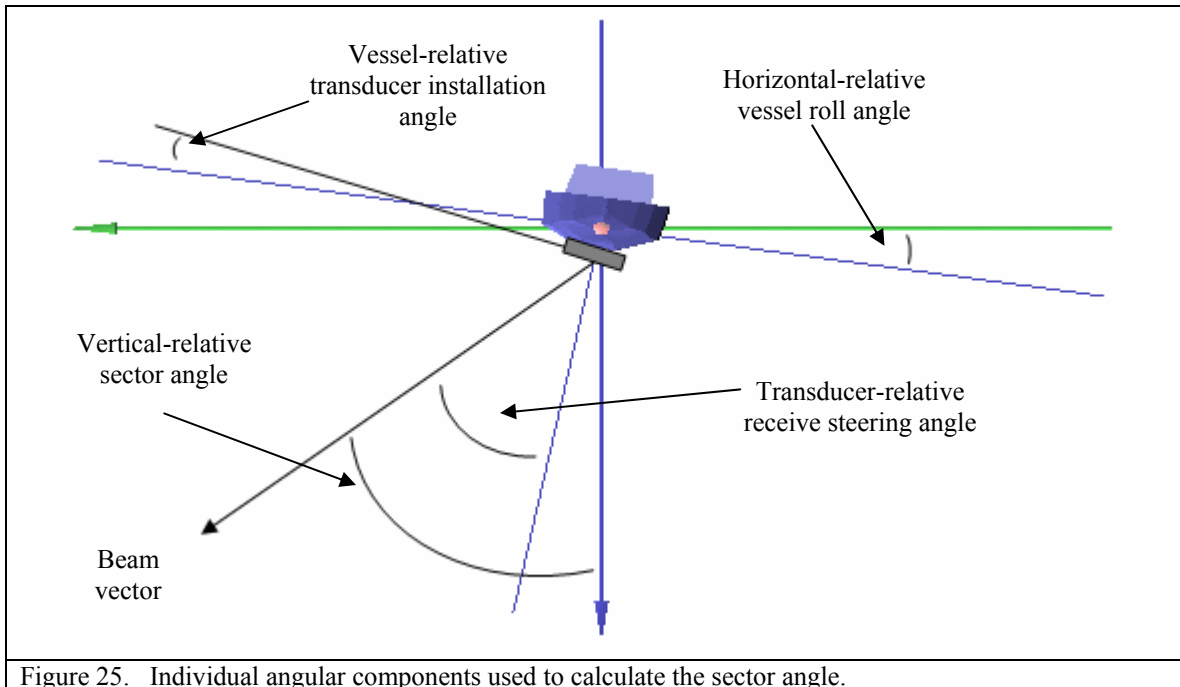


Figure 25. Individual angular components used to calculate the sector angle.

Here the roll of the ship at receive is calculated using an algorithm developed by Jonathan Beaudoin in the UNB Ocean Mapping Group. It uses the information from the attitude telegram contained within the raw data, at the precise moment of receive for that beam. This in turn is calculated using the initial ping transmit time, the two-way-travel time, and the appropriate time offset for whichever sector it belongs to.

$$T_{receive} = T_{initial\ ping\ time} + T_{sector\ offset} + TWTT \quad (17)$$

where:

$T_{initial\ ping\ time}$  = Time of first sector firing (logged in the raw Simrad telegrams)

$T_{sector\ offset}$  = Time delay caused by the interval between sector firing as outlined in Table 3.

TWTT = Two-way travel time of the beam.

The converging algorithm was run using the same approach as outlined above, using this new method of angle determination, and the sector boundaries converged exceptionally well, showing a mean standard deviation of 0.029 degrees between each line. The results using this method of sector angle determination proved to be more accurate as it more precisely matches the angular location of each receive beam in a 2-dimensional across track plane below the transducer. The depression angle is a fairly accurate estimation of this, however it is offset from this across-track plane by the azimuth angle of the beam vector as was shown in Figure 22, introducing a small yet noticeable error in the calculation. Table 5 shows the results with the new calculated sector boundaries.

Table 5. EM300 Sector Boundaries in Use by the System on CCGS Amundsen as Calculated Using Raw Angular Measurements.

Mode	Number of Sectors	Sector Boundaries (degrees) <i>positive=port, negative=starboard</i>
Extra Deep	3	5.0, -5.0
Very Deep	9	36.5, 23.0, 18.0, 5.0 -4.3, -16.2, -24.0, -34.0
Deep	9	53.0, 35.0, 27.0, 9.0 -8.0, -29.0, -36.0, -51.0
Medium	3	47.0, -44.0
Shallow	3	47.0, -44.0
Very-Shallow	3	47.0, -44.0

It is worthwhile to note here that this process was run for data with equidistant beam spacing. These boundaries have been found to change by a few degrees when switching to equiangular mode, however virtually no data has been collected while using this setting.

## 6.2 Redefinition of Launch Angles Using Raw Angle Determination

As mentioned earlier, the 2 steps undertaken with OMG software to process backscatter information are the beam pattern correction and backscatter production software. These are two independent computer programs, with the results of the former being used in the operation of the second to produce mosaics with the proper corrections applied. The cause of the beam pattern residuals becoming apparent in the mosaics was the method of launch angle determination used in both software programs. The launch angle is the exact angle at which a beam is received, measured from the horizon in a 2-dimensional vertically-referenced across-track plane directly underneath the survey vessel. This is equivalent to the sector angle discussed in the previous section, with the exception that this angle is measured from 0° through 180° starting from the starboard side, with a beam received parallel to the water surface on that side being 0°, at nadir being 90°, and so on. Traditionally OMG software has calculated this using the depth of a sounding less the draft of the vessel, and the sounding's across-track distance, as shown in equation 18.

$$\theta_{launch} = \text{atan}\left(\frac{D_{across}}{D_{depth} - D_{draft}}\right) \quad (18)$$

This calculation is used to transform the plane formed by the beam azimuth angle and depth, draft, and across-track distances to a 2-dimensional across-track plane. This transformation results in a fairly accurate but not perfect calculation of the true across-track plane launch angle. The reason for this is that it incorporates the full refracted beam ray path into the vector solution, whereas the launch angle is a simple one-dimensional measurement. This discrepancy causes the beam pattern correction software to model the beam pattern effects slightly inaccurately, resulting in residual effects being

left in the mosaics. These appear predominantly at the boundaries between each transmit sector as the presence of the protective ice window increases the contrast between sector intensity levels beyond those normally found in an EM300 system.

The solution to this is to redefine the definition of each beam launch angle in both the beam pattern correction software as well as the sidescan production software. This is accomplished using the receive steering angle, roll of the ship at receive, and transducer installation angle in the same way as described in section 6.1 using equations 14 and 15. Both methods of angle determination are shown in Figure 26.

When these launch angles are calculated in this fashion, the intensity effects for each beam are correctly modeled, resulting in the removal of these residual boundary effects. Figure 27 shows the processing of the backscatter mosaics using both methods of beam launch angle determination. Table B-1 in Appendix B shows the numerical differences between the two methods of angle determination for the beam pattern shown in the figure.

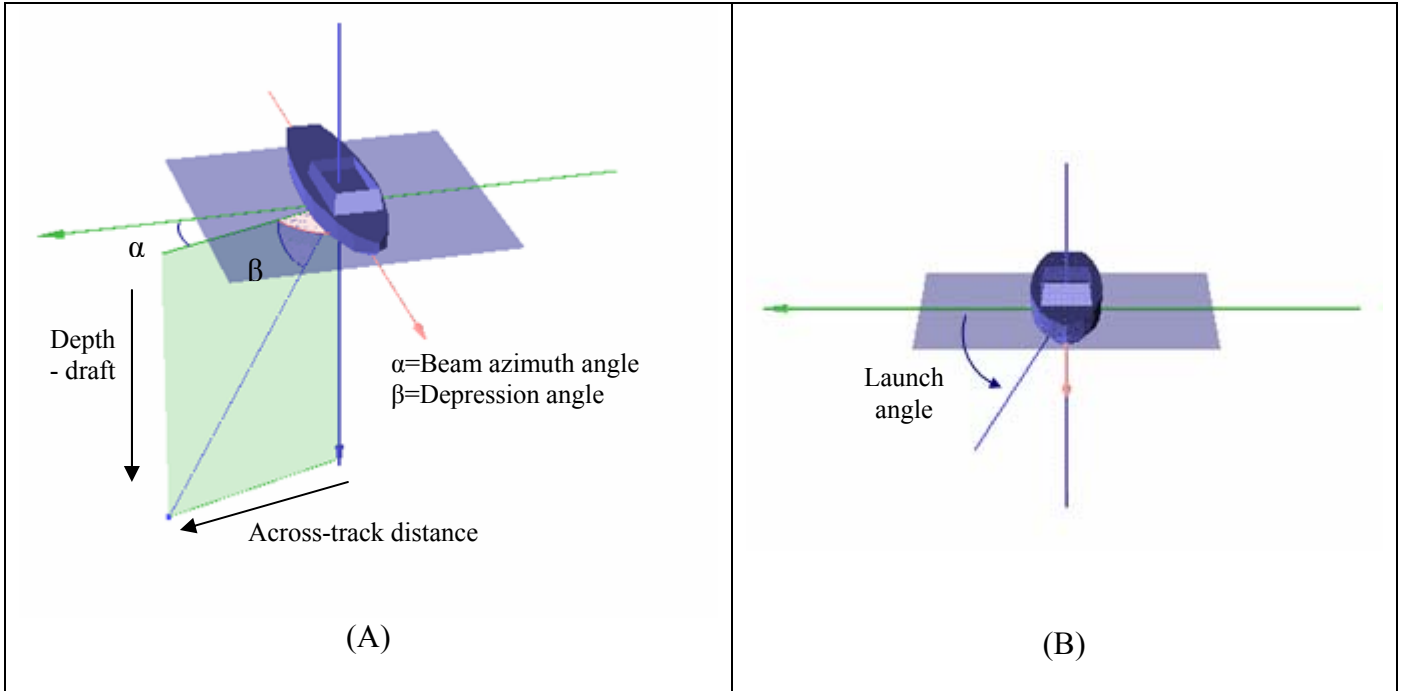


Figure 26. Differing methods of launch angle determination. Figure (A) shows the plane formed by the beam azimuth angle and depth and across-track distances which requires a transformation to reduce to the across-track plane. Figure (B) shows the true 2-dimensional across-track plane in which the launch angle is measured.

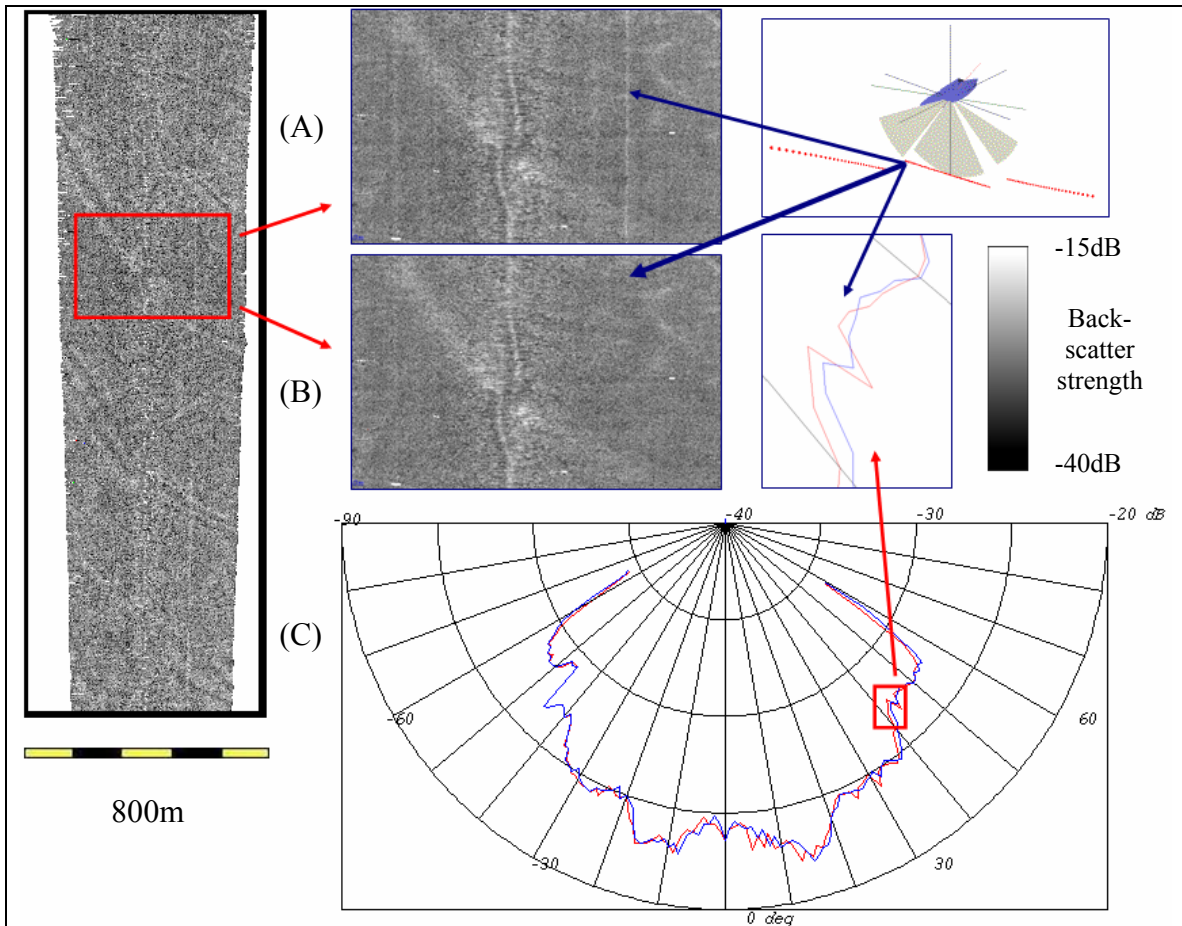


Figure 27. EM300 backscatter mosaiced using raw angle determination. Figures (A) and (B) show the mosaics before and after the sector boundaries residuals are removed. Figure (C) contains the residual beam patterns showing the difference between the beam patterns at the sector boundaries using the two types of angular determination. Here the red pattern shows the method of using the depth and across-track distance transformation, while the blue pattern shows the method of raw angle determination. One can see small yet frequent 1-2 dB shifts in beam pattern intensity between the two plots. Water depth is 180m, with a backscatter range of -15dB to -40dB.

### **6.3 Automatic Mode-Intelligent Beam Pattern Correction Software for Multi-Mode, Multi-Sector Multibeam Systems**

One additional problem with the beam pattern correction software being used by OMG personnel on the Amundsen was the fact that one residual beam pattern average was taken for each line of survey data. This method is acceptable as long as the beam pattern of the sonar does not change within the survey line. This sometimes is not the case with the use of a multi-mode, multi-sector multibeam system such as the EM300. As discussed in section 2.3, changes in water depth will cause the system to automatically change to a different operational mode. This can change the pulse length, angular swath, and number of sectors which are fired. This happens quite frequently between the Medium and Deep modes of the system as the depth ranges for the waters in which EM300 surveys often take place is within the depth ranges of the system which causes a change between those two modes. This mode change increases the number of sectors fired from 3 to 9, which in turn causes a significant change in the beam pattern output of the sonar system. Figure 28 shows an example of one line of survey data in which both the Medium (3 sector, 2ms pulse length), and Deep (9 sectors, 5ms pulse length) modes of the system were used, with the resulting changes in beam patterns. The data was collected from the EM300 system installed on the Research Vessel Thomas G. Thompson operated by the University of Washington. In this figure the residual beam patterns for each mode of the system are shown, as well as the line-averaged beam pattern residual calculated using the conventional beam pattern software. Table B-2 in Appendix B shows the numerical differences between these three beam pattern arrays.

If a line-averaged beam pattern model is applied to data in which several modes are present, not only will some beam pattern effects not be removed, but the software

may actually introduce new artificial beam pattern effects in the resulting mosaics as it will be applying corrections which do not apply to certain sections of the data. To correct for this, there is a mode-intelligent capability of the beam pattern correction software which can be used. The user tells the software which modes the system used during the course of the survey, which will create residual beam pattern models for each used mode of the system. These can be given automatically to the backscatter production software, which will apply the needed corrections to each corresponding section of the file which was operated in that mode. For example, if a file contains 500 pings in Medium mode (3 sectors, 2ms pulse length), and 500 pings in deep mode (9 sectors, 5ms pulse length), then 2 residual beam pattern models will be created, each corresponding to the appropriate section of that line. The required corrections will then be automatically applied in the backscatter production software, again for each corresponding section of the line. The software was upgraded for this project so that the user is not required to specify that the system operates with different ping modes, or which ones were in fact used during the survey. This enables the software to be used without requiring any knowledge of the sonar's mode of operation. Figure 29 shows the results of using this approach on the survey line shown in Figure 28 comprised of different system modes.



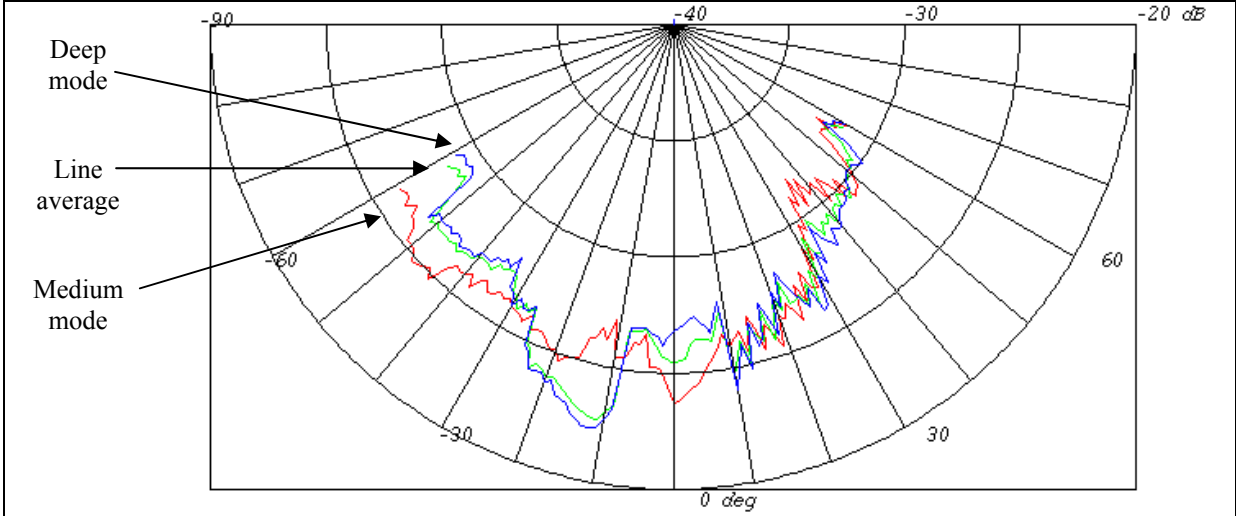
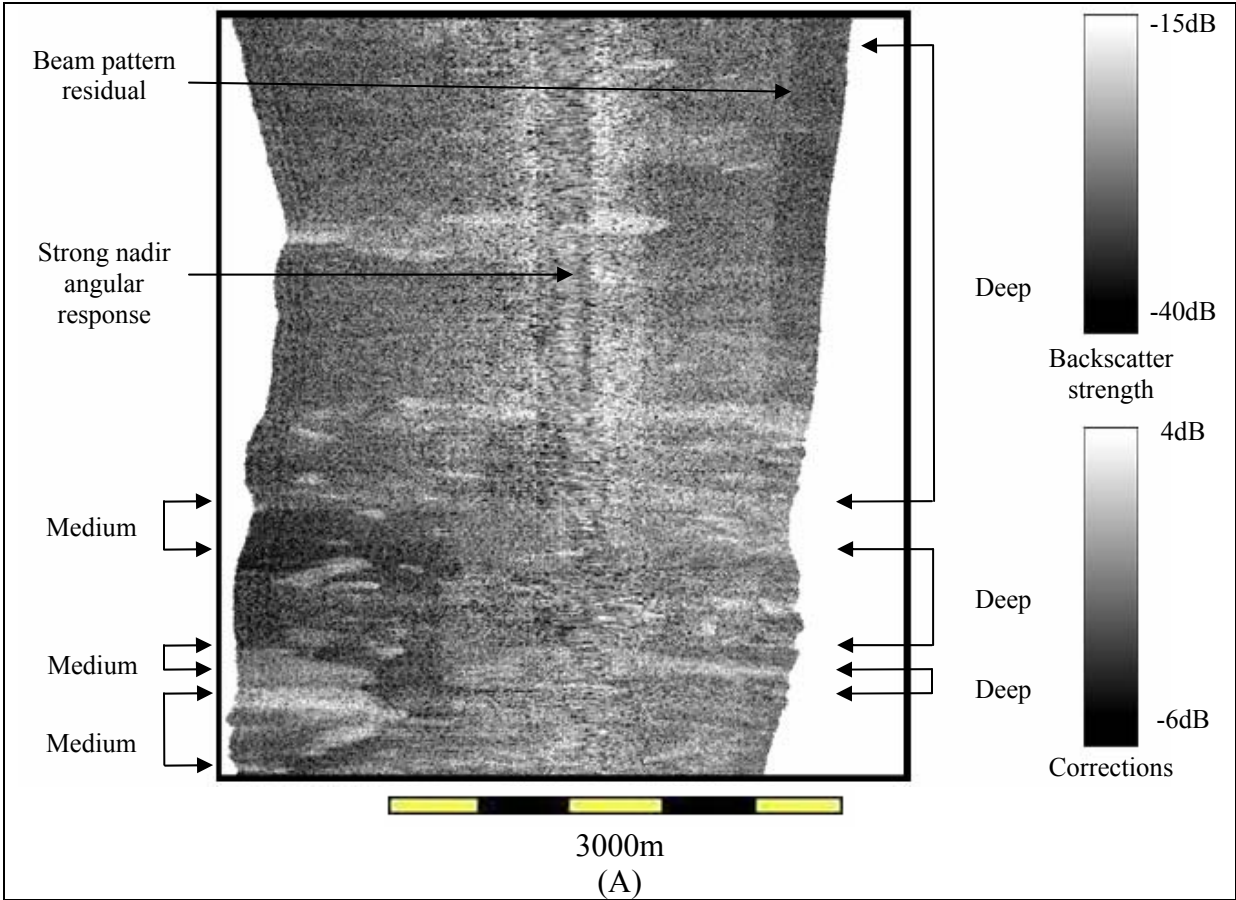
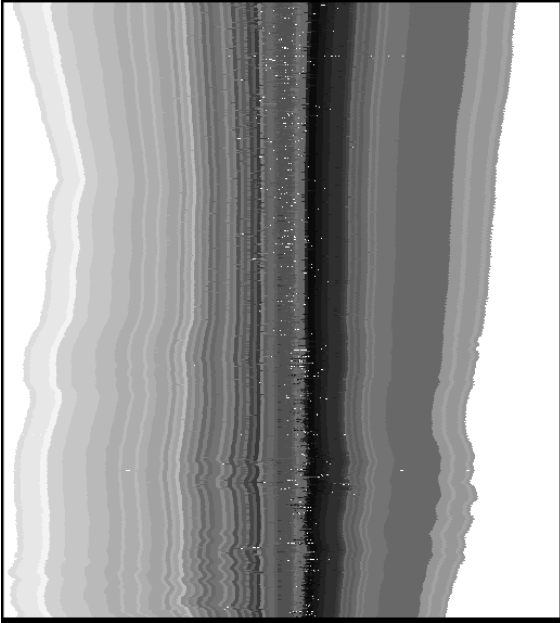
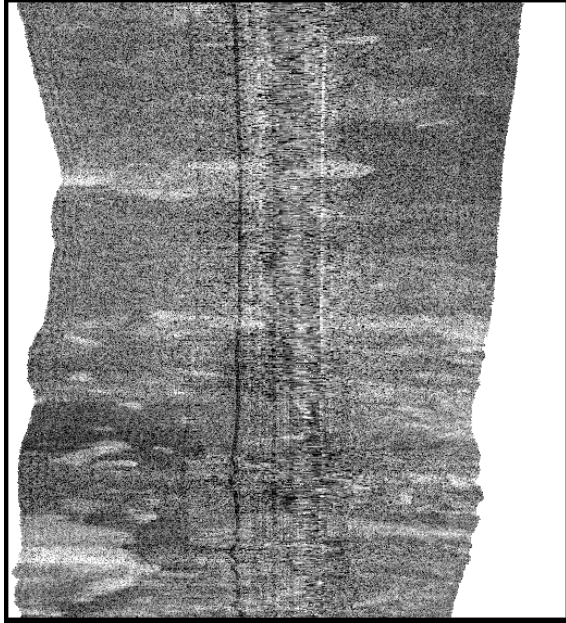


Figure 28. EM300 beam pattern residuals showing the effects of changing pulse length and the number of transmit sectors fired. Here the blue pattern shows the Deep mode, while the red pattern represents the Medium mode. The green line is the line-averaged pattern applied with conventional OMG beam pattern software. Frequent and large differences are visible in beam pattern intensity (up to 5dB) between the different patterns.

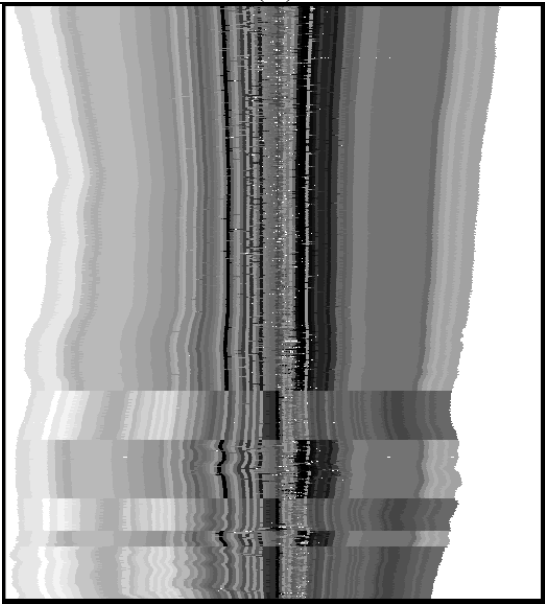




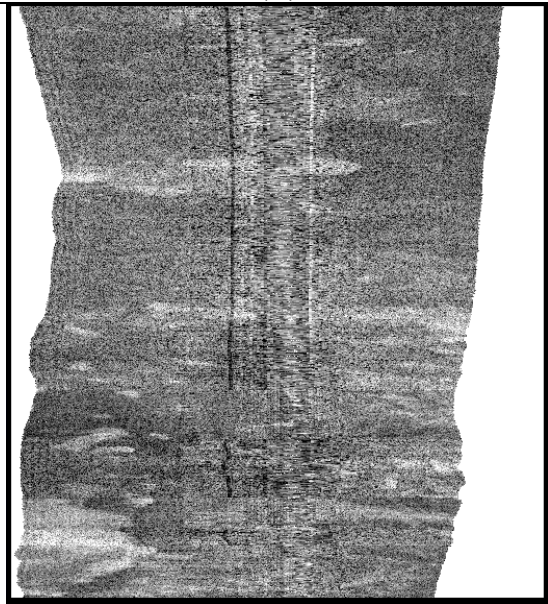
(B)



(C)



(D)



(E)

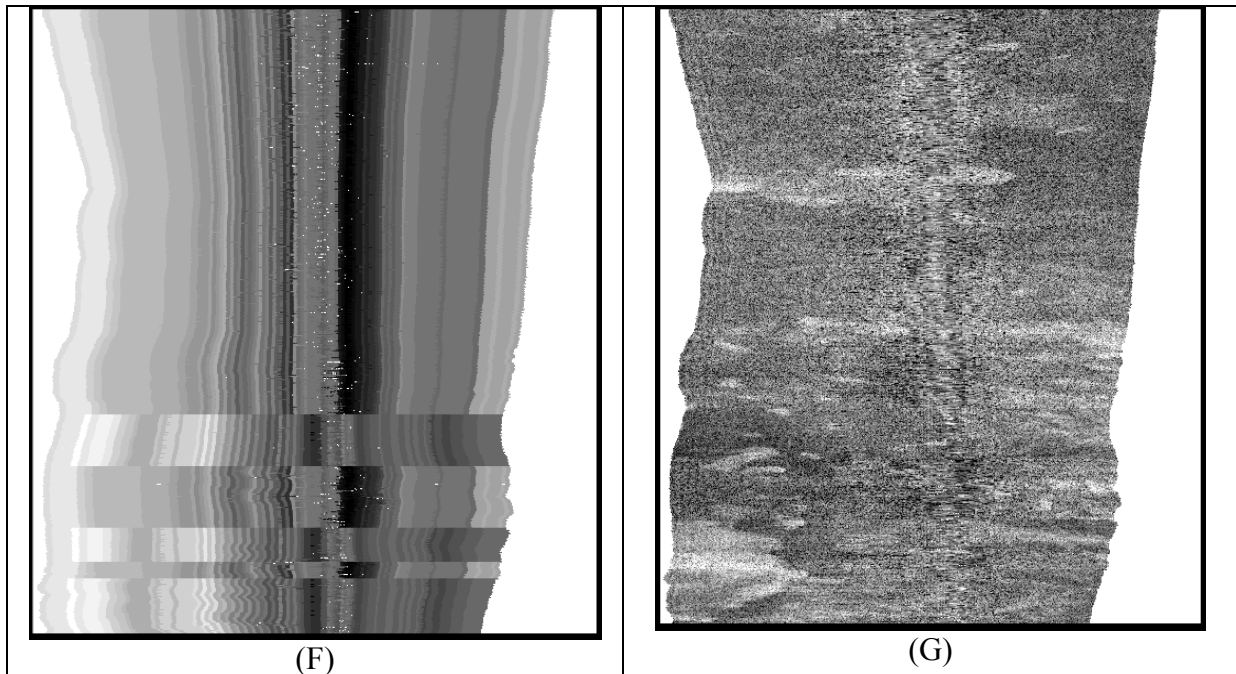


Figure 29. A line of EM300 backscatter mosaiced with multi-mode beam pattern corrections applied. Figure (A) shows the raw backscatter data and at what point which modes were used in the file. Figures (B) and (C) show the corrections and resulting mosaic with conventional OMG beam pattern corrections applied, while Figures (D) and (E) show the corrections and resulting mosaic with multi-mode beam pattern corrections applied. It is clear that neither of these methods is successful in removing all residual effects, and in both cases introduce new, artificial effects. Figures (F) and (G) show the corrections and resulting mosaic with multi-mode beam pattern corrections applied, also incorporating raw angle determination. This solution is finally successful in removing the residual beam pattern effects. Water depth is 850m.

To ensure that enough soundings are acquired within a certain mode to allow for sufficient statistical analysis of that specific mode's beam pattern, a minimum number of pings are required to be present in the file in order to create a valid beam pattern model. The default for this is 250 pings, however the user has the option to change this value if he or she so wishes. In addition to generating a residual beam pattern model for each mode of the system in a file, the software will generate an average beam pattern model for the entire file and apply the averaged result to any section of the line with a number of pings less than the required amount to generate its own model. For example, if a file

contains 300 pings in Shallow Mode, 800 pings in Medium Mode, and 25 pings in Deep mode, then beam pattern models will be created and applied to the Shallow and Medium modes, while a line-averaged model will be applied to the Deep mode.

One additional complication arises when processing the deeper modes of the system. Beam pattern statistics are generally acquired from beams excluding those at nadir, as they are generally most dominated by angular response effects. Beams with launch angles from  $25^{\circ}$  to  $65^{\circ}$  on each side of nadir are used, thus excluding the 25 degrees of beams on each side of nadir. However, the angular swath becomes narrower as water depth increases due to increasing attenuation of the outer beams. In Very Deep mode, the system pings at a maximum of  $\pm 52^{\circ}$  from nadir, which will decrease as water depth increases. In Extra Deep mode the system pings only  $\pm 18^{\circ}$  from nadir, completely within the exclusion window of the beams normally chosen to compute the beam pattern statistics. One additional functionality was included in the new software which will automatically recognize these modes being used. In Very Deep mode, the beams with launch angles from  $15^{\circ}$  through  $52^{\circ}$  on either side of nadir are used to compute the statistics. In Extra Deep mode, the beams with launch angles of  $5^{\circ}$  to  $15^{\circ}$  on either side of nadir are used to compute the statistics. This will allow for as much data as possible to be included in the creation of valid residual beam pattern model, while using the areas of the swath least affected by imperfect angular response modeling. Figure 30 shows the difference in beam patterns between Medium and Extra Deep modes, giving angular swaths of  $\pm 60^{\circ}$  and  $\pm 18^{\circ}$ , respectively.



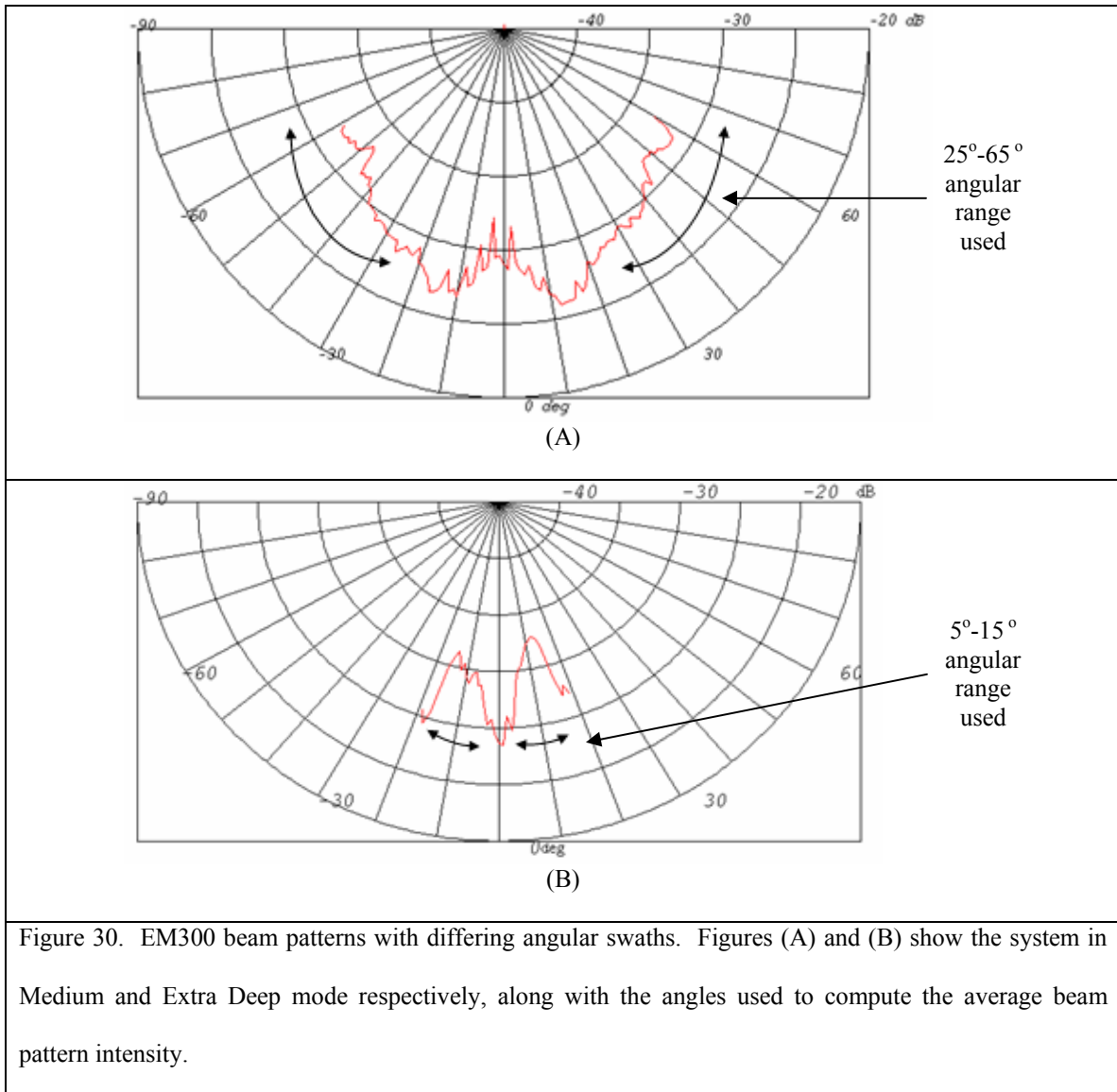
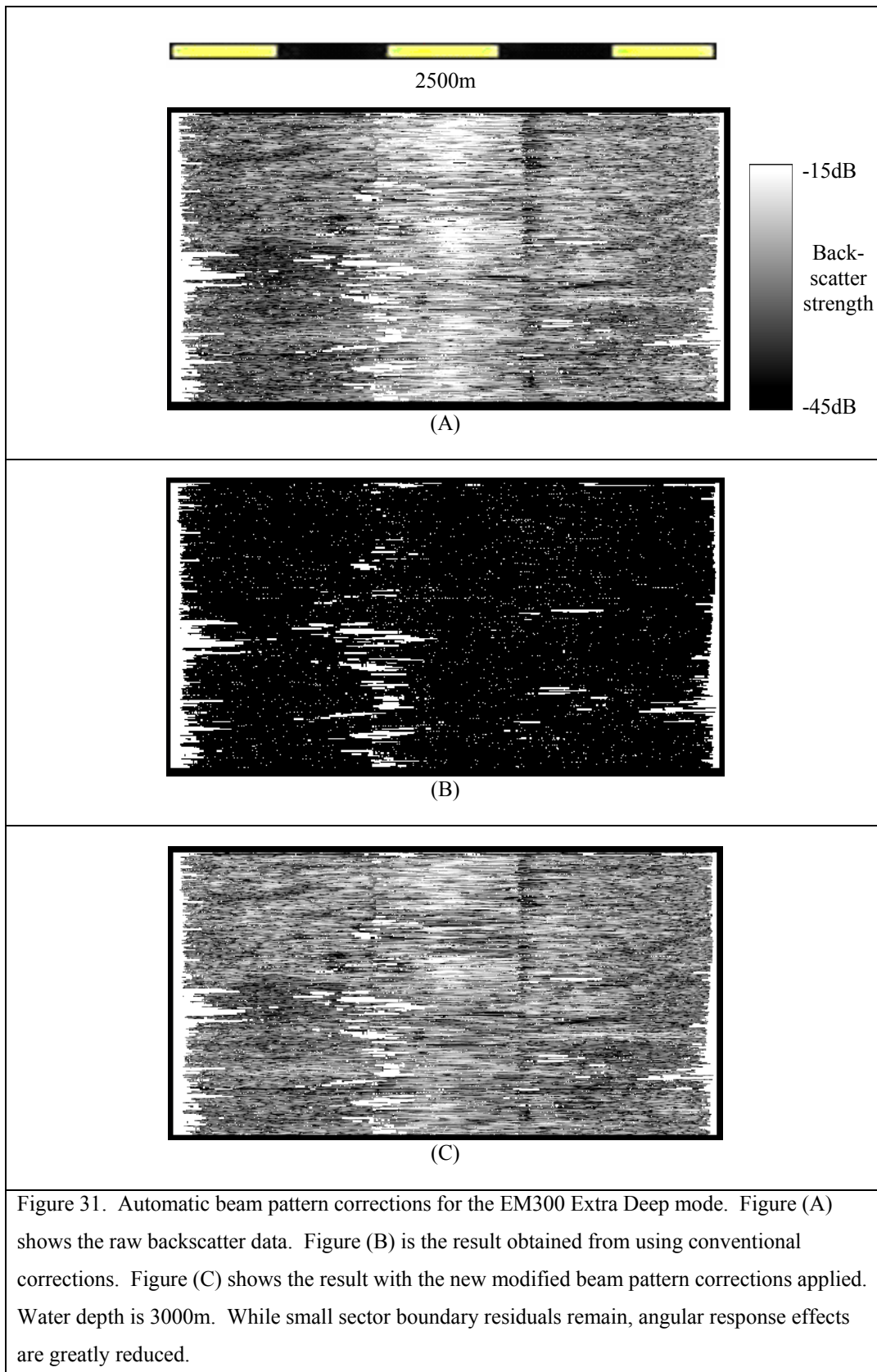


Figure 30. EM300 beam patterns with differing angular swaths. Figures (A) and (B) show the system in Medium and Extra Deep mode respectively, along with the angles used to compute the average beam pattern intensity.

Failure to provide any data for the beam pattern correction will result in null corrections being applied in the backscatter production software. This will cause this process to fail, resulting in a black, washed out mosaic. With this new automation in place, the system will correct for beam pattern residuals using an appropriate amount of the swath. This ensures that data is included in the computation of the statistics and provides improved results. An example of this issue in Extra Deep mode is shown in Figure 31.



## 6.4 Inter-Beam Interpolation Within Beam Pattern Models

Modeling the residual beam pattern of a multibeam sonar system is essentially a statistical algorithm based on the backscatter information recorded by each of the sonar's beams through the length of a survey line. Like all statistical programs, it is dependant on a sufficient amount of data given to it to report accurate results. As was outlined in section 5, all beam launch angles are rounded to the nearest degree during the beam intensity averaging process. These are stored as an array from 0 to 180 degrees, along with the appropriate average beam intensity values, as was shown in Table 2. Occasionally some of these array entries representing certain beam launch angles have little to no data given to them, caused when the sonar does not typically have a beam launch vector which will round to that particular degree. This can happen with any beam of the system, but more often with beams close to nadir, as the system is run in Equidistant mode. This means that all the beams are spread out at fixed intervals to keep inter-beam distances along the seabed equal. To accomplish this, the receive channels are spread out at a fairly large angular distance from one another at nadir, and become closer together towards the outer edges of the swath. This leaves smaller concentrations of beams close to nadir, and hence is more prone to some angular array entries with little or no data. This phenomenon is also more likely with short lines with a small number of pings, or with very noisy data where a large amount of data is cleaned and thus removed from the mosaic. An example of this type of noisy data can be seen in Table 6, showing a sample of the array entries from a line of EM300 data, taken from the Research Vessel Southern Surveyor operated in Australia by the Commonwealth Scientific and Industrial Research Organization. Entries from angles 85 through 90 inclusive are detailed, and it

can be seen that entries 86, 87, and 89 have few data samples present and subsequently report sudden, inaccurate jumps in beam intensity values. Figure 32 shows the residual beam pattern displayed graphically to highlight the beam pattern irregularities for the entire file.

Table 6. Sample Data from a Beam Pattern Structure Resulting from Using Conventional OMG Beam Pattern Correction Software.

BEAM LAUNCH ANGLE	AVERAGE BEAM INTENSITY	DIFFERENCE FROM ARRAY AVERAGE	NUMBER OF INTENSITY SAMPLES
0.0 .....			
85.0	-30.525243	1.274274	4536
86.0	-24.290909	-4.960059	55
87.0	-26.868932	-2.382037	103
88.0	-31.051901	1.800932	3025
89.0	-23.013514	-6.237455	37
90.0	-29.910054	0.659086	2029
..... 180.0			

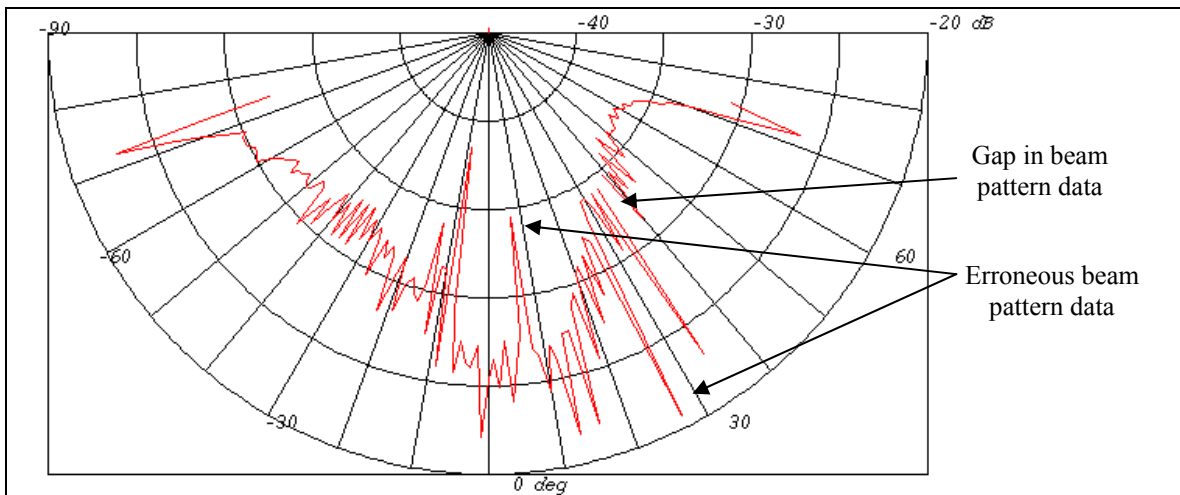


Figure 32. EM300 beam pattern with missing and artificial beam pattern data. This is the pattern for the file shown in Table 6, indicating artificial beam pattern effects due to a statistically low number of backscatter averages used to compute an overall beam intensity.



To account for this problem, additional software was written which can be run on the beam pattern model data structure created by the beam pattern correction software.

The algorithm performs the following functions:

- 1) The entire array of beam pattern average intensities is scanned and the average number of samples for all the angular entries is calculated.
- 2) A minimum number of samples threshold value is calculated as 15% of the average number of samples per entry.
- 3) Those entries with zero or less than the threshold number of samples are flagged.
- 4) For each flagged entry with zero data samples, the entries directly before and after it are examined. If both these entries are not flagged, it will average the two of them and use this new value for that entry. If only one of them is not flagged, it will adopt that entry's statistics exclusively. If the entries on either side are flagged but contain a non-zero number of samples, then it will adopt whichever one contains the greater number of samples.
- 5) For each flagged entry with a non-zero number of data samples, the entries directly before and after it are once again examined. Again if both these entries are not flagged, it will average the two of them and use this new value for that entry. If only one of them is not flagged, it will adopt those entry's statistics exclusively. It will adopt the same logic if the entries on either side are flagged, providing the entry(ies) contain(s) at least twice the number of data samples, indicating an improved statistical result.

The results for this process are displayed in Table 7. The entire contents of the beam pattern array including all entries from 0 through 180 degrees can be found in Appendix B in Table B-3. A graphical display of the interpolated beam patterns can be seen in Figure 33.

Table 7. Sample Data from a Beam Pattern Structure Resulting from Using Inter-Beam Interpolated Beam Pattern Correction Software.

BEAM LAUNCH ANGLE	AVERAGE BEAM INTENSITY	DIFFERENCE FROM ARRAY AVERAGE	NUMBER OF INTENSITY SAMPLES
0.0 .....			
85.0	-30.525244	1.274274	4536
86.0	-30.525244	1.274274	4536
87.0	-31.051901	1.800932	3025
88.0	-31.051901	1.800932	3025
89.0	-30.480976	1.230009	2527
90.0	-29.910053	0.659086	2029
..... 180.0			

In this case the values for launch angles 86, 87, and 89 were altered. Entries 86 and 87 were modified by adopting the intensities from the beams before and after them. The entry for beam 89 was altered by averaging between the beams before and after it.

Failure to correct for these small spikes in the beam pattern models may result in artificial beam patterns appearing in the mosaics. Figure 34 shows the results of this method.

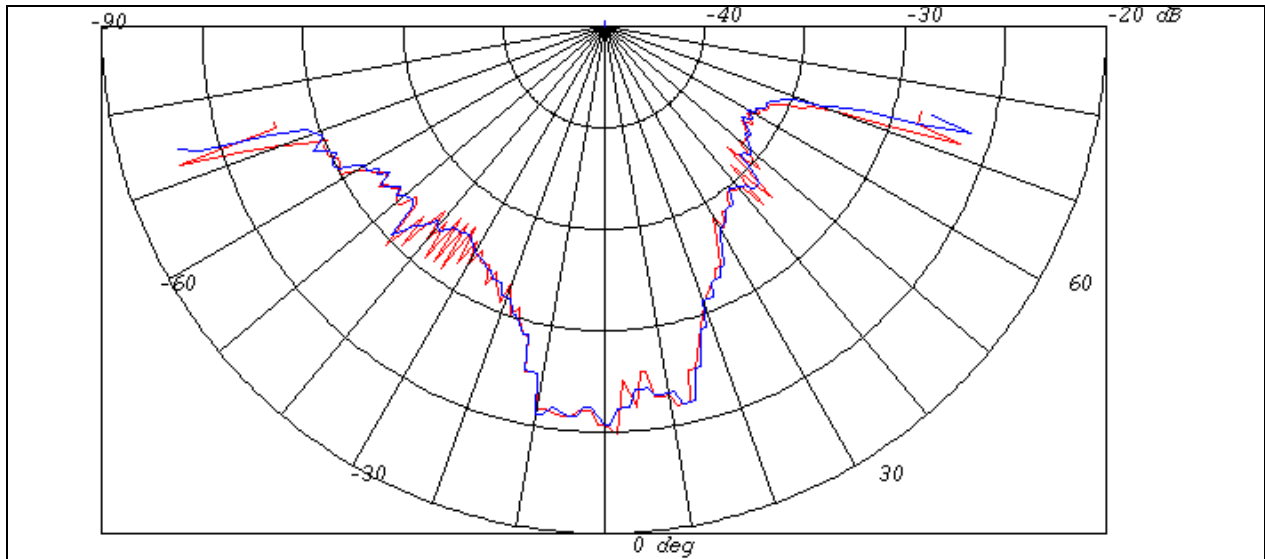
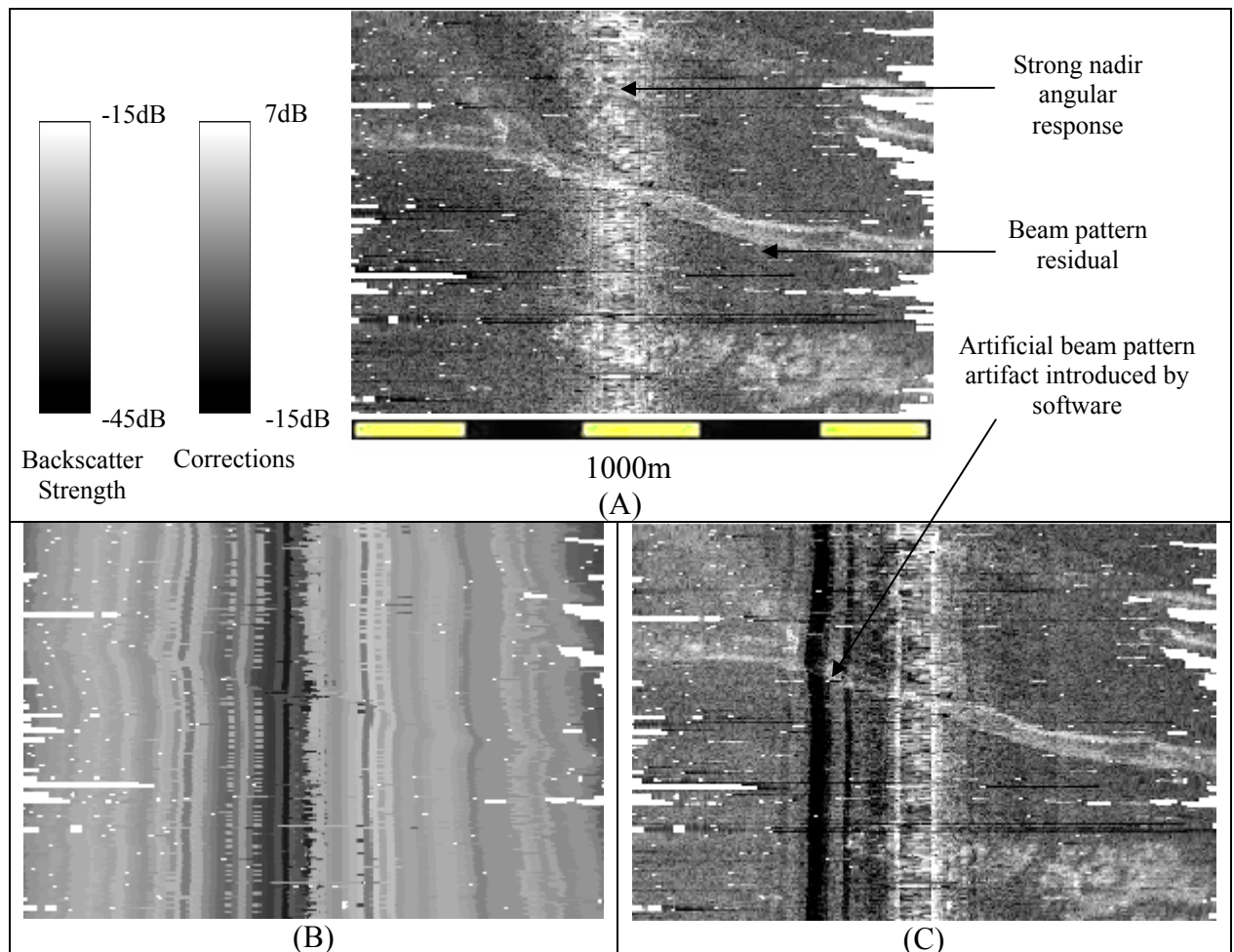


Figure 33. EM300 residual beam pattern with inter-beam interpolation. This red pattern represents the entire beam pattern for the file shown in Table 7, with the artificial beam patterns removed. The blue pattern shows the same pattern as processed using raw angle determination.



Backscatter Strength  
 Corrections

Strong nadir angular response

Beam pattern residual

Artificial beam pattern artifact introduced by software

1000m

(A)

(B)

(C)

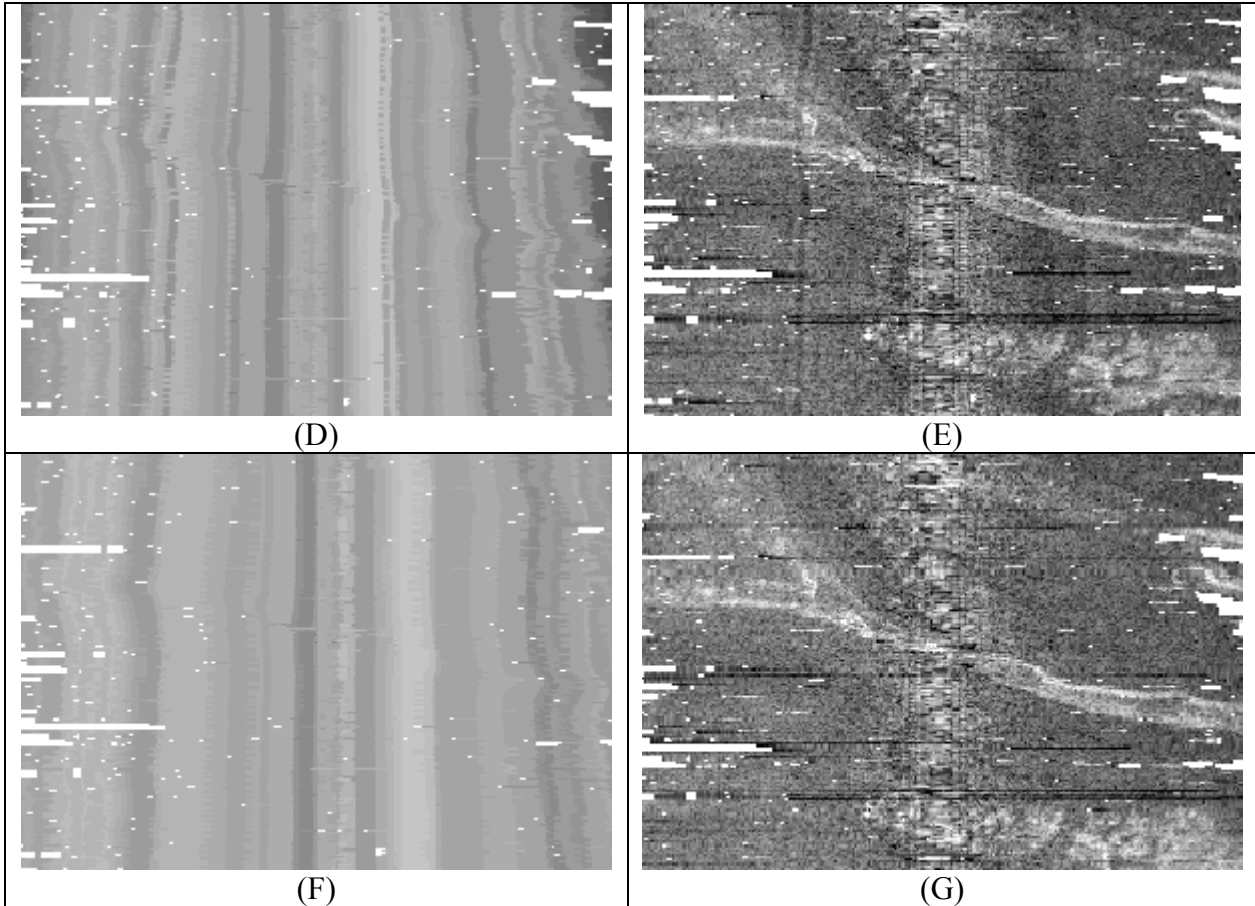


Figure 34. EM300 backscatter mosaiced using interpolated beam pattern model corrections. Figure (A) shows the raw mosaic with no corrections applied. Figures (B) and (C) show the corrections and resulting mosaic with standard beam pattern corrections applied resulting in the creation of artificial beam patterns. Figures (D) and (E) show the corrections and resulting mosaic with interpolated beam pattern model corrections. Figures (F) and (G) show the corrections and resulting mosaic with interpolated beam pattern model corrections applied to the data computed using raw angle determination. This last method is successful in removing almost all remaining beam pattern effects from the multibeam data. Water depth is 230m.

## 7. CONCLUSION

The objective of this project was to improve the beam pattern correction software used by the UNB Ocean Mapping Group for multi-mode, multi-sector multibeam sonar systems, particularly the Kongsberg-Simrad EM300 system installed on the Canadian Coast Guard Ship Amundsen. The installation of the titanium-polymer ice window to protect the transducers further enhances the transmit sector boundary residuals commonly found in EM300 backscatter mosaics. The solution to eliminate these sector boundary residuals was four-fold:

- 1) Determine the exact vertically-referenced angular location of each sector boundary by comparing changing pitch steering angles across the swath for all pings of many survey lines to converge on the true sector boundaries for each mode of the system.
- 2) Redefine the calculation of a beam launch vector from the transformation of the depth and across-track distances to one comprised of the receive steering angle, vessel roll at receive, and roll installation angle of the receive transducer in a true two-dimensional vertical across-track plane below the transducer.
- 3) Automate the mode-intelligent features of the beam pattern correction software which produces residual beam pattern models for each used mode within a single survey line. This in turn can be applied to the appropriate sections of the line in the backscatter production software to correct for true beam patterns effects in the backscatter mosaics. Included in this new automation are the required computational adjustments to account for a narrow swath width used in the Very Deep and Extra Deep mode of the system.

- 4) Perform an inter-beam interpolation on the produced beam pattern models to account for any beams for which an insufficient number of data samples are present to avoid introducing artificial beam pattern effects into the data.

Examples of improvements to backscatter mosaics have been shown throughout this paper to highlight each individual programming improvement. Figure 35 depicts a small survey performed by the CCGS Amundsen during the 2004 field season in the Beaufort Sea. It shows an example of the improvements which can be seen by implementing all the new tools developed in this project by comparing the resulting backscatter mosaic with and without the changes to the beam pattern software.

The end result of this work is that the future backscatter information processed by OMG personnel will reflect more accurate backscatter strength of the seafloor without the distortion of beam pattern residuals. This will have a positive impact on science activities of other groups on board the ship, in particular the ongoing geology and paleo-oceanographic research which involves boxcore and piston-core samples taken from the surface and sub-surface of the seabed. The selection of appropriate locations for these coring samples is aided by the backscatter information provided by the EM300, which will now better reflect true changes in seafloor geology rather than sonar intensity fluctuations from the EM300 system. These programming changes have been implemented thus far solely for the EM300, but are equally applicable to any multi-sector, multi-mode Simrad multibeam system.

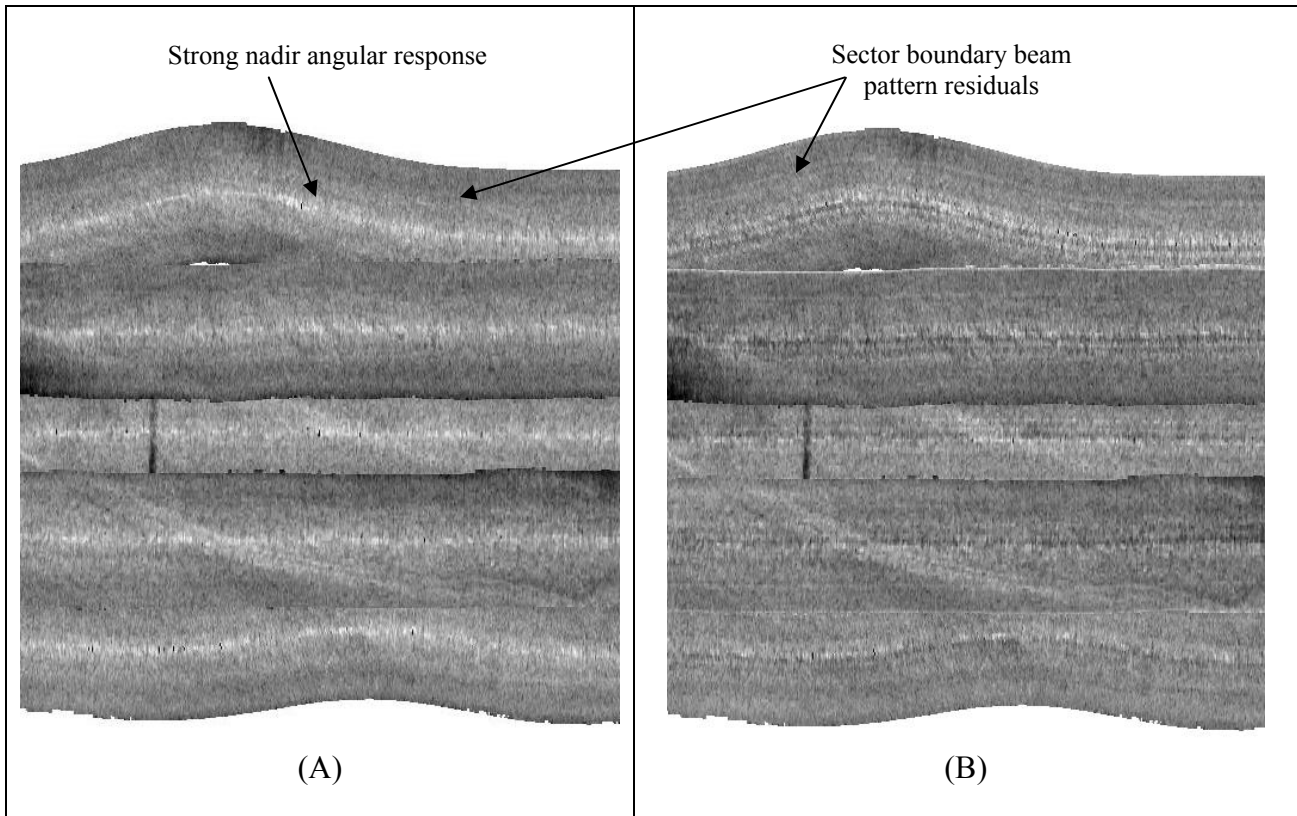
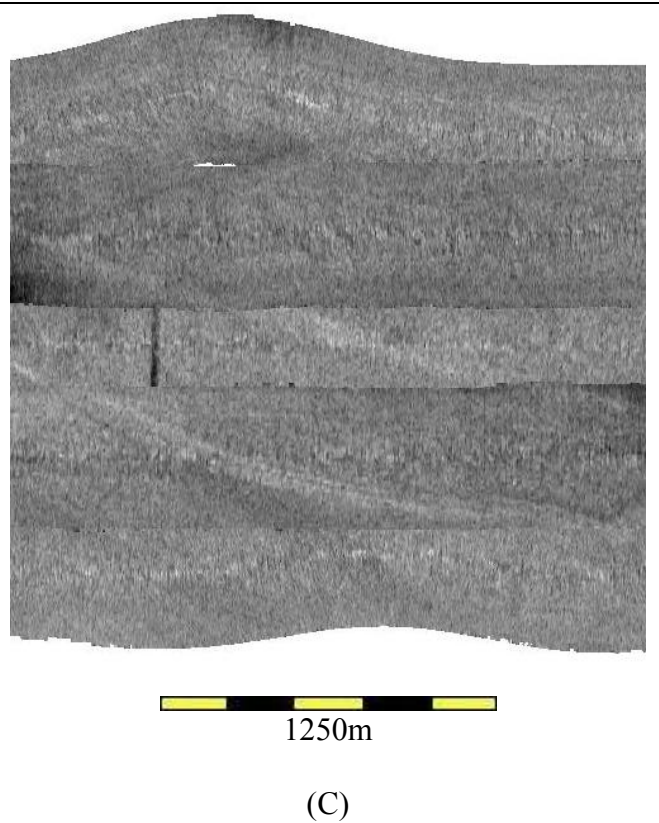
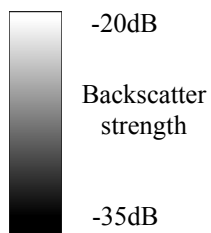


Figure 35. Backscatter mosaics showing the results of using the improved beam pattern correction software tools. Figure (A) shows the raw backscatter, Figure (B) shows the backscatter with conventional beam pattern corrections as processed on the Amundsen, while Figure (C) shows the result using the new improved software tools. A noticeable grayscale difference for the center line in comparison with the other lines exists for both the raw and corrected data, however at this time no research into inter-line backscatter normalization has been undertaken. Water depth is 75m.



## REFERENCES

- Bartlett, J., Hughes Clarke, J.E., and Beaudoin, J. (2004). "CCGS Amundsen: A New Mapping Platform for Canada's North". *Lighthouse*, Edition No. 65, pp. 30-38.
- ArcticNet Inc. (2005). CCGS Amundsen Research Icebreaker. [On-line]. 15 June 2005. <http://www.amundsen.quebec-ocean.ulaval.ca/amundsenenglish.htm>
- Francois R.E. and Garrison G.R., 1982. Sound absorption based on ocean measurements: Part I: Pure Water and magnesium sulfate contributions: *JASA*, v. 72, p.896-907.
- Francois R.E. and Garrison G.R., 1982. Sound absorption based on ocean measurements: Part II: Boric acid contribution and equation for total absorption: *JASA*, v.72, p. 1879-1890.
- Hammerstad, E. (2000). EM Technical Note, Backscattering and Seabed Image Reflectivity.
- Hammerstad, E. (2005), Kongsberg-Simrad. Personal communication via email November 1, 2005. Subject: EM backscatter reduction document
- Hughes Clarke, J.E. (1997) EM300 Yaw Stabilisation, [On-line]. 14 May 2005. [http://www.omg.unb.ca/~jhc/yaw\\_stab/](http://www.omg.unb.ca/~jhc/yaw_stab/)
- Hughes Clarke, J.E. (2003). GGE 3353 Lecture Notes. Department of Geodesy and Geomatics Engineering, University of New Brunswick, Fredericton, New Brunswick
- Hughes Clarke, J.E., Beaudoin, J., Bartlett, J. (2003) CCGS Amundsen Ship Acceptance Trial Report, Sam Ford Fjord, Baffin Island
- Hughes Clarke, J.E. (2004). Multibeam Training Course Notes. Swath sonar training course given as part of the Canadian Hydrographic Conference, Ottawa, Ontario, May, 2005.
- Hughes Clarke, J.E., Llewellyn, K. (2004). Amundsen EM300 Deep Water Performance. [On-line]. 14 May 2005. [http://huron.omg.unb.ca/Projects/Arctic/LabradorSea/Amundsen\\_EM300\\_deep\\_water\\_performance.html](http://huron.omg.unb.ca/Projects/Arctic/LabradorSea/Amundsen_EM300_deep_water_performance.html)
- Kongsberg-Simrad (2002). Simrad EM300 Multibeam Echo Sounder. Product Specification, Horten, Norway.
- Kongsberg-Simrad(2005) Acoustic principles for multibeam systems. Multibeam sonar training presentation, London, UK, May, 2005.
- Lurton, X. (2002). *An Introduction to Underwater Acoustics*. Praxis Publishing, UK.



## **APPENDIX A**

Comparisons of Default EM300 Transmit Beam Pattern Adjustments with those Modified to Account for the Ice Window Installation aboard the CCGS Amundsen

All Data Derived from Original Data Provided by  
Kjell Nielsen of Kongsberg-Simrad

**Table A-1. EM300 Relative Sector Transmit Strengths.**

<b>SECTOR CALIBRATION SETTING</b>	<b>SYSTEM MODE</b>	<b>CALIBRATION VARIABLE</b>	<b>DEFAULT EM300 VALUE (dB)</b>	<b>PREDICTED AMUNDSEN EM300 VALUE (dB)</b>
<b>DeltaSL (Relative Sector Transmit Strength)</b>	Very Shallow, Shallow, and Medium	deltaSL_ShallowBeam0	-5.4	-0.3
		deltaSL_ShallowBeam1	0.0	3.1
		deltaSL_ShallowBeam2	-0.9	4.2
	Deep	deltaSL_DeepBeam0	0.5	5.6
		deltaSL_DeepBeam1	-0.6	3.6
		deltaSL_DeepBeam2	4.3	8.6
		deltaSL_DeepBeam3	2.2	7.8
		deltaSL_DeepBeam4	3.0	5.4
		deltaSL_DeepBeam5	1.2	0.8
		deltaSL_DeepBeam6	2.9	6.0
		deltaSL_DeepBeam7	-2.3	1.4
	Very Deep	deltaSL_VDeepBeam0	1.3	3.3
		deltaSL_VDeepBeam1	0.5	3.1
		deltaSL_VDeepBeam2	2.4	5.3
		deltaSL_VDeepBeam3	0.5	3.7
		deltaSL_VDeepBeam4	0.4	3.2
		deltaSL_VDeepBeam5	-0.1	3.0
		deltaSL_VDeepBeam6	-0.1	3.0
		deltaSL_VDeepBeam7	-0.3	2.7
	Extra Deep	deltaSL_EDeepBeam0	0.0	3.0
		deltaSL_EDeepBeam1	0.0	3.0
		deltaSL_EDeepBeam2	0.0	3.0

**Table A-2. EM300 Transmit Sector Crossover Angles.**

<b>SECTOR CALIBRATION SETTING</b>	<b>SYSTEM MODE</b>	<b>CALIBRATION VARIABLE</b>	<b>DEFAULT EM300 VALUE (degrees)</b>	<b>PREDICTED AMUNDSEN EM300 VALUE (degrees)</b>
<b>TxCrossing (Crossover Angle Between Fired Sectors)  (Positive to Starboard)</b>	Very Shallow, Shallow, and Medium	txCrossingShallowBeam0	-47.0	-47.0
		txCrossingShallowBeam1	45.5	44.0
		txCrossingShallowBeam2	90.0	90.0
	Deep	txCrossingDeepBeam0/1	-53.6	-53.0
		txCrossingDeepBeam1/2	-33.5	-35.0
		txCrossingDeepBeam2/3	-26.4	-27.0
		txCrossingDeepBeam3/4	-9.0	-9.0
		txCrossingDeepBeam4/5	9.0	8.0
		txCrossingDeepBeam5/6	24.8	29.0
		txCrossingDeepBeam6/7	35.0	36.0
		txCrossingDeepBeam7/8	53.6	51.0
	Very Deep	txCrossingVDeepBeam8	90.0	90.0
		txCrossingVDeepBeam0	-36.5	-36.5
		txCrossingVDeepBeam1	-23.0	-23.0
		txCrossingVDeepBeam2	-18.0	-18.0
		txCrossingVDeepBeam3	-5.0	-5.0
		txCrossingVDeepBeam4	4.3	4.3
		txCrossingVDeepBeam5	16.2	16.2
		txCrossingVDeepBeam6	24.0	24.0
		txCrossingVDeepBeam7	34.0	34.0
	Extra Deep	txCrossingVDeepBeam8	90.0	90.0
txCrossingExtraDeepBeam0		-5.0	-5.0	
txCrossingExtraDeepBeam1		5.0	5.0	
		txCrossingExtraDeepBeam2	90.0	90.0

**Table A-3. EM300 Transmit Sector Beam Boresite Pointing Angles.**

SECTOR CALIBRATION SETTING	SYSTEM MODE	CALIBRATION VARIABLE	DEFAULT EM300 VALUE (degrees)	PREDICTED AMUNDSEN EM300 VALUE (degrees)
<b>TXBeamAngle (Across-Track Beam Boresite Angle)</b>  <b>(Positive to Starboard)</b>	Very Shallow, Shallow, and Medium	txBeamAngleShallowBeam0	-60.0	-55.0
		0	0.0	0.0
		txBeamAngleShallowBeam1	60.0	53.5
	Deep	txBeamAngleDeepBeam0	-63.4	-60.0
		txBeamAngleDeepBeam1	-44.7	-44.7
		txBeamAngleDeepBeam2	-29.5	-30.0
		txBeamAngleDeepBeam3	-18.4	-18.4
		txBeamAngleDeepBeam4	0.0	0.0
		txBeamAngleDeepBeam5	17.9	17.9
		txBeamAngleDeepBeam6	30.0	30.5
		txBeamAngleDeepBeam7	44.7	44.0
		txBeamAngleDeepBeam8	63.5	58.0
	Very Deep	txBeamAngleVDeepBeam0	-43.3	-43.3
		txBeamAngleVDeepBeam1	-30.5	-30.5
		txBeamAngleVDeepBeam2	-20.7	-20.7
		txBeamAngleVDeepBeam3	-9.6	-9.6
		0	0.0	0.0
		txBeamAngleVDeepBeam4	9.8	9.8
		txBeamAngleVDeepBeam5	19.9	19.9
		txBeamAngleVDeepBeam6	31.5	31.5
		txBeamAngleVDeepBeam7	44.1	44.1
	Extra Deep	txBeamAngleEDeepBeam0	-9.5	-9.5
		txBeamAngleEDeepBeam1	0.0	0.0
txBeamAngleEDeepBeam2		10.5	10.5	

**Table A-4. EM300 Across-Track Transmit Sector Beamwidths.**

SECTOR CALIBRATION SETTING	SYSTEM MODE	CALIBRATION VARIABLE	DEFAULT EM300 VALUE (degrees)	PREDICTED AMUNDSEN EM300 VALUE (degrees)
<b>TXBeamWidth (Across-Track Transmit Beam Width)</b>  <b>(Beam1 correction not used)</b>	Very Shallow, Shallow, and Medium	txBeamWidthShallowBeam0	31.0	22.0
		txBeamWidthShallowBeam1	200.0	200.0
		txBeamWidthShallowBeam2	31.0	25.0
	Deep	txBeamWidthDeepBeam0	25.0	19.0
		txBeamWidthDeepBeam1	20.0	30.0
		txBeamWidthDeepBeam2	18.0	18.0
		txBeamWidthDeepBeam3	18.0	18.0
		txBeamWidthDeepBeam4	40.0	40.0
		txBeamWidthDeepBeam5	18.0	18.0
		txBeamWidthDeepBeam6	18.0	19.0
		txBeamWidthDeepBeam7	20.0	21.0
		txBeamWidthDeepBeam8	25.0	20.0
	Very Deep	txBeamWidthVDeepBeam0	22.0	22.0
		txBeamWidthVDeepBeam1	20.0	20.0
		txBeamWidthVDeepBeam2	17.0	17.0
		txBeamWidthVDeepBeam3	17.0	17.0
		txBeamWidthVDeepBeam4	14.0	14.0
		txBeamWidthVDeepBeam5	16.0	16.0
		txBeamWidthVDeepBeam6	16.0	16.0
		txBeamWidthVDeepBeam7	24.0	24.0
		txBeamWidthVDeepBeam8	24.0	24.0
Extra Deep	txBeamWidthEDeepBeam0	16.0	16.0	
	txBeamWidthEDeepBeam1	14.0	14.0	
	txBeamWidthEDeepBeam2	16.0	16.0	

## **APPENDIX B**

### Quantitative Comparisons of Beam Pattern Modeling

**Table B-1. Numerical Beam Pattern Structure as Shown Graphically in Figure 27  
Comparing Launch Angle Calculation of Sounding Depth and Across-Track  
Distance Transformation versus Raw Angle Determination**

BEAM LAUNCH ANGLE (deg)	AVERAGE BEAM INTENSITY (dB)		DIFFERENCE FROM ARRAY AVERAGE (dB)		NUMBER OF INTENSITY DATA SAMPLES	
	Transformation	Raw	Transformation	Raw	Transformation	Raw
0.00	0.000000	0.000000	0.000000	0.000000	0	0
1.00	0.000000	0.000000	0.000000	0.000000	0	0
2.00	0.000000	0.000000	0.000000	0.000000	0	0
3.00	0.000000	0.000000	0.000000	0.000000	0	0
4.00	0.000000	0.000000	0.000000	0.000000	0	0
5.00	0.000000	0.000000	0.000000	0.000000	0	0
6.00	0.000000	0.000000	0.000000	0.000000	0	0
7.00	0.000000	0.000000	0.000000	0.000000	0	0
8.00	0.000000	0.000000	0.000000	0.000000	0	0
9.00	0.000000	0.000000	0.000000	0.000000	0	0
10.00	0.000000	0.000000	0.000000	0.000000	0	0
11.00	0.000000	0.000000	0.000000	0.000000	0	0
12.00	0.000000	0.000000	0.000000	0.000000	0	0
13.00	0.000000	0.000000	0.000000	0.000000	0	0
14.00	0.000000	0.000000	0.000000	0.000000	0	0
15.00	0.000000	0.000000	0.000000	0.000000	0	0
16.00	0.000000	0.000000	0.000000	0.000000	0	0
17.00	0.000000	0.000000	0.000000	0.000000	0	0
18.00	0.000000	0.000000	0.000000	0.000000	0	0
19.00	0.000000	0.000000	0.000000	0.000000	0	0
20.00	0.000000	0.000000	0.000000	0.000000	0	0
21.00	0.000000	0.000000	0.000000	0.000000	0	0
22.00	0.000000	0.000000	0.000000	0.000000	0	0
23.00	0.000000	0.000000	0.000000	0.000000	0	0
24.00	0.000000	0.000000	0.000000	0.000000	0	0
25.00	0.000000	-34.215863	0.000000	6.819652	0	11908
26.00	-34.365532	-34.364342	7.058252	6.968131	178362	203250
27.00	-34.195953	-34.175433	6.888673	6.779222	220323	249166
28.00	-33.300647	-33.224957	5.993367	5.828746	219716	244627
29.00	-32.058600	-32.019859	4.751320	4.623648	214070	237801
30.00	-30.883810	-30.865947	3.576529	3.469736	216481	236213
31.00	-30.129688	-30.107519	2.822408	2.711307	144863	162423
32.00	-29.580445	-29.576843	2.273165	2.180632	145633	167374
33.00	-29.334176	-29.304562	2.026896	1.908351	144141	161340
34.00	-28.878820	-28.880361	1.571540	1.484149	142949	159053
35.00	-28.869907	-28.841247	1.562627	1.445036	140092	152536
36.00	-28.561859	-28.595688	1.254579	1.199477	137854	150834

BEAM LAUNCH ANGLE (deg)	AVERAGE BEAM INTENSITY (dB)		DIFFERENCE FROM ARRAY AVERAGE (dB)		NUMBER OF INTENSITY DATA SAMPLES	
	Transformation	Raw	Transformation	Raw	Transformation	Raw
37.00	-28.579365	-28.555828	1.272085	1.159617	136451	151430
38.00	-28.320683	-28.339516	1.013403	0.943305	136680	151529
39.00	-28.359413	-28.380446	1.052133	0.984235	71333	79324
40.00	-28.442548	-28.462548	1.135268	1.066337	132329	146388
41.00	-28.904231	-28.951908	1.596951	1.555697	70127	77664
42.00	-29.326401	-29.324702	2.019121	1.928490	128728	137303
43.00	-29.152183	-29.205834	1.844903	1.809623	66926	78884
44.00	-29.292639	-29.074160	1.985359	1.677949	68646	75944
45.00	-26.584954	-26.584622	-0.722326	-0.811590	66877	73740
46.00	-26.721338	-26.725318	-0.585942	-0.670893	120542	128352
47.00	-27.135362	-27.162130	-0.171918	-0.234081	62883	72747
48.00	-27.300649	-27.312765	-0.006631	-0.083446	62538	69346
49.00	-27.241301	-27.229345	-0.065979	-0.166866	60700	66777
50.00	-26.908670	-26.934333	-0.398610	-0.461878	59630	65543
51.00	-27.235961	-27.197827	-0.071319	-0.198384	58213	63884
52.00	-26.980760	-26.940906	-0.326520	-0.455305	56602	62045
53.00	-26.430507	-26.381619	-0.876774	-1.014592	55811	61222
54.00	-25.784190	-25.762839	-1.523090	-1.633372	54738	59953
55.00	-25.783475	-25.729712	-1.523805	-1.666499	54077	58952
56.00	-25.181238	-25.177339	-2.126042	-2.218873	51275	53020
57.00	-25.047814	-25.063054	-2.259466	-2.333158	50320	54985
58.00	-24.830563	-24.809201	-2.476717	-2.587010	48679	53221
59.00	-25.202571	-24.937030	-2.104710	-2.459181	4396	8115
60.00	-24.775927	-24.754746	-2.531353	-2.641465	47422	51673
61.00	-24.594063	-24.609657	-2.713217	-2.786554	44922	49030
62.00	-24.470153	-24.482368	-2.837127	-2.913843	43639	44834
63.00	-24.431671	-24.426294	-2.875610	-2.969918	42083	45783
64.00	-24.801997	-24.805530	-2.505283	-2.590682	3505	6438
65.00	-24.709930	-24.729169	-2.597350	-2.667042	39525	42977
66.00	-24.875134	-24.883819	-2.432146	-2.512392	38173	39219
67.00	-24.971881	-24.977362	-2.335400	-2.418850	35954	39137
68.00	-25.287879	-25.185200	-2.019401	-2.211011	2574	5027
69.00	-24.750007	-24.743237	-2.557273	-2.652974	33709	34600
70.00	-24.956048	-24.982294	-2.351232	-2.413917	31876	34706
71.00	-24.757509	-24.522425	-2.549771	-2.873786	2497	4593
72.00	-24.415974	-24.396279	-2.891306	-2.999932	30193	31281
73.00	-23.717916	-23.695589	-3.589364	-3.700622	27919	29971
74.00	-23.027872	-22.729610	-4.279408	-4.666601	2063	3850
75.00	-22.835341	-22.815633	-4.471940	-4.580578	25823	26591
76.00	-22.974588	-22.943191	-4.332692	-4.453021	23631	25656
77.00	-23.214058	-23.161102	-4.093223	-4.235109	1565	3175
78.00	-23.133024	-23.123285	-4.174256	-4.272926	21763	22233
79.00	-23.331632	-23.301658	-3.975648	-4.094553	20179	22010



BEAM LAUNCH ANGLE (deg)	AVERAGE BEAM INTENSITY (dB)		DIFFERENCE FROM ARRAY AVERAGE (dB)		NUMBER OF INTENSITY DATA SAMPLES	
	Transformation	Raw	Transformation	Raw	Transformation	Raw
80.00	-22.985480	-22.908029	-4.321800	-4.488182	1343	2740
81.00	-23.200625	-23.189055	-4.106655	-4.207157	17767	18291
82.00	-22.683787	-23.097269	-4.623494	-4.298942	993	2087
83.00	-23.651820	-23.660710	-3.655460	-3.735501	15907	16340
84.00	-23.972666	-23.956650	-3.334614	-3.439561	13646	14706
85.00	-23.828125	-23.932342	-3.479155	-3.463869	768	1648
86.00	-24.404721	-24.395490	-2.902560	-3.000721	11524	11774
87.00	-24.414599	-24.424553	-2.892681	-2.971658	10843	11803
88.00	-24.847682	-24.717849	-2.459598	-2.678362	604	902
89.00	-24.436436	-24.420438	-2.870845	-2.975773	9219	9766
90.00	-23.568888	-23.539840	-3.738392	-3.856371	7367	8007
91.00	-24.234014	-24.216465	-3.073267	-3.179746	9211	9997
92.00	-24.544280	-24.316410	-2.763000	-3.079801	542	1103
93.00	-24.293612	-24.312273	-3.013668	-3.083939	11350	12100
94.00	-24.164055	-24.201812	-3.143225	-3.194399	1021	1821
95.00	-24.207756	-24.216995	-3.099525	-3.179216	11179	11521
96.00	-23.657765	-23.645862	-3.649515	-3.750349	12788	13835
97.00	-24.032779	-23.547170	-3.274501	-3.849041	1083	2173
98.00	-23.110940	-23.119343	-4.196340	-4.276868	15621	15954
99.00	-23.565766	-23.149525	-3.741514	-4.246686	1110	2421
100.00	-22.955472	-22.950290	-4.351809	-4.445921	17618	18075
101.00	-23.149723	-23.157683	-4.157557	-4.238528	19339	21242
102.00	-23.241770	-23.078360	-4.065510	-4.317852	1367	2865
103.00	-22.965294	-22.988221	-4.341986	-4.407990	21855	22455
104.00	-22.530569	-22.534111	-4.776711	-4.862100	23226	25329
105.00	-21.875060	-22.016097	-5.432220	-5.380114	2081	4069
106.00	-22.089292	-22.111570	-5.217988	-5.284641	26419	27095
107.00	-22.444040	-22.447829	-4.863240	-4.948383	27457	29959
108.00	-22.508341	-22.759917	-4.798939	-4.636294	2098	4109
109.00	-22.986502	-23.000552	-4.320778	-4.395659	29931	30796
110.00	-23.692906	-23.705030	-3.614374	-3.691181	31632	34490
111.00	-24.043487	-24.000600	-3.263793	-3.395611	2449	4998
112.00	-24.170899	-24.184149	-3.136381	-3.212062	33587	34559
113.00	-24.642126	-24.638701	-2.665155	-2.757510	35349	38410
114.00	-24.744452	-24.806471	-2.562829	-2.589740	3064	5857
115.00	-24.581279	-24.611221	-2.726001	-2.784990	38946	42519
116.00	-24.649710	-24.643323	-2.657571	-2.752888	40455	41717
117.00	-24.509547	-24.492091	-2.797733	-2.904120	42212	45963
118.00	-24.465341	-24.513217	-2.841939	-2.882994	3722	7112
119.00	-24.736112	-24.717458	-2.571168	-2.678753	45004	49214
120.00	-24.822136	-24.824699	-2.485144	-2.571513	46142	48679
121.00	-25.051025	-25.046816	-2.256255	-2.349395	47643	50901
122.00	-24.564157	-24.577860	-2.743123	-2.818351	48771	53352

BEAM LAUNCH ANGLE (deg)	AVERAGE BEAM INTENSITY (dB)		DIFFERENCE FROM ARRAY AVERAGE (dB)		NUMBER OF INTENSITY DATA SAMPLES	
	Transformation	Raw	Transformation	Raw	Transformation	Raw
123.00	-24.930709	-24.928748	-2.376572	-2.467463	50735	55339
124.00	-25.164534	-24.984633	-2.142746	-2.411578	5002	9273
125.00	-24.967890	-24.949540	-2.339390	-2.446671	52865	58096
126.00	-24.862043	-24.855056	-2.445237	-2.541155	54412	59730
127.00	-24.681387	-24.711363	-2.625893	-2.684848	56429	62052
128.00	-24.929558	-24.942268	-2.377723	-2.453943	58012	63717
129.00	-25.463491	-25.498587	-1.843789	-1.897624	58931	64774
130.00	-25.944856	-25.960664	-1.362424	-1.435547	59399	65614
131.00	-26.228567	-26.259878	-1.078714	-1.136334	61085	67299
132.00	-27.002378	-26.999978	-0.304902	-0.396233	62650	69002
133.00	-27.290736	-27.339598	-0.016544	-0.056613	62426	69538
134.00	-26.987979	-26.956782	-0.319302	-0.439429	123696	131069
135.00	-27.301273	-27.308216	-0.006007	-0.087995	64717	75499
136.00	-27.397457	-27.433624	0.090177	0.037412	63549	70974
137.00	-27.531273	-27.493892	0.223992	0.097681	63426	70318
138.00	-27.402499	-27.394471	0.095218	-0.001740	126993	139057
139.00	-27.352959	-27.378086	0.045679	-0.018125	67947	76382
140.00	-27.127736	-27.158703	-0.179545	-0.237508	128762	139988
141.00	-27.178848	-27.233448	-0.128432	-0.162764	71801	83492
142.00	-27.487249	-27.477379	0.179969	0.081168	135874	150173
143.00	-27.307125	-27.276765	-0.000155	-0.119446	70678	78377
144.00	-27.537657	-27.599095	0.230377	0.202884	136600	152813
145.00	-27.415256	-27.478089	0.107976	0.081878	141308	157341
146.00	-28.089869	-28.111404	0.782589	0.715193	145428	162512
147.00	-29.235449	-29.257720	1.928169	1.861508	154528	171252
148.00	-30.466079	-30.451566	3.158798	3.055355	154062	171338
149.00	-31.517445	-31.863894	4.210165	4.467682	144135	172626
150.00	-33.884340	-33.887722	6.577060	6.491510	193299	197665
151.00	0.000000	0.000000	0.000000	0.000000	0	0
152.00	0.000000	0.000000	0.000000	0.000000	0	0
153.00	0.000000	0.000000	0.000000	0.000000	0	0
154.00	0.000000	0.000000	0.000000	0.000000	0	0
155.00	0.000000	0.000000	0.000000	0.000000	0	0
156.00	0.000000	0.000000	0.000000	0.000000	0	0
157.00	0.000000	0.000000	0.000000	0.000000	0	0
158.00	0.000000	0.000000	0.000000	0.000000	0	0
159.00	0.000000	0.000000	0.000000	0.000000	0	0
160.00	0.000000	0.000000	0.000000	0.000000	0	0
161.00	0.000000	0.000000	0.000000	0.000000	0	0
162.00	0.000000	0.000000	0.000000	0.000000	0	0
163.00	0.000000	0.000000	0.000000	0.000000	0	0
164.00	0.000000	0.000000	0.000000	0.000000	0	0
165.00	0.000000	0.000000	0.000000	0.000000	0	0

BEAM LAUNCH ANGLE (deg)	AVERAGE BEAM INTENSITY (dB)		DIFFERENCE FROM ARRAY AVERAGE (dB)		NUMBER OF INTENSITY DATA SAMPLES	
	Transformation	Raw	Transformation	Raw	Transformation	Raw
166.00	0.000000	0.000000	0.000000	0.000000	0	0
167.00	0.000000	0.000000	0.000000	0.000000	0	0
168.00	0.000000	0.000000	0.000000	0.000000	0	0
169.00	0.000000	0.000000	0.000000	0.000000	0	0
170.00	0.000000	0.000000	0.000000	0.000000	0	0
171.00	0.000000	0.000000	0.000000	0.000000	0	0
172.00	0.000000	0.000000	0.000000	0.000000	0	0
173.00	0.000000	0.000000	0.000000	0.000000	0	0
174.00	0.000000	0.000000	0.000000	0.000000	0	0
175.00	0.000000	0.000000	0.000000	0.000000	0	0
176.00	0.000000	0.000000	0.000000	0.000000	0	0
177.00	0.000000	0.000000	0.000000	0.000000	0	0
178.00	0.000000	0.000000	0.000000	0.000000	0	0
179.00	0.000000	0.000000	0.000000	0.000000	0	0

**Table B-2. Numerical Beam Pattern Structure as Shown Graphically in Figure 28  
Comparing Beam Pattern Statistics Calculated for Each Used Mode in a  
Survey Line versus an Average of the Entire Line**

BEAM LAUNCH ANGLE (deg)	AVERAGE BEAM INTENSITY (dB)			DIFFERENCE FROM ARRAY AVERAGE (dB)		
	Mode 2	Mode 3	Original Average	Mode 2	Mode 3	Original Average
0.00	0.000000	0.000000	0.000000	0.000000	0.000000	0.000000
1.00	0.000000	0.000000	0.000000	0.000000	0.000000	0.000000
2.00	0.000000	0.000000	0.000000	0.000000	0.000000	0.000000
3.00	0.000000	0.000000	0.000000	0.000000	0.000000	0.000000
4.00	0.000000	0.000000	0.000000	0.000000	0.000000	0.000000
5.00	0.000000	0.000000	0.000000	0.000000	0.000000	0.000000
6.00	0.000000	0.000000	0.000000	0.000000	0.000000	0.000000
7.00	0.000000	0.000000	0.000000	0.000000	0.000000	0.000000
8.00	0.000000	0.000000	0.000000	0.000000	0.000000	0.000000
9.00	0.000000	0.000000	0.000000	0.000000	0.000000	0.000000
10.00	0.000000	0.000000	0.000000	0.000000	0.000000	0.000000
11.00	0.000000	0.000000	0.000000	0.000000	0.000000	0.000000
12.00	0.000000	0.000000	0.000000	0.000000	0.000000	0.000000
13.00	0.000000	0.000000	0.000000	0.000000	0.000000	0.000000
14.00	0.000000	0.000000	0.000000	0.000000	0.000000	0.000000
15.00	0.000000	0.000000	0.000000	0.000000	0.000000	0.000000
16.00	0.000000	0.000000	0.000000	0.000000	0.000000	0.000000
17.00	0.000000	0.000000	0.000000	0.000000	0.000000	0.000000
18.00	0.000000	0.000000	0.000000	0.000000	0.000000	0.000000
19.00	0.000000	0.000000	0.000000	0.000000	0.000000	0.000000
20.00	0.000000	0.000000	0.000000	0.000000	0.000000	0.000000
21.00	0.000000	0.000000	0.000000	0.000000	0.000000	0.000000
22.00	0.000000	0.000000	0.000000	0.000000	0.000000	0.000000
23.00	0.000000	0.000000	0.000000	0.000000	0.000000	0.000000
24.00	0.000000	0.000000	0.000000	0.000000	0.000000	0.000000
25.00	0.000000	0.000000	0.000000	0.000000	0.000000	0.000000
26.00	0.000000	0.000000	0.000000	0.000000	0.000000	0.000000
27.00	0.000000	0.000000	0.000000	0.000000	0.000000	0.000000
28.00	0.000000	0.000000	0.000000	0.000000	0.000000	0.000000
29.00	0.000000	0.000000	0.000000	0.000000	0.000000	0.000000
30.00	0.000000	0.000000	0.000000	0.000000	0.000000	0.000000
31.00	-26.209381	-29.055588	0.000000	-1.847751	0.743815	0.000000
32.00	-26.389042	-29.360806	-28.526701	-1.668091	1.049033	0.202266
33.00	-26.353100	-29.308428	-28.727705	-1.704034	0.996656	0.403270
34.00	-26.046659	-29.200018	-28.840570	-2.010474	0.888245	0.516136
35.00	-26.473991	-29.400997	-28.642502	-1.583142	1.089225	0.318066
36.00	-25.995438	-29.258137	-28.885704	-2.061695	0.946365	0.561269

BEAM LAUNCH ANGLE (deg)	AVERAGE BEAM INTENSITY (dB)			DIFFERENCE FROM ARRAY AVERAGE (dB)		
	Mode 2	Mode 3	Original Average	Mode 2	Mode 3	Original Average
37.00	-25.943029	-29.026169	-28.468622	-2.114104	0.714396	0.144188
38.00	-25.786509	-26.582142	-27.490520	-2.270624	-1.729630	-0.833914
39.00	-25.231943	-27.048630	-26.512453	-2.825189	-1.263142	-1.811981
40.00	-25.239414	-26.891182	-26.701109	-2.817717	-1.420591	-1.623325
41.00	-25.140003	-26.955645	-26.579712	-2.917130	-1.356127	-1.744722
42.00	-24.840204	-27.041098	-26.609716	-3.216928	-1.270674	-1.714718
43.00	-24.855213	-26.843224	-26.631863	-3.201920	-1.468549	-1.692572
44.00	-25.023046	-27.053972	-26.587355	-3.034087	-1.257799	-1.737080
45.00	-25.173502	-27.040791	-26.682049	-2.883630	-1.270982	-1.642386
46.00	-24.741367	-26.732641	-26.473845	-3.315765	-1.579130	-1.850591
47.00	-25.677408	-26.868168	-26.641426	-2.379725	-1.443604	-1.683007
48.00	-26.062500	-26.918497	-26.678440	-1.994633	-1.393274	-1.645994
49.00	-25.928246	-26.835157	-26.694246	-2.128887	-1.476615	-1.630187
50.00	-25.996048	-27.201626	-26.946749	-2.061085	-1.110146	-1.377686
51.00	-26.170395	-27.135889	-26.973534	-1.886738	-1.175882	-1.350902
52.00	-25.693554	-27.119463	-26.959480	-2.363579	-1.192309	-1.364953
53.00	-26.228748	-27.467094	-26.837202	-1.828383	-0.844678	-1.487232
54.00	-26.345421	-27.460705	-27.276283	-1.711713	-0.851067	-1.048151
55.00	-25.980988	-27.628048	-27.178249	-2.076146	-0.683725	-1.146185
56.00	-26.008141	-27.374750	-27.285639	-2.048993	-0.937021	-1.038796
57.00	-26.259056	-28.034515	-27.380098	-1.798076	-0.277256	-0.944335
58.00	-26.109894	-26.673187	-27.292683	-1.947240	-1.638585	-1.031753
59.00	-26.251837	-26.611076	-26.581985	-1.805296	-1.700696	-1.742449
60.00	-25.988659	-26.071848	-26.537615	-2.068474	-2.239924	-1.786820
61.00	-25.971741	-26.543974	-26.043516	-2.085392	-1.767798	-2.280918
62.00	-25.872980	-26.181503	-26.436558	-2.184152	-2.130269	-1.887878
63.00	-25.625053	-26.235226	-26.126698	-2.432079	-2.076547	-2.197737
64.00	-26.132326	-26.500412	-26.432121	-1.924806	-1.811360	-1.892312
65.00	-25.515364	-24.819757	-24.936884	-2.541769	-3.492015	-3.387550
66.00	-25.643368	-24.577360	-24.770433	-2.413766	-3.734412	-3.554001
67.00	-25.610291	-23.940025	-23.970249	-2.446843	-4.371747	-4.354185
68.00	-25.325239	-23.974831	-24.237211	-2.731894	-4.336941	-4.087223
69.00	-25.040188	-24.009638	-24.155323	-3.016944	-4.302135	-4.169111
70.00	-25.109241	-23.645317	-23.877626	-2.947892	-4.666454	-4.446808
71.00	-24.707966	-23.819056	-23.940813	-3.349167	-4.492717	-4.383622
72.00	-24.916565	-23.276728	-23.735371	-3.140567	-5.035045	-4.589065
73.00	-25.021049	-23.176231	-23.529926	-3.036084	-5.135542	-4.794508
74.00	-25.125532	-23.075733	-23.375526	-2.931601	-5.236039	-4.948907
75.00	-26.081709	-22.677860	-23.109310	-1.975424	-5.633911	-5.215124
76.00	-26.081709	-22.509935	-22.984314	-1.975424	-5.801836	-5.340120
77.00	-26.577929	-22.283482	-22.859320	-1.479205	-6.028290	-5.465116
78.00	-26.139080	-22.284927	-22.708717	-1.918051	-6.026845	-5.615716
79.00	-27.034168	-22.353382	-22.671642	-1.022964	-5.958388	-5.652793

BEAM LAUNCH ANGLE (deg)	AVERAGE BEAM INTENSITY (dB)			DIFFERENCE FROM ARRAY AVERAGE (dB)		
	Mode 2	Mode 3	Original Average	Mode 2	Mode 3	Original Average
80.00	-25.471760	-22.773130	-23.072889	-2.585374	-5.538640	-5.251545
81.00	-25.471760	-23.192879	-23.402719	-2.585374	-5.118893	-4.921716
82.00	-25.587597	-26.803724	-26.675434	-2.469537	-1.508047	-1.648999
83.00	-26.196234	-26.836071	-26.714121	-1.860899	-1.475701	-1.610313
84.00	-26.196234	-26.868416	-26.752808	-1.860899	-1.443355	-1.571628
85.00	-26.630636	-26.902948	-26.838705	-1.426496	-1.408824	-1.485730
86.00	-25.226290	-26.727985	-26.494328	-2.830843	-1.583786	-1.830107
87.00	-25.226290	-26.553024	-26.149950	-2.830843	-1.758747	-2.174484
88.00	-25.107563	-26.189318	-25.764400	-2.949570	-2.122454	-2.560034
89.00	-24.419325	-26.503769	-25.590105	-3.637808	-1.808002	-2.734329
90.00	-23.731087	-26.818222	-25.415810	-4.326047	-1.493550	-2.908625
91.00	-23.777567	-26.910530	-25.542269	-4.279567	-1.401241	-2.782166
92.00	-24.056660	-27.102013	-25.616665	-4.000474	-1.209759	-2.707771
93.00	-24.335751	-27.293493	-26.230787	-3.721382	-1.018278	-2.093646
94.00	-24.502697	-27.411816	-26.412220	-3.554436	-0.899956	-1.912215
95.00	-24.903538	-27.171036	-26.401110	-3.153595	-1.140737	-1.923325
96.00	-25.304379	-26.930256	-26.389999	-2.752755	-1.381517	-1.934435
97.00	-25.589741	-26.650631	-26.293163	-2.467392	-1.661141	-2.031271
98.00	-26.059231	-27.298815	-26.898548	-1.997902	-1.012957	-1.425887
99.00	-26.528721	-27.946999	-27.503933	-1.528412	-0.364773	-0.820502
100.00	-25.973850	-24.054266	-24.666418	-2.083282	-4.257506	-3.658016
101.00	-26.243935	-24.989922	-25.386189	-1.813199	-3.321851	-2.938246
102.00	-26.514017	-25.925575	-26.105959	-1.543115	-2.386196	-2.218476
103.00	-25.456120	-24.803825	-24.997337	-2.601013	-3.507946	-3.327096
104.00	-27.081139	-26.744474	-26.614204	-0.975994	-1.567297	-1.710230
105.00	-26.467581	-25.698814	-26.208878	-1.589552	-2.612958	-2.115557
106.00	-25.438646	-25.957348	-25.803549	-2.618487	-2.354425	-2.520885
107.00	-26.488338	-27.455259	-27.164059	-1.568795	-0.856512	-1.160376
108.00	-25.942381	-26.672489	-25.746731	-2.114753	-1.639284	-2.577704
109.00	-25.396423	-25.889717	-26.582577	-2.660710	-2.422055	-1.741857
110.00	-26.648933	-27.760666	-27.418425	-1.408199	-0.551106	-0.906010
111.00	-26.469086	-26.971579	-26.821863	-1.588047	-1.340194	-1.502571
112.00	-27.049423	-28.463530	-28.029991	-1.007710	0.151757	-0.294443
113.00	-26.569626	-27.923847	-26.957497	-1.487507	-0.387924	-1.366939
114.00	-26.089828	-27.384167	-27.027878	-1.967305	-0.927605	-1.296556
115.00	-27.608101	-26.902620	-27.117918	-0.449031	-1.409152	-1.206516
116.00	-26.809919	-26.453806	-26.557123	-1.247213	-1.857966	-1.767311
117.00	-28.063679	-27.204048	-27.452763	0.006546	-1.107722	-0.871672
118.00	-27.187662	-26.085911	-26.437174	-0.869469	-2.225862	-1.887262
119.00	-27.079906	-26.226088	-27.892502	-0.977226	-2.085684	-0.431933
120.00	-28.921831	-27.492060	-27.353397	0.864698	-0.819712	-0.971036
121.00	-28.219433	-27.033035	-29.269369	0.162299	-1.278736	0.944935
122.00	-29.845055	-28.424620	-28.428661	1.787922	0.112847	0.104228







**Table B-3. Numerical Beam Pattern Structure as Shown Graphically in Figures 32 and 33 Comparing Original Beam Pattern Modeling versus Inter-Beam Interpolation Modeling**

BEAM LAUNCH ANGLE (deg)	AVERAGE BEAM INTENSITY (dB)		DIFFERENCE FROM ARRAY AVERAGE (dB)		NUMBER OF INTENSITY DATA SAMPLES	
	Original	Interpolated	Original	Interpolated	Original	Interpolated
0.00	0.000000	0.000000	0.000000	0.000000	0	0
1.00	0.000000	0.000000	0.000000	0.000000	0	0
2.00	0.000000	0.000000	0.000000	0.000000	0	0
3.00	0.000000	0.000000	0.000000	0.000000	0	0
4.00	0.000000	0.000000	0.000000	0.000000	0	0
5.00	0.000000	0.000000	0.000000	0.000000	0	0
6.00	0.000000	0.000000	0.000000	0.000000	0	0
7.00	0.000000	0.000000	0.000000	0.000000	0	0
8.00	0.000000	0.000000	0.000000	0.000000	0	0
9.00	0.000000	0.000000	0.000000	0.000000	0	0
10.00	0.000000	0.000000	0.000000	0.000000	0	0
11.00	0.000000	0.000000	0.000000	0.000000	0	0
12.00	0.000000	0.000000	0.000000	0.000000	0	0
13.00	0.000000	0.000000	0.000000	0.000000	0	0
14.00	0.000000	0.000000	0.000000	0.000000	0	0
15.00	0.000000	0.000000	0.000000	0.000000	0	0
16.00	0.000000	0.000000	0.000000	0.000000	0	0
17.00	0.000000	0.000000	0.000000	0.000000	0	0
18.00	0.000000	0.000000	0.000000	0.000000	0	0
19.00	-17.253205	-22.726887	-14.928776	-9.455094	156	4121
20.00	-22.726887	-22.726887	-9.455094	-9.455094	4121	4121
21.00	-25.269198	-25.269197	-6.912783	-6.912783	5821	5821
22.00	-27.077996	-27.077995	-5.103985	-5.103985	15193	15193
23.00	-28.175476	-28.175476	-4.006505	-4.006505	30138	30138
24.00	-28.861757	-28.861757	-3.320224	-3.320224	45901	45901
25.00	-29.817936	-29.817936	-2.364046	-2.364046	55549	55549
26.00	-29.746697	-29.746696	-2.435284	-2.435284	56839	56839
27.00	-30.485515	-30.485516	-1.696466	-1.696466	62653	62653
28.00	-30.544382	-30.544382	-1.6376	-1.637600	65624	65624
29.00	-31.230246	-31.230246	-0.951735	-0.951735	65556	65556
30.00	-31.066321	-31.066320	-1.11566	-1.115660	44654	44654
31.00	-31.590063	-31.590063	-0.591918	-0.591918	68319	68319
32.00	-31.577442	-31.577442	-0.604539	-0.604539	42593	42593
33.00	-32.047026	-32.047028	-0.134955	-0.134955	62497	62497
34.00	-32.205535	-32.205536	0.023554	0.023554	47819	47819
35.00	-32.315825	-32.315826	0.133844	0.133844	42438	42438
36.00	-32.507502	-32.507504	0.32552	0.325520	41191	41191
37.00	-33.067711	-33.067711	0.88573	0.885730	40850	40850

BEAM LAUNCH ANGLE (deg)	AVERAGE BEAM INTENSITY (dB)		DIFFERENCE FROM ARRAY AVERAGE (dB)		NUMBER OF INTENSITY DATA SAMPLES	
	Original	Interpolated	Original	Interpolated	Original	Interpolated
38.00	-33.127048	-33.127048	0.945067	0.945067	39119	39119
39.00	-32.688903	-32.688904	0.506922	0.506922	38983	38983
40.00	-32.722769	-32.722771	0.540788	0.540788	37898	37898
41.00	-33.264221	-33.264221	1.08224	1.082240	34895	34895
42.00	-31.877651	-31.877651	-0.30433	-0.304330	9052	9052
43.00	-32.816475	-32.816475	0.634494	0.634494	31508	31508
44.00	-33.446647	-33.446648	1.264666	1.264666	36774	36774
45.00	-30.696182	-30.696182	-1.485799	-1.485799	33339	33339
46.00	-30.318626	-30.318626	-1.863355	-1.863355	2969	2969
47.00	-30.963407	-30.963408	-1.218574	-1.218574	35977	35977
48.00	-31.259584	-31.259584	-0.922397	-0.922397	30624	30624
49.00	-29.011638	-29.011639	-3.170343	-3.170343	4425	4425
50.00	-31.781521	-31.781521	-0.40046	-0.400460	34818	34818
51.00	-29.423913	-31.703152	-2.758068	-0.478831	46	33928
52.00	-31.624781	-31.624781	-0.557201	-0.557201	33038	33038
53.00	0	-32.051109	0	-0.130873	0	32574
54.00	-32.477438	-32.477440	0.295456	0.295456	32111	32111
55.00	-31.984962	-32.466431	-0.197019	0.284445	133	31908
56.00	-32.455416	-32.455418	0.273435	0.273435	31704	31704
57.00	-31.272727	-32.491833	-0.909254	0.309851	44	30614
58.00	-32.528248	-32.528248	0.346267	0.346267	29524	29524
59.00	0	-32.470123	0	0.288144	0	29242
60.00	-32.412002	-32.412003	0.230021	0.230021	28961	28961
61.00	0	-32.400307	0	0.218325	0	27826
62.00	-32.38861	-32.388611	0.206629	0.206629	26690	26690
63.00	-33.679775	-32.388611	1.497794	0.206629	445	26690
64.00	0	-32.360737	0	0.178753	0	24859
65.00	-32.360735	-32.360737	0.178753	0.178753	24859	24859
66.00	0	-32.214310	0	0.032326	0	23814
67.00	-32.06788	-32.067879	-0.114101	-0.114101	22768	22768
68.00	0	-32.067879	0	-0.114101	0	22768
69.00	-27	-31.417501	-5.181981	-0.764480	27	20376
70.00	-31.417501	-31.417501	-0.76448	-0.764480	20376	20376
71.00	-29.04	-31.417501	-3.141981	-0.764480	25	20376
72.00	-30.471014	-31.245762	-1.710967	-0.936220	207	17930
73.00	-31.245761	-31.245762	-0.93622	-0.936220	17930	17930
74.00	0	-30.361443	0	-1.820539	0	13762
75.00	-29.477124	-29.477123	-2.704858	-2.704858	9595	9595
76.00	-31.021357	-31.021357	-1.160624	-1.160624	6087	6087
77.00	-22.5	-29.817347	-9.681981	-2.364635	10	8562
78.00	-28.613336	-28.613337	-3.568645	-3.568645	11038	11038
79.00	-30.361345	-28.613337	-1.820637	-3.568645	1904	11038
80.00	0	-27.704741	0	-4.477241	0	8650
81.00	-27.70474	-27.704741	-4.477241	-4.477241	8650	8650

BEAM LAUNCH ANGLE (deg)	AVERAGE BEAM INTENSITY (dB)		DIFFERENCE FROM ARRAY AVERAGE (dB)		NUMBER OF INTENSITY DATA SAMPLES	
	Original	Interpolated	Original	Interpolated	Original	Interpolated
82.00	-30.740558	-27.704741	-1.441423	-4.477241	1721	8650
83.00	0	-28.538912	0	-3.643070	0	3932
84.00	-28.538911	-28.538912	-3.64307	-3.643070	3932	3932
85.00	-29.713017	-29.713017	-2.468964	-2.468964	3772	3772
86.00	-20.818182	-29.713017	-11.363799	-2.468964	11	3772
87.00	-30.098214	-30.382683	-2.083767	-1.799298	56	5255
88.00	-30.382683	-30.382683	-1.799298	-1.799298	5255	5255
89.00	0	-29.562487	0	-2.619494	0	3811
90.00	-28.74229	-28.742290	-3.439691	-3.439691	2367	2367
91.00	0	-28.742290	0	-3.439691	0	2367
92.00	-29.5	-29.317104	-2.681981	-2.864877	6	4344
93.00	-29.317104	-29.317104	-2.864877	-2.864877	4344	4344
94.00	-24.125	-29.317104	-8.056981	-2.864877	8	4344
95.00	0	-29.929663	0	-2.252319	0	7272
96.00	-29.929662	-29.929663	-2.252319	-2.252319	7272	7272
97.00	-27.291667	-29.929663	-4.890314	-2.252319	12	7272
98.00	0	-27.977385	0	-4.204596	0	9286
99.00	-27.977385	-27.977385	-4.204596	-4.204596	9286	9286
100.00	0	-27.977385	0	-4.204596	0	9286
101.00	-23.633333	-28.300507	-8.548648	-3.881475	15	11855
102.00	-28.300506	-28.300507	-3.881475	-3.881475	11855	11855
103.00	-27.619048	-28.300507	-4.562934	-3.881475	21	11855
104.00	0	-29.296955	0	-2.885025	0	14029
105.00	-29.296956	-29.296955	-2.885025	-2.885025	14029	14029
106.00	-25.3125	-29.296955	-6.869481	-2.885025	24	14029
107.00	0	-31.119757	0	-1.062224	0	17356
108.00	-31.119757	-31.119757	-1.062224	-1.062224	17356	17356
109.00	0	-31.119757	0	-1.062224	0	17356
110.00	-29.124242	-31.547047	-3.057739	-0.634935	165	18854
111.00	-31.547046	-31.547047	-0.634935	-0.634935	18854	18854
112.00	-31.9375	-31.662819	-0.244481	-0.519163	32	19864
113.00	-31.77859	-31.778589	-0.403392	-0.403392	20873	20873
114.00	-28.670455	-31.778589	-3.511527	-0.403392	88	20873
115.00	-31.585714	-31.911798	-0.596267	-0.270182	35	23180
116.00	-31.911799	-31.911798	-0.270182	-0.270182	23180	23180
117.00	-29.472222	-32.278545	-2.709759	0.096565	36	24208
118.00	-32.645294	-32.645294	0.463313	0.463313	25235	25235
119.00	-32.345395	-32.645294	0.163414	0.463313	152	25235
120.00	-30.951737	-32.761093	-1.230244	0.579111	259	25987
121.00	-32.761092	-32.761093	0.579111	0.579111	25987	25987
122.00	-32.813725	-32.932190	0.631744	0.750211	51	27590
123.00	-33.103292	-33.103291	0.921311	0.921311	29194	29194
124.00	-34.949153	-32.682953	2.767171	0.500975	59	29356

BEAM LAUNCH ANGLE (deg)	AVERAGE BEAM INTENSITY (dB)		DIFFERENCE FROM ARRAY AVERAGE (dB)		NUMBER OF INTENSITY DATA SAMPLES	
	Original	Interpolated	Original	Interpolated	Original	Interpolated
125.00	-32.262619	-32.262619	0.080638	0.080638	29518	29518
126.00	0	-32.621178	0	0.439198	0	30676
127.00	-32.979739	-32.979740	0.797758	0.797758	31834	31834
128.00	-31.637255	-32.693745	-0.544726	0.511764	51	32161
129.00	-32.407751	-32.407749	0.225769	0.225769	32488	32488
130.00	-29.008744	-32.102844	-3.173237	-0.079138	1887	31960
131.00	-31.797935	-31.797935	-0.384046	-0.384046	31433	31433
132.00	-31.202325	-31.202326	-0.979656	-0.979656	33587	33587
133.00	-31.015317	-31.299759	-1.166664	-0.882223	457	33419
134.00	-31.397191	-31.397190	-0.78479	-0.784790	33251	33251
135.00	-31.672966	-31.672966	-0.509015	-0.509015	26962	26962
136.00	-34.006247	-34.006248	1.824266	1.824266	8804	8804
137.00	-32.478604	-32.478603	0.296622	0.296622	33744	33744
138.00	-32.478493	-32.478493	0.296512	0.296512	34314	34314
139.00	-31.963031	-31.963032	-0.21895	-0.218950	22262	22262
140.00	-33.407725	-33.407726	1.225744	1.225744	16505	16505
141.00	-33.835847	-33.835846	1.653866	1.653866	33280	33280
142.00	-34.34963	-34.349628	2.167649	2.167649	37165	37165
143.00	-33.178393	-33.178394	0.996412	0.996412	34396	34396
144.00	-34.023974	-34.023975	1.841993	1.841993	36790	36790
145.00	-33.885775	-33.885777	1.703793	1.703793	33644	33644
146.00	-33.462673	-33.462673	1.280692	1.280692	39743	39743
147.00	-34.037446	-34.037445	1.855465	1.855465	49631	49631
148.00	-34.044405	-34.044407	1.862423	1.862423	36190	36190
149.00	-32.585385	-32.585384	0.403404	0.403404	35410	35410
150.00	-33.429925	-33.429924	1.247944	1.247944	49540	49540
151.00	-32.804243	-32.804241	0.622262	0.622262	35991	35991
152.00	-33.440177	-33.440178	1.258196	1.258196	38965	38965
153.00	-33.023354	-33.023354	0.841373	0.841373	36461	36461
154.00	-32.867246	-32.867245	0.685265	0.685265	30470	30470
155.00	-33.599075	-33.599075	1.417094	1.417094	26278	26278
156.00	-34.159302	-34.159302	1.97732	1.977320	17153	17153
157.00	-31.347398	-31.347399	-0.834583	-0.834583	6245	6245
158.00	-28.696336	-31.347399	-3.485645	-0.834583	1938	6245
159.00	-26.9125	-31.347399	-5.269481	-0.834583	200	6245
160.00	0	0.000000	0	0.000000	0	0
161.00	0	0.000000	0	0.000000	0	0
162.00	0	0.000000	0	0.000000	0	0
163.00	0	0.000000	0	0.000000	0	0
164.00	0	0.000000	0	0.000000	0	0
165.00	0	0.000000	0	0.000000	0	0
166.00	0	0.000000	0	0.000000	0	0
167.00	0	0.000000	0	0.000000	0	0
168.00	0	0.000000	0	0.000000	0	0

BEAM LAUNCH ANGLE (deg)	AVERAGE BEAM INTENSITY (dB)		DIFFERENCE FROM ARRAY AVERAGE (dB)		NUMBER OF INTENSITY DATA SAMPLES	
	Original	Interpolated	Original	Interpolated	Original	Interpolated
169.00	0	0.000000	0	0.000000	0	0
170.00	0	0.000000	0	0.000000	0	0
171.00	0	0.000000	0	0.000000	0	0
172.00	0	0.000000	0	0.000000	0	0
173.00	0	0.000000	0	0.000000	0	0
174.00	0	0.000000	0	0.000000	0	0
175.00	0	0.000000	0	0.000000	0	0
176.00	0	0.000000	0	0.000000	0	0
177.00	0	0.000000	0	0.000000	0	0
178.00	0	0.000000	0	0.000000	0	0
179.00	0	0.000000	0	0.000000	0	0

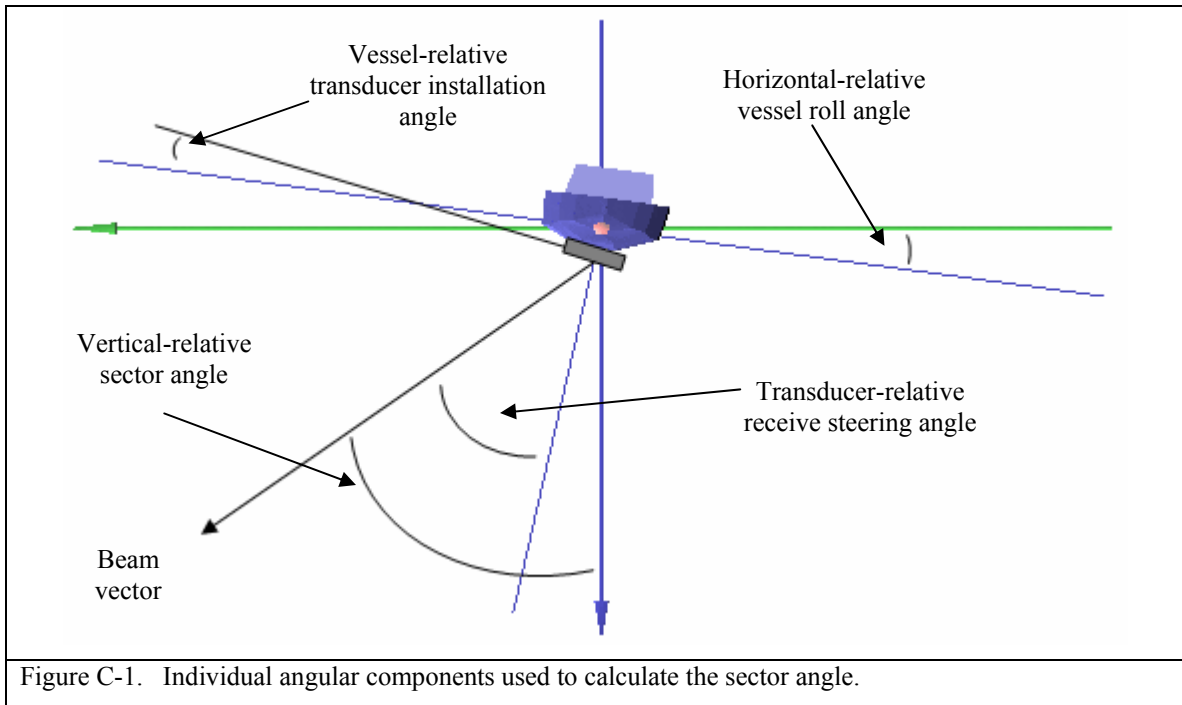
## **APPENDIX C**

### **Overview of Angular Definitions**

## **1) Steering and Sector Angles**

The beam steering angle is a transducer-relative angle to which a receive beam is pointed. Beams are steered in such a way as to ensure that all available beams in the system are spread out to acquire soundings across the entire desired across-track angular swath. The convention used for Simrad systems is to measure these angles from the vertical, with angles to port being positive, and angles to starboard being negative. The system will automatically steer all beams depending on the desired angular swath, type of beam spacing (equidistant, equiangular, or in-between), installation angle of the receive transducer, and roll angle of the vessel at the time of receive.

The sector angle is a vertically-references angle which represents the final pointing vector of a receive beam in the across-track direction. It employs the same sign convention as that of the beam steering angle, in that it is measured from the vertical, with the port being positive and starboard being negative. It is calculated as the sum of the receive steering angle, the vessel roll angle, and the receive transducer installation angle, as shown in Figure C-1.



## 2) Launch Angle

The launch angle is equivalent to the sector angle in that it is a vertically-references angle which represents the final pointing vector of the receive beam in the across-track direction. The difference between the two is that the launch angle is an OMG convention used for in-house software which is measured from  $0^\circ$  through  $180^\circ$  starting from the starboard side, with a beam received parallel to the water surface on that side being  $0^\circ$ , at nadir being  $90^\circ$ , and so on, as shown in Figure C-2.



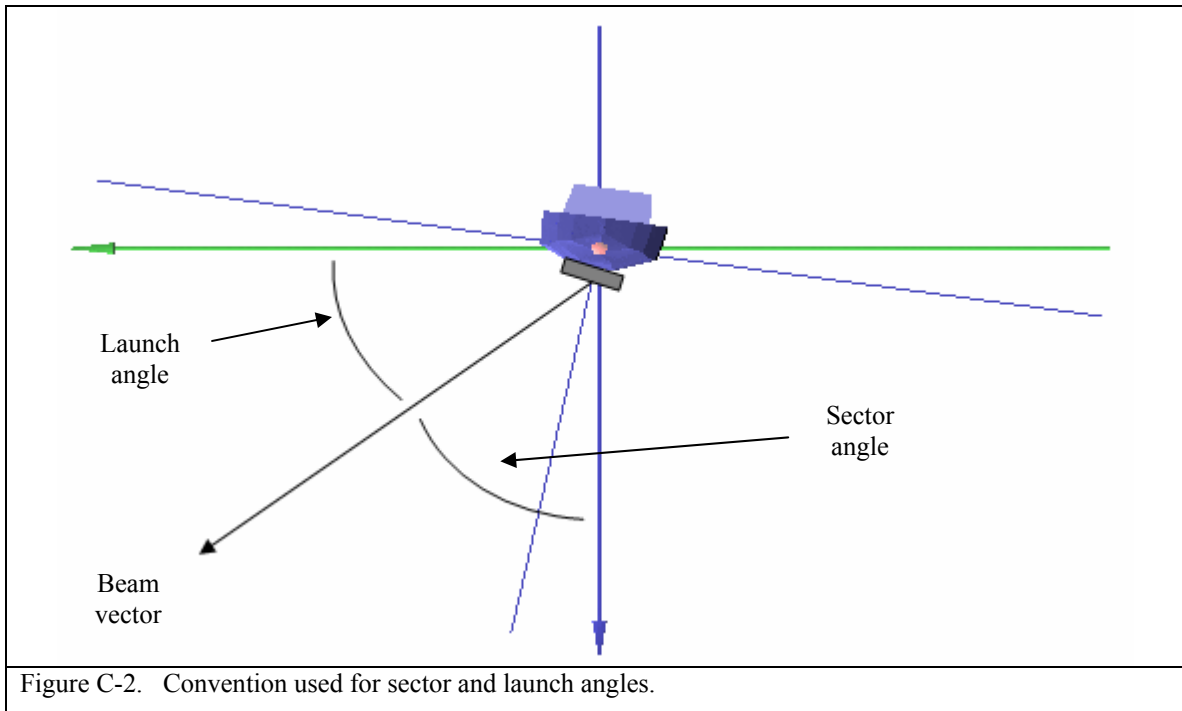


Figure C-2. Convention used for sector and launch angles.

### 3) Azimuth and Depression Angle

Simrad multibeam systems report the position of soundings in 3-dimensional space using water depth and transducer-relative along-track and across-track distances. These are calculated using a range (distance to seabed from transducer), and azimuth and depression angles (direction to seabed from transducer). Before this research was undertaken, sector and launch angles were calculated using the depression angle and across-track distances to the final sounding solutions show in Figure C-3, rather than the angular measurements of the raw receive beams and transducer installation geometry as discussed in section 6 of this report.

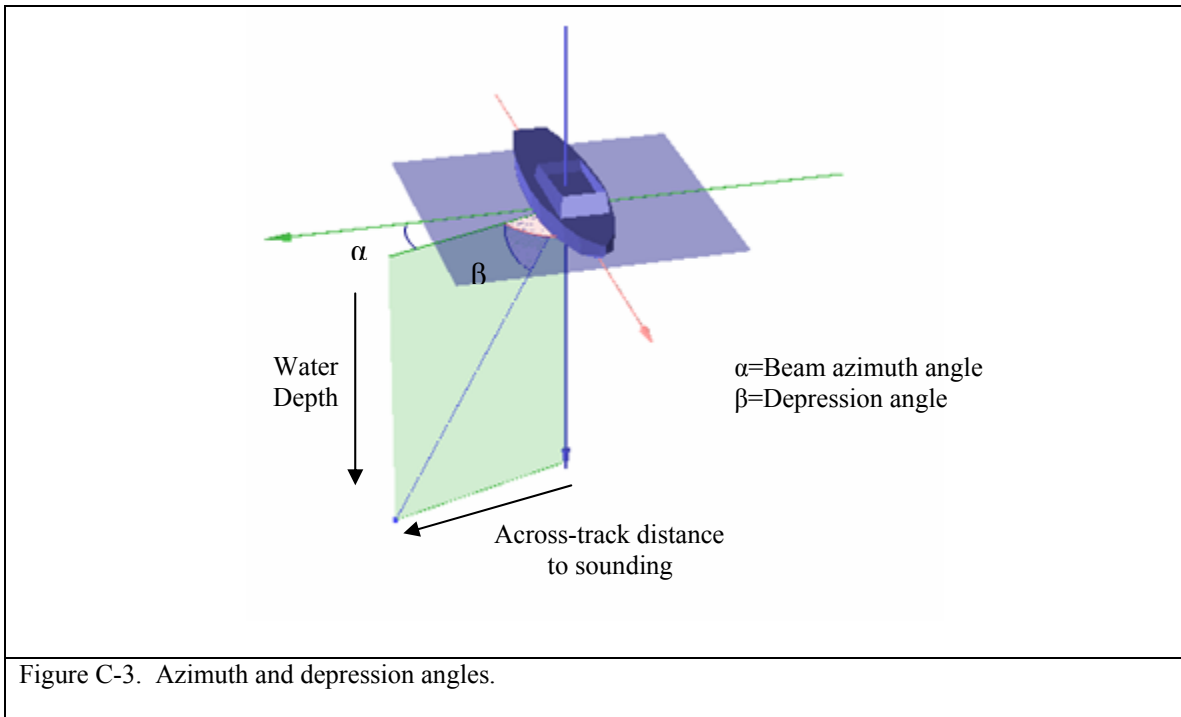


Figure C-3. Azimuth and depression angles.

#### 4) Incidence Angle

The incidence angle is the angle between the vertical and the vector of a beam of a multibeam system as shown in Figure C-4. The angle at which the acoustic wave interacts with the seabed has as great impact on the amount of energy which will be backscattered by that beam as discussed in section 4 of this report.

It is important to note, however, that this angle definition holds true only when the seabed is flat. In this case it is a valid definition since the seafloor is assumed to be flat by the Simrad system. The true incidence angle will depend on the seabed slope if it changes across the width of the swath.

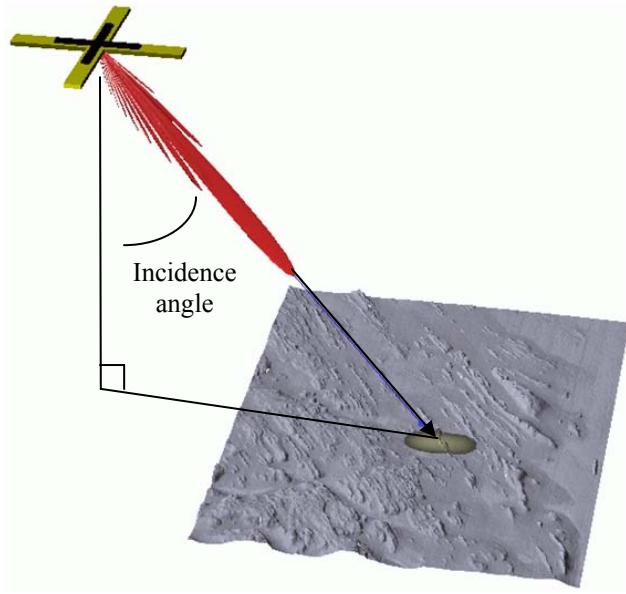


Figure C-4. Seabed incidence angle. Image derived from [Hughes Clarke, 2004].

## **CURRICULUM VITAE**

# KRISTIAN CHARLES LLEWELLYN

---

- PERSONAL INFORMATION** : Date of birth : 23 March 1979  
Nationality : Canadian
- EDUCATION** : Masters of Engineering, Geodesy and Geomatics, Ocean Mapping Group – University of New Brunswick, Fredericton, New Brunswick, Canada
- Bachelor of Science in Engineering, Mechanical – University of New Brunswick, Fredericton, New Brunswick, Canada
- SAFETY COURSES** : Offshore Personal Survival Techniques, Warsaw Maritime Centre, Southampton, UK. June 2005 (expires June 2007).
- TECHNICAL COURSES** : CARIS HIPS – Ocean-mapping software training course using HIPS and SIPS 6.0 products, Fredericton, NB, Canada. August 2005.
- EXPERIENCE** : Study within the Ocean Mapping Group, including underwater acoustic imaging, oceanography, hydrographic data management, GIS, remote sensing, and survey economics and business management.
- Primary thesis work included post-processing algorithm design to correct for beam pattern residuals in backscatter mosaics arising from using a sonar system which features a multi-sector motion-stabilized transducer which is protected by a titanium-polymer ice window.
- Participated in a conference on uncertainty representation on nautical charts at the University of Southern Mississippi at Stennis Space Center, Mississippi, USA. March 2004.
- Co-authored and presented a paper on nautical chart uncertainty at the Canadian Hydrographic Conference in Ottawa, Canada. May 2004.
- Authored a new education module for the [Canadian Power & Sail Squadrons](#), teaching about uncertainty representation on nautical charts to recreational boaters. May 2004.

**FIELD EXPERIENCE** : 3-week cruise in Long Reach in the St. John river, NB, Canada, involving installation and monitoring of tide gauges, mobilization and calibration of UNB's survey launch the [CSL Heron](#), acquisition and processing of a variety of hydrographic and oceanographic data, and geoid-ellipsoid separation modeling of the river. May 2004.

6-week cruise in the Beaufort Sea and Amundsen Gulf in the Canadian Arctic aboard the [CCGS Amudsen](#) as part of the [ArcticNet](#) project, seabed mapping using a Simrad EM300 and Knudsen 320R subbottom profiler. Summer 2004.

2-week cruise aboard the [CCGS Amudsen](#) down the coast of Labrador, Canada, performing deep-water trials of the EM300 as installed on the ship. September 2004.

2-week cruise around Deer Island, NB, Canada, involving habitat analysis mapping using a Simrad EM3000 and Knudsen keel-mounted sidescans aboard the [CSL Heron](#). May 2005.

3-week cruise off the coast of Fraser Island in Australia mapping sediment transport for Australian geologists using the Simrad EM300 on the CSIRO RV [Southern Surveyor](#). January 2005.

4-week cruise off the coast of Scotland with [Gardline Hydro](#) aboard the [RV Triton](#) running a Simrad EM1002 survey for the [UK Maritime and Coastguard Agency](#). July 2005.

3-week cruise off the coast of Malaysia with [Fugro Survey](#) aboard the Geo Surveyor running a towed EM2000 survey using the [Edgetech DT-1](#) deep-tow vessel. September 2005.

6-week cruise in the Gulf of Mexico aboard the Moana Wave with [C&C Technologies](#) performing block hazard surveys utilizing seismic, single-beam, sidescan, and subbottom acoustic systems. November/December 2005.

Professional SCUBA diver. Certified PADI & SSI Divemaster, Assistant Instructor (AI), and Oxygen Provider. Professional experience including the role of DiveMaster/AI on the Great Barrier Reef in Australia, and as AI in local SCUBA clubs. Significant experience in worldwide diving, including the eastern seaboard of Canada and throughout the South Pacific. High interest and experience in all types of diving including shore, boat, warm-water, cold-water, reef, ocean-bottom, drift, and wreck diving.



**Jan 1995 – March 2005**

**Hospitality/Food and Beverage, Various Organizations**

Nine years experience working in the F&B hospitality industry. Work has included all types of establishments including the 4-star level at a Sheraton Resort Hotel. Significant supervisory experience, including the responsibility of general store and bar operations and entire staff. Duties have included the hiring, training, scheduling, and rotation of staff, as well as promotional work and human resource management.

**EQUIPMENT USED:**

Positioning:

Kongsberg Seatex 200 DGPS systems with Fugro differential correction service  
Trimble DGPS positioning systems  
C-Nav globally-corrected DGPS systems  
Coda-Octopus F-180 DGPS positioning systems  
Underwater positioning systems including Doppler and USBL positioning

Hydrographic Systems:

Simrad EM3000 multibeam sonar system  
Simrad EM2000 multibeam sonar system  
Simrad EM1002 multibeam sonar system  
Simrad EM300 multibeam sonar system  
Knudsen 320 single-beam sonars  
EchoTrac single-beam sonars  
RDI Instruments Acoustic Doppler Current Profilers  
Brooke-Ocean Moving Vessel Profilers with CTD sensors  
Various carousel/rosette systems with CTD sensors  
Kongsberg Seatex 200, Kongsberg MRU-6 Coda-Octopus F-180, and Applanix POS/MV integrated positioning/orientation systems  
Edgetech DT-1 combined sonar system deep-tow vessels

Geophysical Systems:

Knudsen 320R subbottom profilers  
GeoAcoustics subbottom profilers  
Knudsen 320 keel-mounted sidescan sonars  
GeoAcoustics sidescan sonars  
Klein 5000 focused multibeam sidescan sonar

**COMPUTER SKILLS:**

Very proficient computer skills in all aspects of general use, including Windows, UNIX, and Linux, as well as Microsoft, Adobe, and Corel Office Packages.

Hydrographic processing software including:

Caris HIPS/SIPS  
IVS Fledermaus  
Fugro Starfix  
UNB Ocean Mapping Group in-house tools



Hydrographic surveying systems including:  
Kongsberg-Simrad Multibeam Sonar Systems  
Knudsen sidescan, single-beam, and subbottom profiler systems  
Aldebaran-Regulus ENC & survey planning software  
Winfrog survey planning software  
SonarWiz sonar acquisition software  
Brooke Ocean Technology Moving Vessel Profilers.

Extensive programming experience using C and Fortran.

Engineering software including Arcview GIS, PCI, AutoCad, and TKSolver.

**LANGUAGES SPOKEN**

Fluent in English and French